UNIVERSITÀ DEGLI STUDI DI MESSINA

DIPARTIMENTO DI

SCIENZE MATEMATICHE ED INFORMATICHE, SCIENZE FISICHE

E SCIENZE DELLA TERRA

DOTTORATO DI RICERCA IN FISICA

XXXI CICLO

CLIMATE CHANGE IN THE MEDITERRANEAN AREA AND IN SICILY: TIME SERIES ANALYSIS OF TEMPERATURE AND PRECIPITATION USING WAVELET

Tesi di dottorato di:

Franco COLOMBO

Coordinatore: **Chiar.mo Prof. Lorenzo TORRISI**

Tutor: **Chiar.mo Prof. Salvatore MAGAZU'**

Contents

Introduction

The topic of climate change involves and directly or indirectly affects every inhabitant of the planet Earth. The magnitude of the problems that poses and the repercussions on many aspects of the daily life of every human being have turn the spotlight on one of the hottest and debated themes of the last 40 years. Terms like "Kyoto[1] Protocol", "global warming" or "COP21[2]" are now of public domain, despite their real meaning is still barely known, if not unknown, for the vast majority of the world population. The presence of two opposite schools of thought, on the one hand sees the **deniers** who claims that the on-going warming is only the result of a natural phenomenon linked to the Earth's climate cycles and on the other, the **supporters of warming** resulted from anthropogenic factors has further complicated and confused ideas on the matter.

The Earth's climate system is a **complex** system made of the atmosphere, the geosphere, the cryosphere, the biosphere and the hydrosphere and their complex and multiple interactions.

The characteristics of the earth's climate and its variability are often associated only with the atmospheric element of the climate system being the influence exerted by the other

[1] Kyoto Protocol: it is an international agreement to combat global warming, an environmental phenomenon that science has never questioned and whose human responsibility is absolutely clear and proven. The treaty, of a voluntary nature, was signed in Kyoto on December 11, 1997, during the Conference of the Parties (COP3) but entered into force only on February 16, 2005 after the ratification of Russia.

[2] At the Paris climate conference (COP21) of December 2015, 195 countries adopted the first universal and legally binding global climate agreement. The agreement sets out a comprehensive action plan to put the world on track to avoid dangerous climate changes by limiting global warming below 2º C.

components less evident. Due to such complexity, understanding the dynamics that underlie its variability, noticed starting from the observation of the data itself, requires the use of refined physical and mathematical tools. Temporal series analysis was one of the key tools in the interpretation of climate dynamics, since the collection and cataloguing of the various meteorological parameters began.

The climate of a place is often defined in a very restrictive sense, such as the average weather conditions of a given location. A definition of the term in a broader meaning is as follows: "state of the climate system" where the term **state** means the statistical description in terms of mean value and variance of the most important meteorological parameters, such as temperature, precipitation, distribution of winds, etc. in a sufficiently long timeframe and in any case not less than 30 years. From this point of view, we can say with certainty that the Earth's climate has never been constant, but over the time has undergone to various changes due to natural factors. Mainly in the 80s started a strong dispute over the anthropogenic nature of climate change that has involved both the scientific and the political world globally. Starting from that period, in fact, a long sequence of years characterized by average temperatures record has induced the scientific community to investigate the nature and causes of such global warming. Today, despite the understanding on the origin and evolution of global warming has greatly improved; the climate change thematic remains one of the most debated among the entire international scientific community. As matter of fact, the chaotic nature of the atmosphere and the complexity of the Earth's climate system makes the issue far from being resolved.

The work dealt with in this doctoral thesis is placed in such context and aims to provide a historical framework to the science of climate change (Chap.1) to subsequently pass on to the evidence and consequences of global warming already observed in atmosphere, in the oceans and in the Cryosphere (Chap.2). Chapter 3 of the thesis will be described both natural and

anthropogenic climate changes scientifically most credited causes. The next chapter will provide an overview of climate models currently used globally, their development over the last 20 years and the climate scenarios envisaged, both globally and regionally, by the end of the century. Chapter 5 depicts the analysis and description of the main climatic changes observed and the future scenarios envisaged by the models for the Mediterranean area.

Finally, in Chapter 6, will be reviewed some of the techniques of analysis of the climates time series, applying the Wavelet analysis technique to some historical series of temperatures observed on some locations of Sicily.

1

The Science of the climate changes: historical overview

1.1 From Aristotle to XVIII Century

Even before Aristotle, Thales of Miletus that lived between 624 and 565 B.C. dealt with meteorology. He is the author of the first meteorological calendar, used by sailors in their increasingly frequent journeys due to the flourishing trade between Greece and the colonies in the Mediterranean. He is the first who affirms that the Sun illuminates the Moon. However, **Aristotle** (384-322 B.C.) is the first the fully and systematically dealt on climate. In fact, he is the author of a work destined to remain the reference of the entire Western world for almost twenty centuries: *Meteorology*. The Greek philosopher examines and tries to scientifically interpret numerous phenomena, explaining how water condensation occurs: "when the heat that brings up the damp disappears, then the humid, cooling down, and because the heat is lacking and for the place itself, it condenses again, and from the air it generates water that thus falls back on Earth" (Meteorology II, 4). The logic of Aristotle considers that if on the one hand that for the knowledge of philosophical truths the deductive method is necessary, from the universal to the particular, on the other hand it recognizes that the *inductive* method is valid for the study of natural phenomena from the observation of particular cases are reached universal conclusions. To complete the *Meteorology*, Theophrastus (373 circa -287 BC), and best known of his students adds a treatise on the winds who also observes how the draining

of the wetlands eliminates the power of moderation of the water and leads to extreme colds. At the same time, cutting the forests to make room for agricultural fields exposes the soil directly to the sun's rays with the effect of increasing the temperatures. It is the first suggestion that human activities can change the climate, at least locally. The recommendation to the methodology of observations and inductive method proposed by Aristotle, exhausted in a short time. Since the ancient Rome, the foundation of meteorology turns into the observation of the stars and the behaviour of animals. **Pliny the Elder** (23-79 AC) states "The Red Moon announces the wind, the black Moon the rain" while **Virgil** (70-19 BC) describes in the *Georgic* the reactions of swallows, cows and frogs as the storm approaches. Finally, for **Lucretius** (95-55 BC), nature and the unleashing of its elements are a spectacle for the eyes, the inspiration to write passages of poetry and not the object of a series of scientific investigations. Once the Greek cogitators' impulse has definitively ceased, the study of the Climate and its elements does not take any step forward and indeed throughout the **Middle Age** it is confused with astrology and assimilated to occult practices.

According to medieval man, the motion of the stars obeys exclusively the will of God, from which obviously every meteorological phenomenon derives. The sky watch is exclusively to gather its premonitions: many falling stars announce a cold winter; the passage of a comet is an omen of calamity, epidemics or droughts. This is a period where God is subject of prayers and processions to send rain or sun and when these invocations are vain, only one person is responsible: the devil "prince of the powers of the air".

The **Renaissance** is when things start to change for most of the sciences. A new, more open cultural climate and tools like the press that allow the rapid dissemination and easy preservation of experimental results support the rebirth of scientific research. Also the discovery and exploration of the new territories gets ready to knowledge the climate and its differences on a global scale.

However, the superstition resists and in 1677 the English parliament promulgates a law that punishes with the stake anyone who “makes the rain come or prophesy the weather” (law abrogated repealed in 1959 only).

A first attempt to restore order and return dignity to the science of the climate is carried out by the French ecclesiastical **Edme Mariotte** (1620-1684) who observes and writes that Sun light and heat easily pass through glass and other transparent materials, while the heat of other sources (such as fire) does not have the same capacity.

It is an insignificant statement for us, but an important intuition for the time. Its implications will be clear only long afterwards, precisely with the discoveries made by Fourier and other scientists.

Meanwhile, at the court of **Ferdinando II**, Grand Duke of Tuscany, are invented many of the instruments that will give an important impulse to meteorology. In 1641, was developed the first thermometer with liquid, which applies the principles already established by Galileo in 1597.

In 1643 the physicist **Evangelista Torricelli** (1608-1647) student and successor of Galileo, demonstrates the existence of atmospheric pressure, inventing the barometer. In 1664 is invented the hygrometer that measures the humidity contained in the air. During the eighteenth century, all these devices were improved. In particular, the thermometer, until then equipped with arbitrary measurement scales, is made “standard” by adopting universal measurement scales.

In 1724, the German physicist **Gabriel Daniel Fahrenheit** (1686-1736) invented the mercury thermometer and introduced the homonym scale, while a few years later the Swedish astronomer **Anders Celsius** (1701-1744) proposed the centigrade scale.

Driven by the new instruments and the exploration of the terrestrial globe, also for the science of climate comes the moment of development. In 1686, the astronomer **Edmond**

Halley (1656-1742) published the first wind map (Fig.1), with a description of trade winds and monsoons, to which he tries to explain: he links the general circulation of atmospheric currents to the homogeneous distribution of solar heat on the earth's surface.

In 1735, **George Hadley** (1685-1768) improved the above-said theory. He enunciates the trade winds theory, making them derive from the rotation of the Earth, as well as from the movements of the air masses. The research of Halley and Hadley are real milestones and both English scientists are considered the fathers of dynamic climatology.

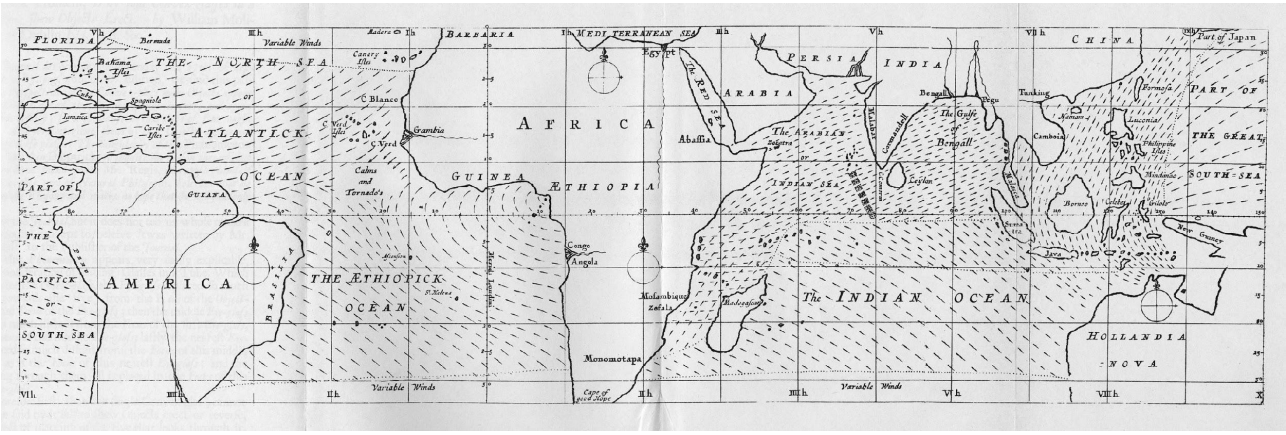

Fig.1 Halley's Winds Map with trade winds representation (Phil. Trans.,1686 n. 183).

In 1765, the French scientist **Antoine Laurent de Lavoisier** (1743-1794) enunciated the rules of meteorological science based on the laws and instruments that from Galileo on were developed: "the prediction of climate changes is an art which has specific principles and well-defined norms and which requires a long experience and constant attention from the scientist. The essential bases of this science are the systematic and daily observation of changes in the mercury height of the barometer, the strength and direction of the winds at different altitudes, the hygrometric state of the air. By having all these data, it is often possible to predict the weather a day or two in advance and with a very high probability". Meteorology develops along with technological innovation.

In 1783, the invention of the air balloons by the **Montgolfier brothers** allows to study the atmosphere conditions at great heights. It's also fundamental the exploration of the mountains and the birth of alpinism symbolized by the name of the Swiss scientist **Horace-Benedict de Saussure** (1740-1799). He graduated in 1859 with a thesis on fire, in which he demonstrates that the bodies absorb the heat the better the darker they are. To study solar heat, he builds a special instrument: the helium-thermometer.

The instrument consists of a container covered by one or more glass plates, separated by air spaces, with a blackened bottom and a thermometer to measure the temperatures. De Saussure utilized it to measure the effect of solar heat on the air contained in the spaces between glass plates. In 1774, he conducted a series of observations with the helium-thermometer in different positions, which were on the mountains peaks and in the valleys underneath, demonstrating a significant growth of heat while the altitude increases: it is a step towards the determination of solar power.

1.2 The Fathers of the Science: Fourier, Tyndall e Arrhenius

One of the first scientists to suggest that the gases in the atmosphere could absorb part of the radiation coming from the Earth's surface and thus contribute to the warming of the atmosphere was **Jean-Baptiste-Joseph Fourier** (1768-1830). In one of his submissions to the Paris Academy of Sciences in 1824, Fourier compared the warming of the atmosphere to what was happening in a solar thermometer (helium-thermometer).

For Fourier the atmosphere behaved exactly like a giant solar thermometer having the same radiative properties. "This is how the temperature of the Earth is increased by the interposition of the atmosphere, because the heat in the state of light finds less resistance to penetrating the air than when bounces back converted into non-luminous heat".

In this description, the French scientist bases on the distinction between "bright heat" and "dark heat" recently introduced. Fourier can thus improve the intuition of Mariotte in the

seventeenth century, stating that sunlight has the property of crossing transparent substances such as air, but loses almost entirely such property when converted into dark heat, that is infrared rays. By retaining the latter, the atmosphere acts more or less like a glass and contributes to raising the earth's temperature.

Claude-Servais-Mathias Pouillet (1790-1868) further elaborated Fourier's idea. He argued that the atmosphere equilibrium temperature had to be higher than that of outer space and lower than the ground temperature due to the different absorption of the atmosphere with respect to solar radiation. The atmosphere absorbs more radiation from the earth than from the sun [1].

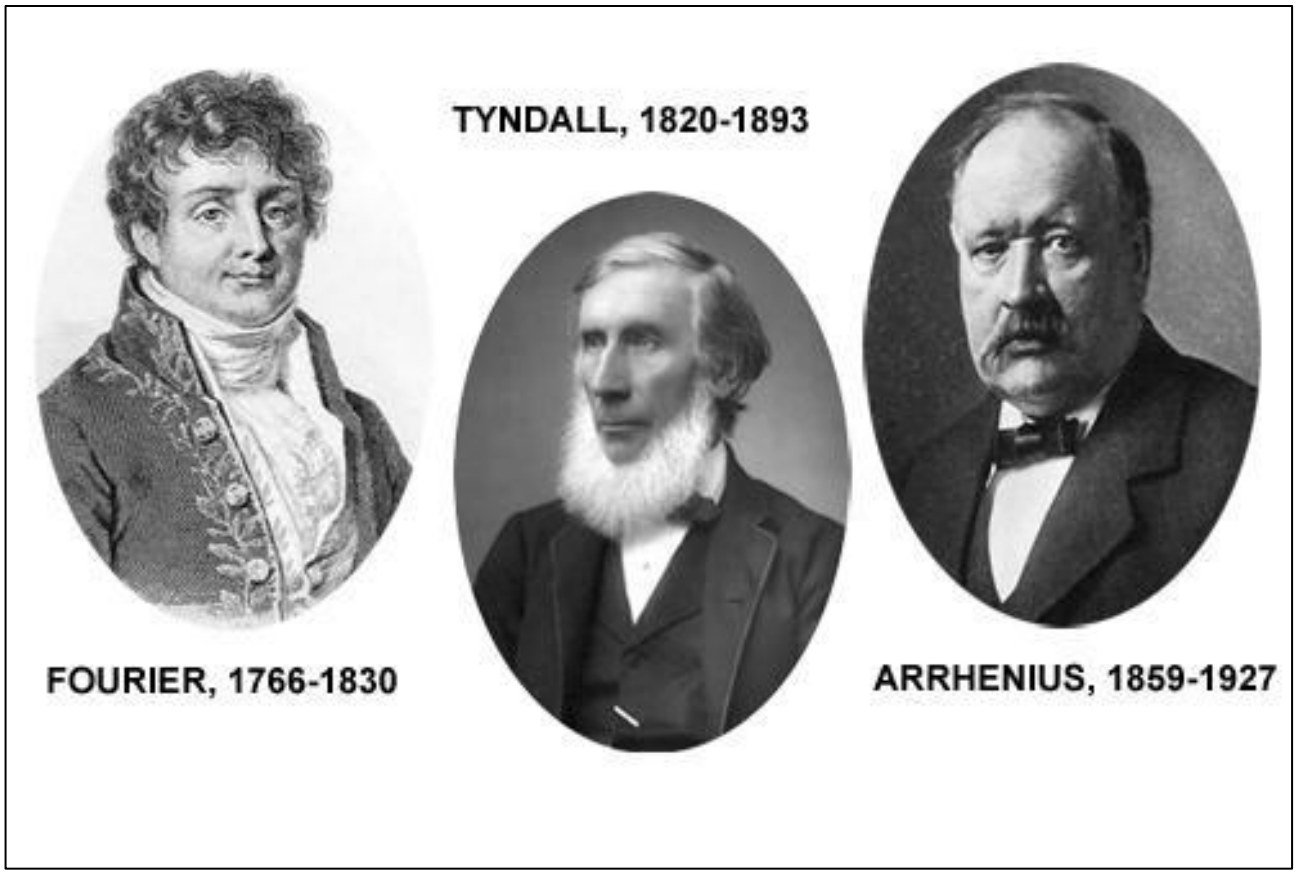

Fig. 2 The Fathers of the climate science

However, neither Fourier nor Pouillet was able to explain why the atmosphere was able to absorb heat, if not in very general terms [2]. To understand the role of water vapor and carbon dioxide was the contribution of the British naturalist **John Tyndall** (1820-1893). He led the first and convincing experiment on the radiative properties of gases, showing that perfectly colourless and invisible, gas and vapor were able to absorb and emit heat. In 1861, the Philosophical Magazine published the results of this experiment.

Tyndall's measurements indicated that both the water vapor and the carbon dioxide in the air were able to absorb more heat than the pure air and consequently exert a great influence on the climate. The importance of this discovery made it possible to understand immediately that the carbon dioxide increase of concentration in the atmosphere, caused by the combustion of coal and oil, would have been able to cause climate change. Tyndall described what Fourier had only sensed: the mechanisms of the greenhouse effect.

In 1986, the Swedish chemist **Svante Arrhenius** (1859-1927) published the first work predicting that human activities could change the earth's climate. The presentation of the long essay “On the influence of atmospheric carbon dioxide over the terrestrial temperatures” took place on 11 December 1895 at the Royal Academy of Sciences of Sweden. The year after the Philosophical Magazine publishes the essay. The scientist develops a theory to explain the causes of glaciations and other major climate changes that is based on the capacity of carbon dioxide and other gases to absorb infrared radiation reflected from the Earth's surface.

The scientist also suggested that the use of fossil fuels could produce so much carbon to heat the Earth, estimating that a doubling of the carbon dioxide in the atmosphere could cause the average temperature increase of 4-6 °C. To perform his calculations he used the radiation measurements coming from the Moon in different humidity conditions performed by Langley, to assess the amount of radiation absorbed by the atmosphere due to steam and carbon dioxide. Arrhenius reached the conclusions were that “if the quantity of carbon dioxide

increases in geometric progression, the temperature of the planet increases in quasi-arithmetic progression".

1.3 The astronomical theories and the climate dynamics

At the beginning of the twentieth century, a Serb-Yugoslav astronomer, **Milutin Milankovitch** (1879-1958), proposed the hypothesis according to which the oscillations of the Earth's axis and the mutations of the orbit cause variations in the quantity of solar energy reaching Earth, such to alter the intensity of the seasons and consequently determine the glacial cycles. The astronomical cycles would somehow upset the balance between winter and summer that is between the ice expansion and withdrawal, to the benefit of the first phase. Milankovitch hypothesis seems confirmed by the duration of the glacial cycles, whose period of formation and melting of the ice is about 100,000 years, while it is about 10,000 years for the interglacial warm intervals.

However, even within the theory of astronomical cycles there are at least two schools of thought. Some scientists hypothesize that the variations triggered by the orbital oscillations act directly on the local climate, particularly in the northern hemisphere: a reduction of the summer sunstroke would correspond to an ice increase. Others, on the other hand, think that the increase in ice and its extension have been the consequence of widest changes: in practice, the decrease in solar radiation, although acting mainly at the northern latitudes, would have changed the climate of the whole world.

In 1998, a partial clarification on this matter came from the data extracted from the glacial carrot of Vostok in Antarctica. Between 1992 and 1998, a team of Russian, French and American scientists, analysed data from the Vostok carrot rebuilding the climatic conditions of the last 420 thousand years. The data show that the four interglacial periods would have started 335 thousand, 245 thousand, 135 thousand and 18 thousand years ago, in substantial

harmony with the changes in the terrestrial orbit parameters that seem to cause the beginning and the end of the ice ages.

From the data extracted, there is also a close correlation between the presence in the atmosphere of some greenhouse gases, carbon dioxide and methane above all. The temperatures instead: every time a glacial period ends and the temperatures start to rise again, the carbon dioxide concentration increases a third while the methane almost doubles.

Thomas Chrowder Chamberlin (1843-1928), U.S. geologist, is the first sensing that there is not just one reason that causes climate change. He describes the climate as a dynamic factor. An approach that proceeds parallel with the meteorological research that intensifies between the nineteenth and twentieth century with the aim to obtain reliable weather forecasts.

The consequence is that all the causes suggested in previous decades to explain climate changes, including the Sun, the orbits, the oceans, the atmosphere, the earth's crust, the vegetation and the volcanoes, become part of a unique system: the complex interactions makes the climate formed and transformed (Fig.3). The twentieth century climatology task will be to understand, among many difficulties, the mechanisms and the dimensions of these relationships. Will no longer be “the” cause but factors that trigger reactions whose result makes the climate system more stable or unstable.

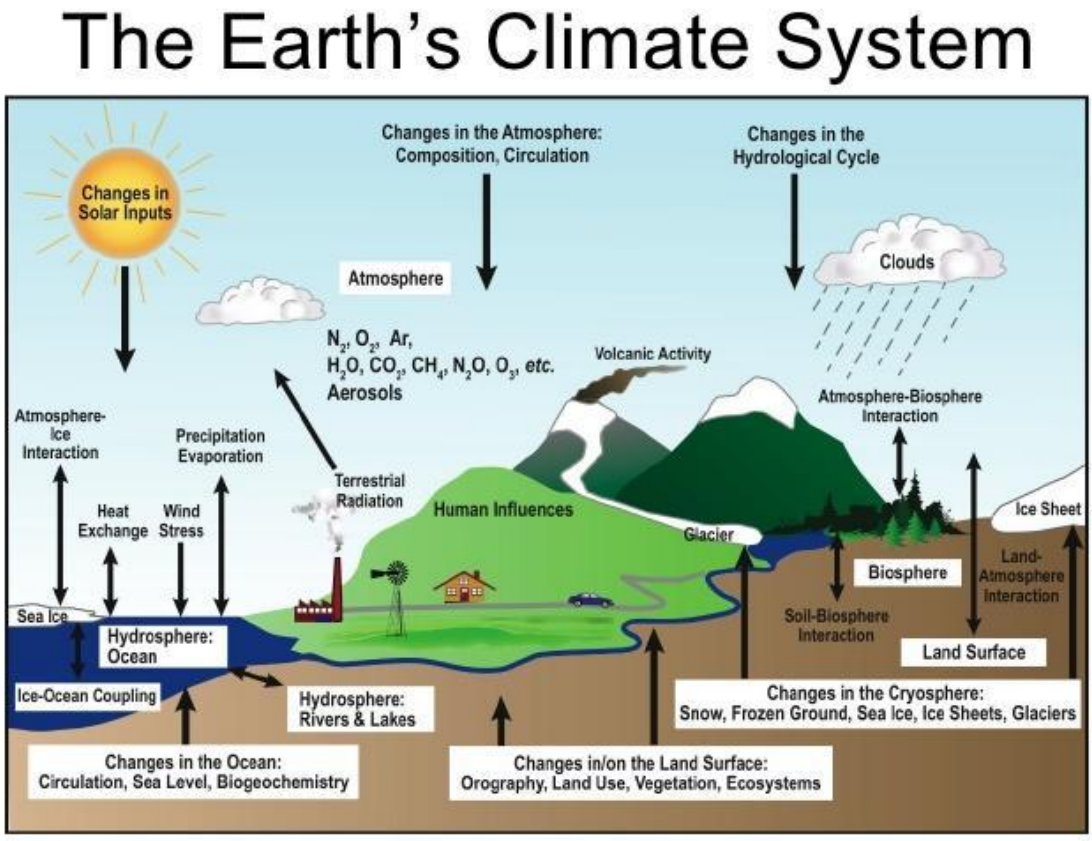

Fig. 3 The earth climate system

1.4 The global warming theory: from Revelle to Callendar, from Plass to Keeling

In 1957, the scientific community proclaims the International Geophysical Year. Among the most debated topics, there are certainly those concerning the space race, which in those years had re-awakened the cold war between the two superpowers of the time, the theory of continental drift and the study of the atmosphere. The interest of scientists in the atmosphere and climatology also had a practical interest. In fact, between the end of the Forties and the beginning of the Fifties, the first signs of a climate change, that is particularly affecting the northern hemisphere, are being felt. In 1948, the Swedish climatologist Hans Ahlmann reports in the Geographical Journal that the average annual temperatures in Iceland have increased by almost a degree and a half between the beginning and the middle of the century and that many glaciers are retreating. Two years later, the English meteorologist Hurd Willet, at the

Royal Meteorological Society in London, confirms the data. Analysing measurements from around the world, the scientist notes that global temperatures have "significantly increased" since 1885 and most of the warming is affecting areas north of the 50th parallel. The question of why the Earth is heating up and the causes of this warming, affects both public opinion and scientists. In this last field, **Roger Revelle** (1909-1991), an American geologist and oceanographer, member of the organizing committee of the geophysical year, publishes together with Hans Suess an article in the magazine Tellus, whose subject is the exchange of carbon dioxide between the atmosphere and ocean. Combining Revelle's marine chemistry research and the knowledge of Suess about the carbon cycle, in the article is analysed the attitude of atmosphere, oceans, biosphere and lithosphere to retain carbon and estimates are made about the reserves of carbon they contain. At the time, it was widely believed among scientists that the CO_2 produced by combustion or deforestation, in addition to that produced naturally, was almost completely absorbed by the oceans. The importance of the work of Revelle and Suess is to have shown that these theories were wrong and that in the atmosphere are concentrated significant amounts of CO_2, such as to amplify the greenhouse effect. Other previous works that indicate carbon dioxide as a potential cause of climate change also support the theory. Of particular interest, in this regard, are the studies of the English engineer Guy Stewart Callendar (1897-1964). Referring to the studies of Arrhenius, he tries to verify if there is a connection between the heating of the Earth and a possible increase of carbon dioxide in the atmosphere. In his first article published in 1938 on the “Quarterly Journal of the Royal Meteorological Society”, Callendar argues that in the last 50 years, the burning of coal and oil produced emissions of about 150 billion tons of carbon dioxide and that three quarters of this CO2 remained the atmosphere. The consequence is that the CO_2 concentration has increased by 6 percent between 1900 and 1936 and, according to Callendar, these emissions are responsible for at least 50 percent of the heating measured by

meteorological stations since 1850. In a later work published in 1939 on the “Meteorological Magazine”, Callendar argues that man has now become an "*agent of global change*", capable of disrupting the normal evolution of the biosphere. Also according to Callendar, humanity is conducting a "*great experiment*" on a planetary scale, an affirmation that will later be taken up by many of the scientists involved in the greenhouse effect and climate change. Thanks to the work of Chamberlin and Callendar, the theory of carbon dioxide as an agent of climate change definitively acquires credibility. To complete the work will be a Canadian physicist, Gilbert **Norman Plass** (1920-2004), who is one of the first researchers to introduce computer simulations in the study of climate. Aided by the enormous technological development that took place in those years, Plass brings together new and detailed spectroscopic measurements in the band of absorption of water vapor, carbon dioxide and ozone, new information on the carbon cycle and industrial emissions using computers, for the first time available. Thanks to his research, the Canadian physicist reaches the same conclusions as Callendar, meaning that the man is conducting a large-scale experiment in the atmosphere, the results of which will not be available before many years. Interest in climate change, in addition to involving scientists, also involves public opinion. However, there are still huge gaps in the knowledge of the climate and its mechanisms, especially due to the lack of monitoring stations for the actual values of CO_2 concentration in the atmosphere. To overcome these shortcomings in the basic monitoring for the study of the climate, the American Weather Bureau decided in 1956 to allocate funds for the construction of an observatory, choosing as location Mauna Loa, the largest island in Hawaii. The task is entrusted to a Californian chemist: Charles D. Keeling (1928-2005). The birth of the observatory marks a real turning point in the study of the earth's climate. The continuous measurements allow the scientist to control step by step the concentration of carbon dioxide in the atmosphere. Already in the early sixties, just 4 years after its birth, the acquired data

allow the scientist to reach an unequivocal conclusion: the presence of CO_2 in the atmosphere increases with a rate of 0.3 percent per year, drawing a diagram from the profile serrated, but always growing, which is given the name of "Keeling curve" (Fig.4). Thanks to the data collected at Mauna Loa and previous estimates, it has been possible to reconstruct the concentration of carbon dioxide in the atmosphere over the last two hundred years: from 290 parts per million (p.p.m.) of the eighteenth century to the current 410, a total growth of 40 percent. The paleoclimatic data obtained from the Antarctic glacial cores confirm the conclusion that before the man had the possibility to alter its composition, the atmosphere contained about 180 p.p.m. of CO_2 at the peak of the glaciations and no more than 280-300 during the following warm periods.

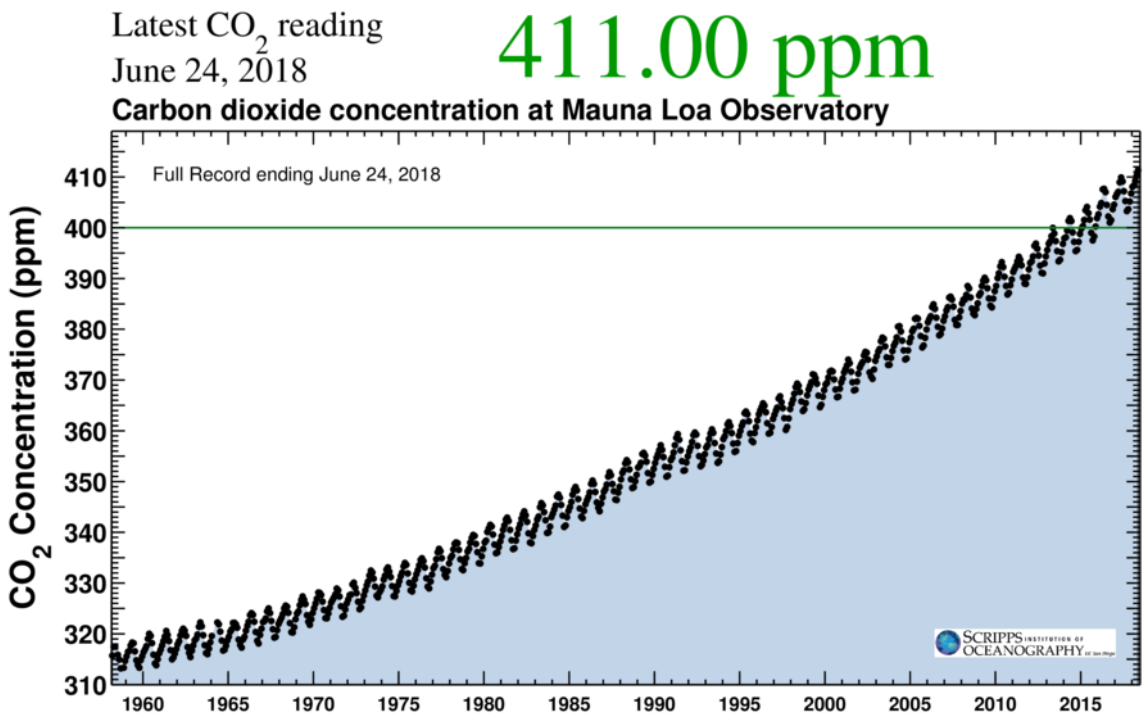

Fig.4 Keeling curve observed from 1958 to June 2018 in the Mauna Loa observatory.
(source: http://scrippsco2.ucsd.edu/data/atmospheric_co2/primary_mlo_co2_record)

2

Climate Change causes

Which and how many natural causes can determine climate change is as of yet not fully understood. Over the years, many theories have attempted to provide an overall explanation of the climate change causes. None of them, however, can alone explain in a complete and exhaustive way all the climatic variations that have occurred in the Earth geological history. One of the reasons that strongly limit the problem resolution is undoubtedly the intricate correlation between the elements involved. The Earth's climate and its variability depend on the interactions between different components, heterogeneous in structure, characteristics and time scales. The climate is a complex system, whose components are in turn complex systems, which have their own internal dynamics and condition each other with multiple interactions. The study of the climate necessarily involves the atmosphere, the hydrosphere, the cryosphere, the biosphere as well as external factors such as the variability of solar activity and earth orbit, volcanic eruptions and the distribution of oceans and emerged lands. If, for example, the global average temperature changes, it affects many other components of the climate system, consequently making the interactions between atmosphere, oceans, cryosphere etc. extremely complex. The following are some of the most scientifically accredited theories and able to explain, at least partially, the origin and evolution of climate changes.

2.1 Astronomical changes

Over the last 500.00 years, the glacial cycles have dominated the climate with periods around 23, 41 and 100 thousand years [3]. Each cycle results linearly correlated with the Earth's orbital parameters that control the quantity and distribution of the incident solar radiation: the precession cycle, the obliquity cycle and the eccentricity cycle [4].

These statistical correlations support the astronomer **Milutin Milankovitch** theory, the first to suggest that the Earth's orbital variations could have influences on the climate. The premise of his idea, publicly presented in 1930 was that the Earth during its orbital motions around the sun had three separate cyclical movements (Fig.5).

According to Milankovitch, the combination of these three distinct motions would have produced a significant variation of the amount of solar radiation arriving on Earth.

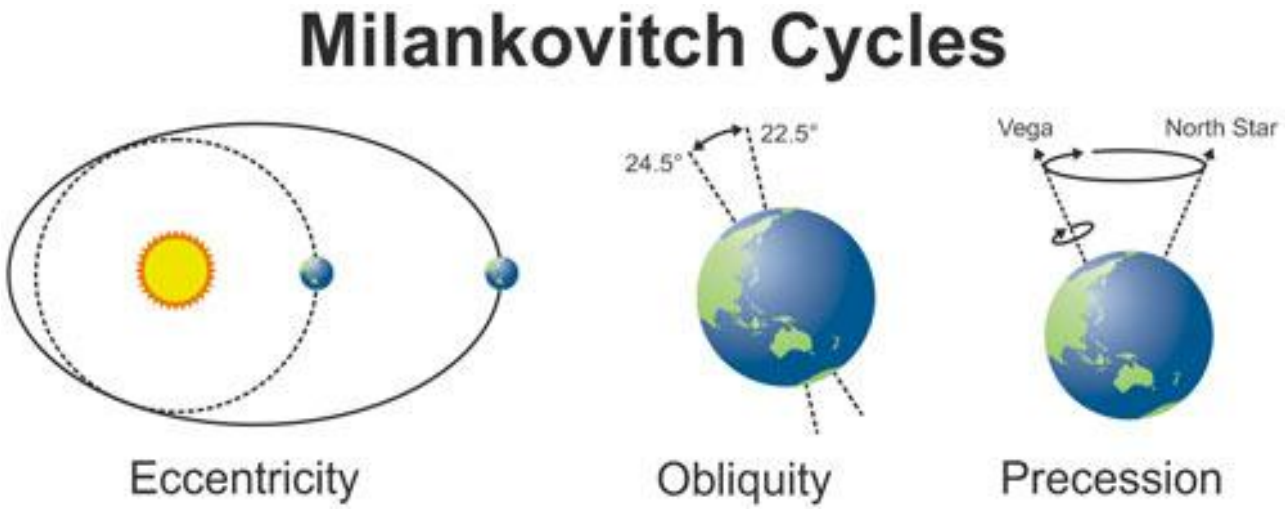

Fig.5 The three main orbital variations of Milankovitch theory: eccentricity, obliquity e precession.

The first of these cycles involves a change in the shape of the terrestrial revolution orbit (eccentricity). It passes from an elliptical to an almost circular shape and completes the period in about 100,000 years. The greater the eccentricity of the orbit is, the greater the variation of solar energy received from Earth between the nearest point (aphelion) and the farthest (perihelion) of the orbit. Currently the earth's orbit shape is of low elliptic, which

results of a small difference in distance from the Sun of about 3 percent. This difference causes a gap of about 7 percent between the energy received at the top of the atmosphere in July and that received in the month of January. During periods of high eccentricity, the different distance from the Sun between summer and winter is about 9 percent, and the gap between the energy received increases of about 20 percent. Furthermore, a more eccentric orbit changes the duration of the seasons in each hemisphere due to the different temporal length between the two equinoxes. The second cycle analysed by Milankovitch takes into consideration the fact that while the Earth rotates around its own axis it oscillates like a spinning top. This oscillation, defined as precession of the earth's axis, occurs with a period of about 23 thousand years. Currently our planet is closer to the Sun in January and further away in July. Because of the precession movement, in about 11 thousand years the situation will be exactly to the opposite. Finally, the third cycle, which takes about 41 thousand years to complete, is that of obliquity. It involves the variation of the terrestrial axis inclination on the plane of the ecliptic that would pass from about 22 ° to 24.5 ° in a cycle. At lower axis inclinations would correspond less seasonal variations between summer and winter at medium and high latitudes: winters tends to be milder and the summers cooler.

During this phase, due to the mildness of the winters more snow could probably accumulate in both polar region due to the increased capacity of the air to contain water vapor. Likewise, during the cooler summers, less snow would melt. Consequently, in periods with the minimum inclination of the terrestrial axis there would be a tendency to form glaciers at high latitudes. Taking into account only the influence of astronomical cycles, current trend should lead to a colder climate in the northern hemisphere.

Ultimately, the cycles of Milankovitch, whose combination is able to modulate the amount of solar energy that reaches the top of the Earth's atmosphere, includes:

– Variations in the shape of the earth's orbit (eccentricity);

– Motions of precession of the Earth rotation axis;

– Changes in the inclination of the Earth's rotation axis.

Several scientific papers published between the years 70 and 80, have highlighted the strong correlation existing between the changes of composition of the deep oceanic sediments, due to changed climatic conditions and the Milankovitch cycles. The same relationship was also found analysing the air bubbles trapped in the Antarctic ice extracted from the glacial carrots coming from the Vostok base, which allowed recreating the CO2 concentrations and temperatures of the last 600 thousand years.

2.2 Variation of energy emitted by the Sun

Recent measurements performed by means of sophisticated radiometers placed on board satellites have changed the opinion, deep in the past, that the energy emitted by the Sun was constant. In fact, through these measurements it has been possible to verify that the energy emitted by the Sun can vary considerably over time. One of the factors that regulates the energy emitted by our star is the number of sunspots on its surface. Sunspots are huge magnetic storms that occur on the solar surface and appear as darker areas. They occur in periodic cycles of 11 years, during which the spots increase in number and extent. During periods when the spots reach their peak, the Sun emits more energy (about 0.1 percent) than during the minimum periods.

Between 1645 and 1715, during the period known as the "Little Ice Age" [5], in which the global average temperatures were lowered by about 0.5 ° C, the "Maunder minimum"[3] also occurred. During this chronological interval the solar spots were very few (Fig.6) if not completely absent. This consideration allowed some scientists to relate the two events, arguing that the cold at that time was in relation to the reduction of sunspots.

[3] This period is named after the British astronomer E.W. Maunder that discovered the period with few solar spots at the end of the 1880.

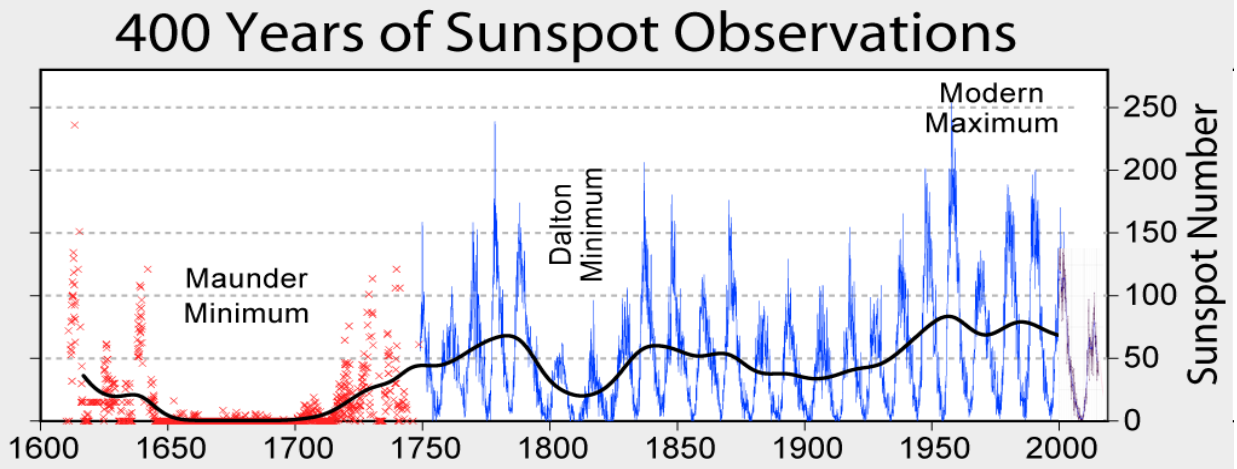

Fig. 6 Solar spots cycle trend from 1600 to nowadays. This figure was prepared by Roert A. Rohde and is part of the Global Warming Art project.

Several scientists have tried to relate the sunspots cycle with some weather anomalies of the same duration: twenty years cycle of drought in the great plains of the United States [6], growth of tree rings in Australia [7] or relationship with some weather characteristics in Europe [8]. Ultimately, the periodic fluctuations of energy emitted by the Sun exert an influence on climate change on time scales ranging from tens to hundreds of years. Despite the rich scientific literature on the subject, no certain evidence has emerged on the relationship between the sunspots cycle and climate change.

2.3 Atmospheric aerosol effects

Among the factors that influence the earth's climate, aerosols are undoubtedly the largest and most difficult class to understand. Composed of solid and liquid microscopic particles, aerosols can have both an anthropogenic and natural origin and are transported around the globe by winds and meteorological phenomena. Diffused in the atmosphere, they can modify the climate either directly, through the scattering and absorption of solar radiation, and indirectly through their impact on some clouds properties. These effects are complex and influenced by a large number of factors.

Among the most significant are the size, shape, colour, chemical composition and quantity. The main types of aerosols include sea salt, powder, sulphur compounds and coal powder resulting from incomplete combustion. Most of these, act by reflecting part of the solar radiation and consequently producing a cooling. Instead, the black coal powder absorbs solar radiation and consequently performs a heating action similar to that of greenhouse gases. Moreover, when it settles on snow-covered surfaces or on ice, it is able to modify the albedo of these surfaces, causing extensive melting. Finally, the aerosols generated by the great volcanic eruptions are able to produce important climatic changes that can be observed and measured on the entire earth surface. Aerosols in the atmosphere are commonly classified as **primary** (direct emissions) or **secondary** (products), and **natural** (resulting from natural processes) or **anthropogenic** (resulting from industrial products or human activities).

2.3.1 Volcanic aerosol

Volcanoes are natural and unpredictable sources of atmospheric aerosols. Their effects on the climate are potentially very large even if temporally limited. On 15 June 1991, the eruption of the Pinatubo volcano in the Philippines occurred. Billions of tons of magmatic particles were released into the atmosphere accompanied by more than 20 million tons of sulphates. The column of powders and volcanic ash reached 20 kilometres in height, reaching the stratosphere and in the following months, distributed to the entire planet (Fig.7).

Following the eruption, global average temperatures dropped by about 0.5 °C and remained low for about two years. The Pinatubo eruption and its influence on global temperatures is an important and dramatic example of the impact that these tiny particles suspended in the atmosphere can have on the Earth's climate.

Furthermore, this eruption marked a turning point in the scientific study of aerosols, including them as important and complex factors of climate change. From a scientific point of

view, there is substantial agreement among researchers that volcanic eruptions that have a greater impact on the climate are those whose gases have a high concentration of sulphides. These gases, for several months are able to combine with water vapor to produce small particles of sulphuric acid able to reflect solar radiation.

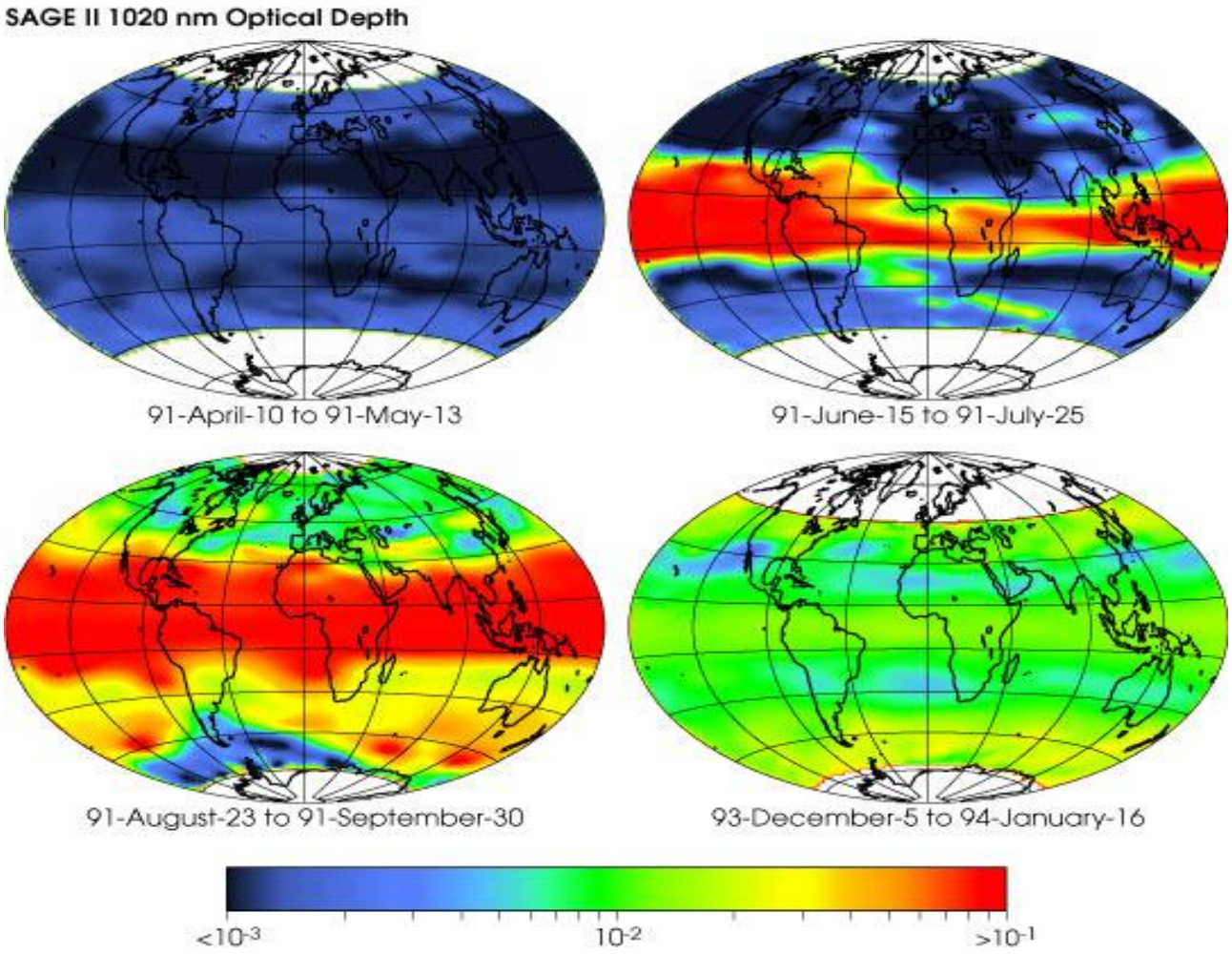

Figure 7. Stratospheric optical depth at wavelength 1,020 nm for four periods just preceding and following the eruption of Mount Pinatubo. The images above were acquired by the Stratospheric Aerosol and Gas Experiment II (SAGE II) flying aboard NASA's Earth Radiation Budget Satellite (ERBS). The false-color images represent aerosol optical depth in the stratosphere during four different time spans, ranging from before the June 1991 Pinatubo eruption to two years after the event. Red pixels show the highest values, while dark blue shows the lowest values, which are normally observed in the stratosphere. Notice how the volcanic plume gradually spreads across virtually the entire globe, hence the global-scale impact on climate. (NASA Langley Research Center Aerosol Research Branch

These sulphuric aerosols may remain in the stratosphere for up to a few years, absorbing and reflecting toward the space a portion of the solar radiation. This effect can cause a warming of

the stratosphere and a cooling of the underlying troposphere with a consequent decrease in surface temperatures, especially in the hemisphere where the eruption has occurred.

2.3.2 Anthropogenic aerosol

The action of anthropogenic aerosols on climate is twofold: some of them are in fact able to reflect solar radiation, in particular powders and sulphates, while others, like coal powder, absorb heat and release it into the atmosphere. The production of these aerosols and their accumulation in the lower troposphere takes place in various ways. Among the best known, the production of emissions from factories and automobiles, some agricultural practices, forest fires and sandstorms. Some aerosols are able to selectively absorb and emit infrared radiation toward the earth's surface, helping to determine the surface nighttime warming.

Other aerosols are able to reduce the amount of solar radiation that reaches the surface, partly reflecting this radiation and causing a cooling action of the surface during the daylight hours. The overall action of anthropogenic aerosols on the climate produces a cooling of the surface. Among the anthropogenic aerosols, a primary role on the climate is due to the sulphates action. This category of aerosol is the result of the sulphides combustion that are contained in new generation of fuels. The concentration levels of sulphide-based pollutants have more than doubled globally compared to pre-industrial values. They are composed mainly of SO_2 emissions that in the atmosphere modifies into tiny droplets that remain in the atmosphere for a short time that is of few days. These aerosols not only reflect solar radiation, but also behave as “condensation nuclei” for cloud formation. As a result, they are potentially able to alter the clouds physical characteristics. This alteration concerns the sharing of humidity contained inside the clouds among many more condensation nuclei, with consequent production of a larger number of smaller water droplets. The increase in the number of water droplets contained in the clouds determines a greater brightness of the

clouds, with the consequent effect of reflecting solar radiation more effectively. Ultimately, the action of anthropogenic aerosols (more specifically the sulphur derivatives) is carried out in two different ways: on the one hand, in the lower troposphere they are able to reflect part of the incident solar radiation carrying out a surface diurnal cooling action; on the other hand, by modifying the brilliance of the clouds they increase the reflective action in the upper part of the troposphere.

2.4 Greenhouse Effect and Feedback Mechanisms

On first chapter, Figure 3 shows the Earth's climate system as hypothesized by **Chamberlain**. This system is the result of the equilibrium between the incoming energy, coming from the Sun and the energy reflected from the Earth towards the Space (Fig.8).

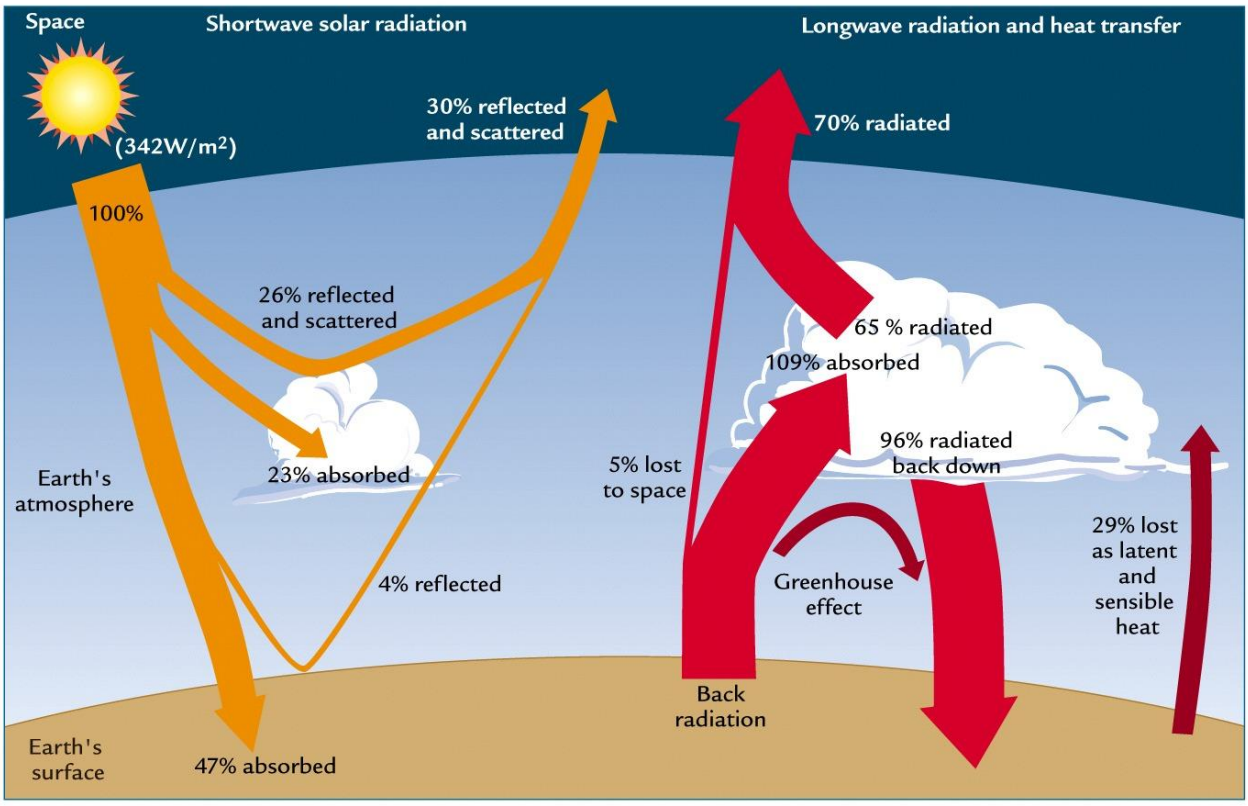

Fig.8 Earth energetic balance

The greenhouse effect is a natural phenomenon that allows life on Earth, as it determines an average temperature of about 15°C. Without greenhouse effect, our planet would have an average temperature of -18°C, which is the equilibrium value in absence of atmosphere. From a physical point of view, the greenhouse effect is based on the fact that the Earth's atmosphere is transparent to a part of the solar radiation, which then reaches the surface and is absorbed, while another part of about 30% of the total radiation is reflected. The phenomenon that regulates the reflection of solar radiation is defined albedo and has a value between zero and one. The part of energy coming from the Sun that is absorbed produces a warming of the Earth that, cooling down, emits heat in the form of infrared radiation (IR) that has a wavelength greater than the incoming one. A part of the IR radiation crosses the atmosphere and is dispersed in space, while some gases that compose it, among which there are water vapor, carbon dioxide (CO_2), methane (CH_4), the nitrogen protoxide (N_2O), ozone (O_3) and chlorofluorocarbons (CFC), hold another part. An increase in the concentrations of these atmosphere constituents would therefore be able to let increase the temperature of the planet. The findings made on the solar system planets confirm this statement. In particular, Venus has an average surface temperature of 480°C, a temperature due to the greenhouse effect of its atmosphere composed of about 95% of carbon dioxide. The second half of the nineteenth century hosts the first scientific surveys on the greenhouse effect. However, it was 1957 when was built in Mauna Loa, Hawaii a permanent meteorological observatory equipped with instruments for measuring the air CO_2 concentrations. Since 1979, CO2 concentration measurements is carried out in Italy by the Monte Cimone Air Force Observatory, located on the Tosco-Emilian Apennines at an altitude of 2167 meters, which constitute the longest data series at European level (Fig. 9).

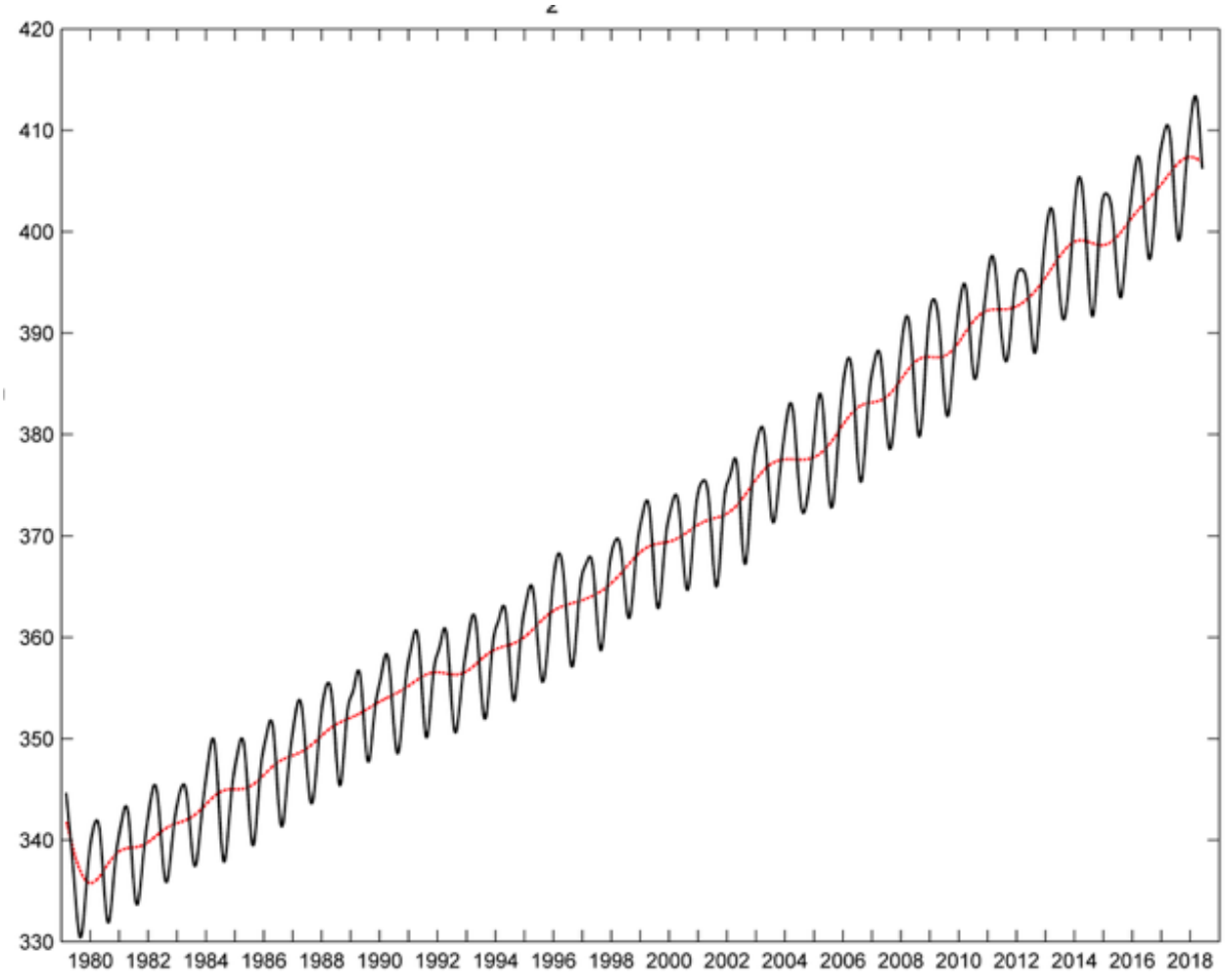

Fig.9 CO_2 concentration in atmosphere. Historical series observed at the Monte Cimone Italian Air Force observatory.

From the end of the nineteenth century up to nowadays, the increment has reached 50 percent, having grown from 270 ppm in 1850 to 410 ppm in 2018. It is difficult to define precisely how much the increase of the concentrations of these gases linked to human activities has contributed to the Earth global warming. Despite these uncertainties, in the various reports published by the Intergovernmental Panel on Climate Change (IPCC), it is clear that emissions resulting from human activities contribute to the on-going climate change. To make further complicate the reference framework occurs some mechanisms called "Feedback".

For example, if we consider the warming trend of the Earth, one of its consequences is greater oceans evaporation. The increase of vapor in the atmosphere absorbs more heat (IR) emitted by Earth, further strengthening the greenhouse effect. This would support a further temperatures increase that in turn would generate further evaporation. This situation, known as vapor-temperature feedback, represents a positive feedback mechanism whereby an initial temperature rise would follow a chain reaction that would accelerate the process. Negative feedback mechanisms act in the opposite direction. As example, a warmer and more humid Earth would see a significant increase of the low clouds percentage. The latter tends to reflect a higher percentage of incident solar radiation, facilitating the increase of albedo. The result of this feedback mechanism is that the initial temperatures increase would rapidly counterbalanced by the increase in the Earth's albedo. As we have seen, many positive and negative feedback mechanisms exist in the climate system. Detecting, understanding and accurately quantifying climate feedback have been the focus of a research project. Detecting, understanding and accurately quantifying climate feedbacks have been the focus of a great deal of research by scientists unravelling the complexities of Earth’s climate.

3

Globally Observed Climate Change: temperature and precipitation

The evidence of global climate change is based on the analysis of the long-term variability that affects the different components of the climate system (atmosphere, oceans, cryosphere, etc.). The long datasets are based on paleoclimatic archives and observations collected in situ or by remote sensing, often integrated through numerical models and reconstructions. The available observations of the atmosphere, the oceans and the earth's surface indicate unequivocally that since the nineteenth century the Earth has undergone a global warming [9]. Land and Ocean temperatures have increased in recent decades, not homogeneously, but with a greater warming near polar latitudes, especially in the Arctic. The ice and snow coverage has decreased in different areas of the planet. The atmospheric water vapor content has increased everywhere due to the higher temperature of the atmosphere. Sea level has also increased. Changes in other climatic indicators have also been observed, such as seasonal elongation in many places on the planet, often accompanied by an increase in the tendency of extreme events such as heat waves or heavy rainfall and a general decrease in extreme cold events. [10]. If we consider the only natural forcings, they are not able to justify these climate changes [11]. Most of the warming observed globally over the last 50 years can only be explained if one considers the effect produced by human activities [12] [13] and in particular emissions from fossil fuels and deforestation.

3.1 Global temperature changes

Shortly after the invention of the thermometer in the early 1600s, efforts began to quantify and record the weather. The first meteorological network was formed in northern Italy in 1653 [14] and reports of temperature observations were published in the earliest scientific journals. By the latter part of the 19th century, systematic observations of the weather were being made in almost all inhabited areas of the world. Formal international coordination of meteorological observations from ships commenced in 1853 [15]. Inspired by the paper Suggestions on a Uniform System of Meteorological Observations (Buys-Ballot, 1872), the International Meteorological Organization (IMO) was formed in 1873. Its successor, the World Meteorological Organization (WMO), still works to promote and exchange standardised meteorological observations. Based on the data coming from WMO and published on the book "WMO Statement on the State of the Global Climate 2017" [16], the year 2017 was one of the world's three warmest years on record. A combination of five datasets, three of them using conventional surface observations and two of them reanalyses[4], shows that global mean temperatures were 0.46 °C ± 0.1 °C above the 1981–2010 average[5], and about 1.1 °C ± 0.1 °C above pre-industrial levels. By this measure, 2017 was the world's second and 2015 the third warmest years on record, ranking only behind 2016, which was 0.56 °C above the 1981–2010 average. The years 2015, 2016 and 2017 were clearly warmer than any year prior to 2015, with all pre-2015 years being at least 0.15 °C cooler than 2015, 2016 or 2017 (Fig.10)

[4] The conventional datasets used are those produced by the US National Oceanic and Atmospheric Administration (NOAA); the US National Aeronautics and Space Administration (NASA); and the Met Office, Hadley Centre/Climatic Research Unit (CRU), University of East Anglia (United Kingdom). The two reanalysis datasets used are the ERA-Interim dataset, produced by the European Centre for Medium-Range Weather Forecasts (ECMWF), and the JRA-55 dataset, produced by the Japan Meteorological Agency (JMA).

[5] For purposes other than comparison of temperatures with pre-industrial levels, this report uses 1981–2010 as a standard baseline period, as this is the period for which the widest range of datasets (especially satellite-based datasets) is available.

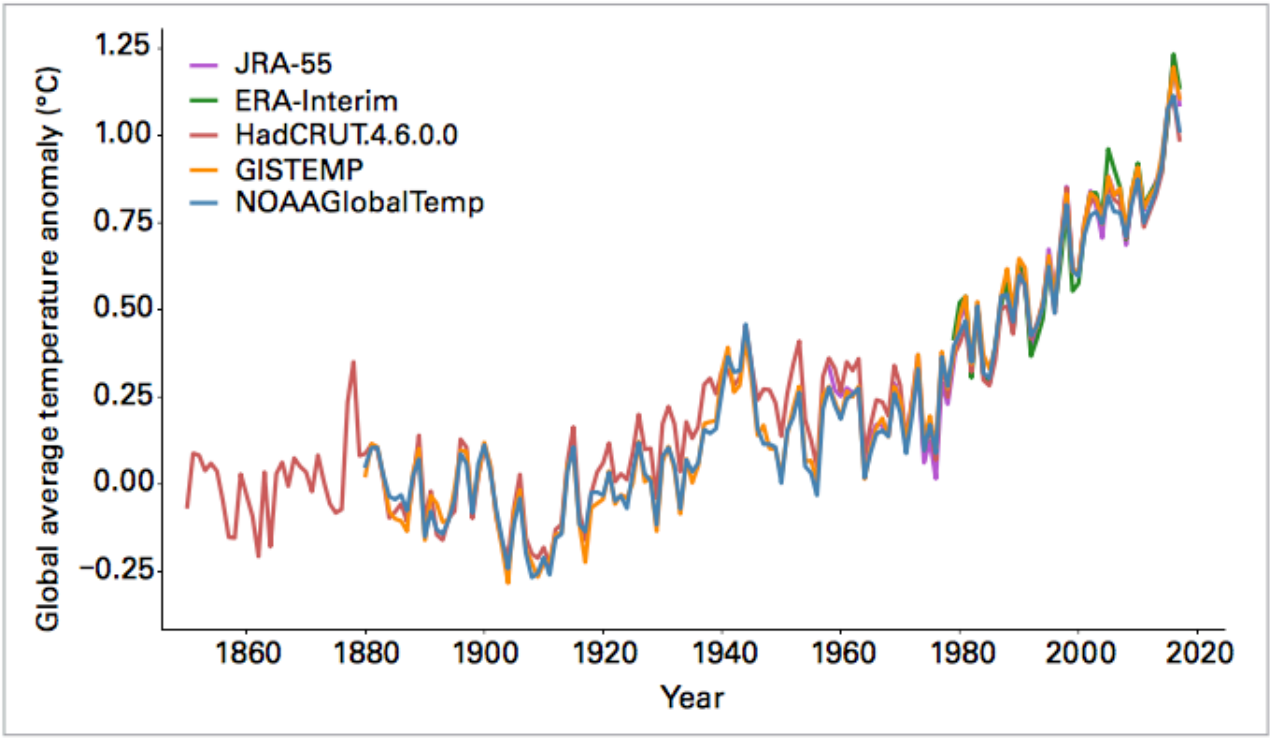

Fig. 10 Global mean temperature anomalies, with respect to the 1850–1900 baseline, for the five global datasets *(Source: UK Met Office Hadley Centre)*

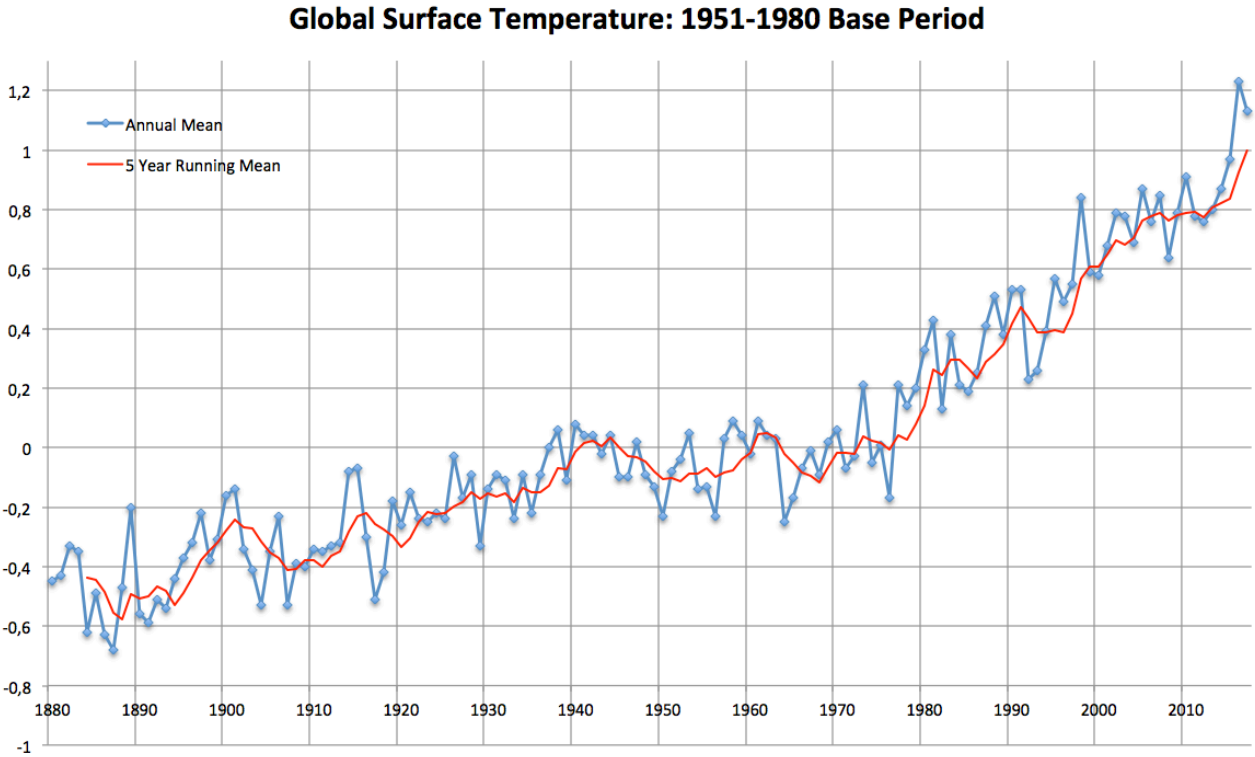

Fig.11 Global surface temperature anomaly 1880-2017 (Data: NASA Goddard Institute for Space Studies. Dataset accessed 2018-06-14 at https://data.giss.nasa.gov/gistemp/)

The series of global temperatures analysed over the period 1880-2017 (Fig.11) shows a heating trend interrupted only for short periods. In particular, the decade between 1900 and 1910 and that between 1942 and 1950 represent the only time intervals in which global temperatures have undergone a trend reversal. Moreover, starting from 1970 the slope of the regression line is undergoing a substantial increase, which brings the heating values between 1970 and 2017 to about 0.17 ° C / decade. The spatial distribution of annual mean surface temperature of 2015-2016 and 2017 shows how the polar latitude, specially the Artic area, results to be the place of Planet with the maximum warming trend. Moreover, huge portions of the northern hemisphere, show temperature anomalies relative to 1951-1980 mean bigger than +2°C (Fig.12).

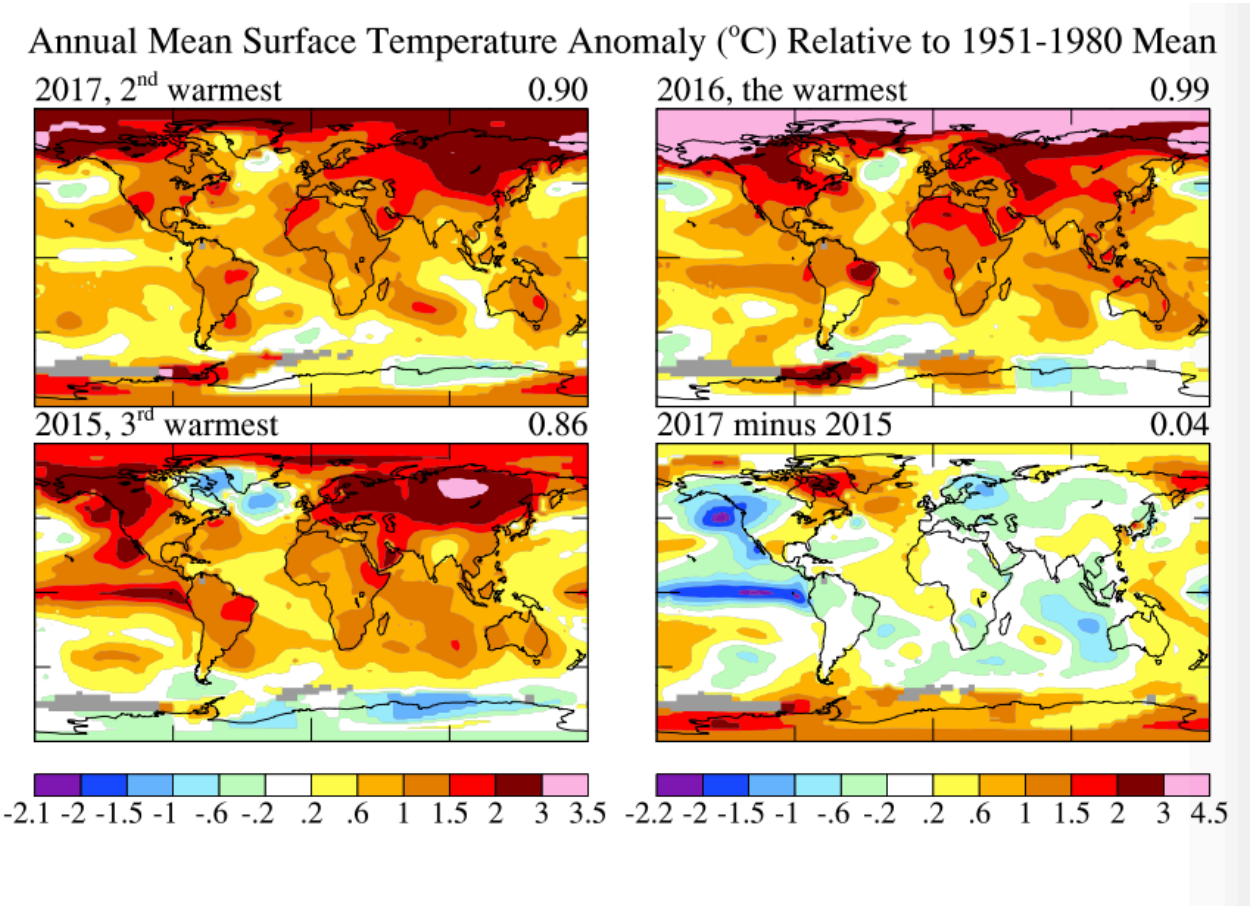

Fig 12. Spatial distribution of annual mean surface temperature of 2015-2016 and 2017 relative to 1951-1980 mean (source: Columbia University Earth Institute).

3.2 Global precipitation changes

Precipitation has been measured on the Planet at various locations for centuries, beginning with simple and then more complex surface gauges. As the record at individual locations and over regions lengthened, long-term means were calculated and seasonal and inter-annual variations at those locations were examined. Over many land areas, especially populated areas, these became very valuable to understand the climatology of precipitation across the globe (Fig.13).

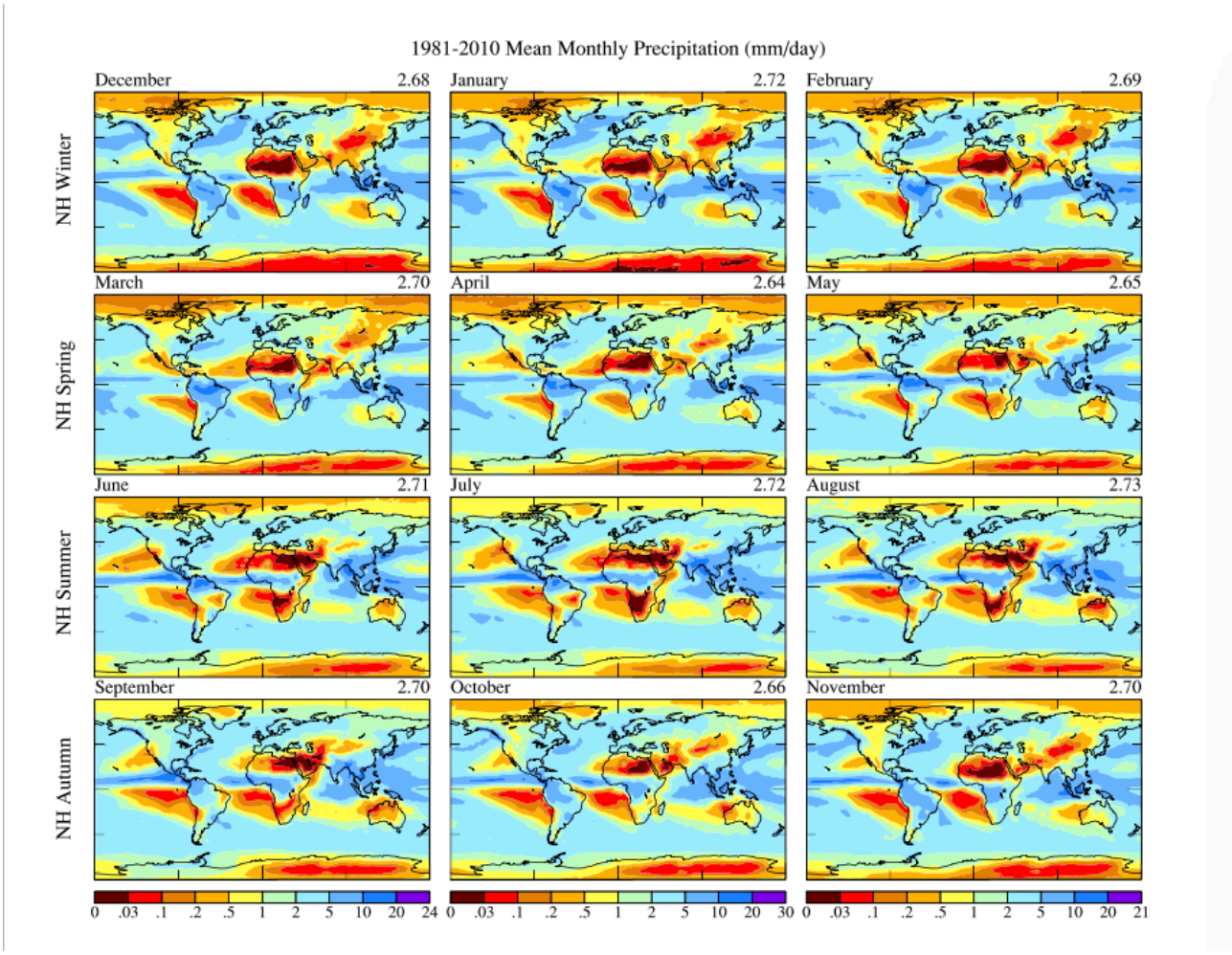

Fig.13 Global precipitation climatology 1981-2010 based on GPCP Version 2.3 Combined Precipitation Data Set

The increased atmospheric moisture content associated with global warming might be expected to lead to increased global mean precipitation. Global annual land mean precipitation showed a small, but uncertain, upward trend over the 20th century of

approximately 1.1 mm per decade. Trends in global annual land precipitation were analysed using data from different database. In Figure 14 the Global Annual Land Precipitation Anomalies are shown, using the Global Historical Climatology Network (GHCN) data of anomalies with respect to the 1981 to 2000 base period. The observed GHCN linear trend over the 106-year period from 1900 to 2005 is not statistically significant. However, the global mean land changes are not at all linear, with an overall increase until the 1950s, a decline until the early 1990s and then a recovery.

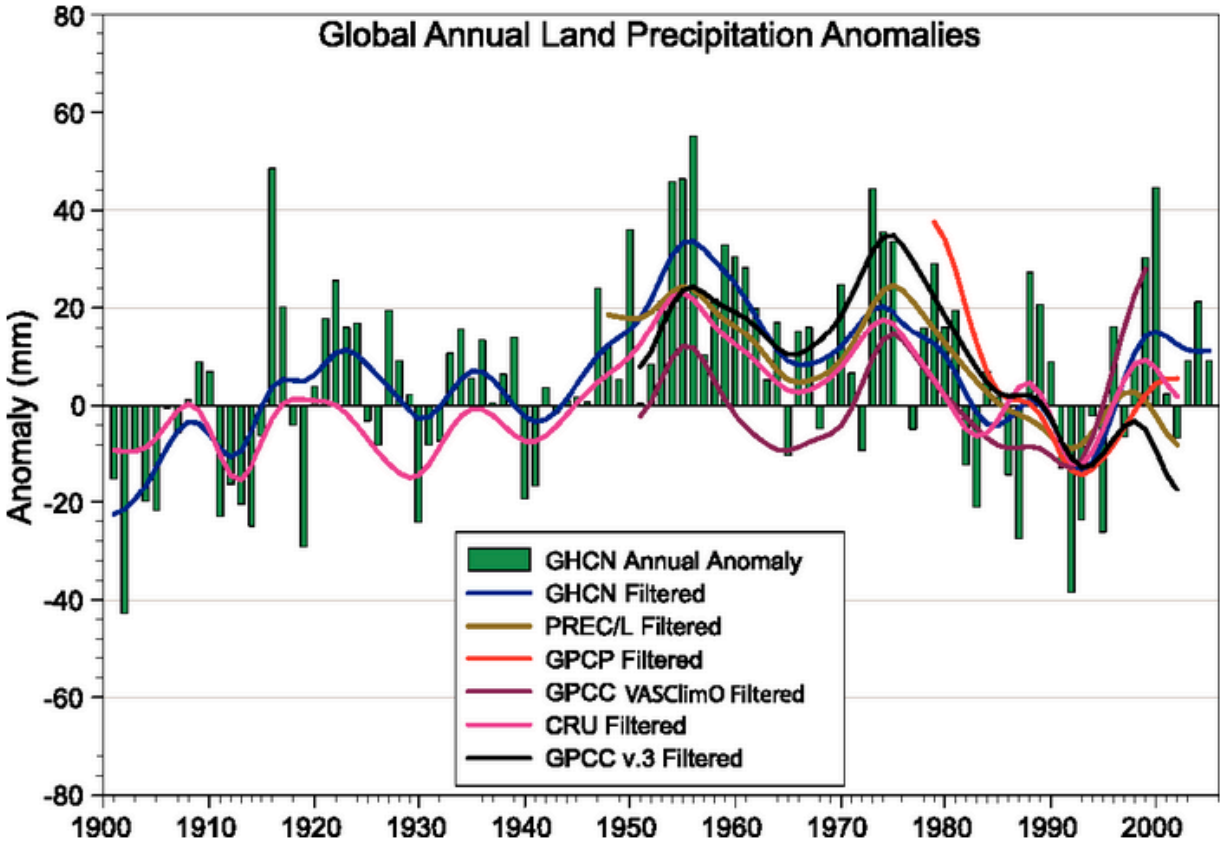

Fig.14 *Time series for 1900 to 2005 of annual global land precipitation anomalies (mm) from GHCN with respect to the 1981 to 2000 base period. The smooth curves show decadal variations for the GHCN[17], PREC/L [18], GPCP [19], GPCC [20] and CRU [21] data sets.*

4

Climate Change in the Mediterranean Area

The climate of the Mediterranean region—its past evolution, present variability, trends, and changes projected for the next decades—has been the object of many research studies and has attracted the interest of a large group of scientists. Such focus of international climate research on a relatively small region can be explained by three fundamental facts—its specific phenomenology, the well-developed cultural background of most Mediterranean countries, and the important social–economical–environmental impacts of climate variability and change [22]. The last report from the International Panel on Climate Change (IPPC, 2013) highlights the Mediterranean as one of the most vulnerable regions in the world to the impacts of global warming. The area that overlooks the Mediterranean basin takes the name of Mediterranean Region and is, from the climatic point of view, strongly characterized by the presence of a semi-enclosed deep sea. The complex morphology of the region and its geographical location halfway between the sub-tropical zone to the south and the temperate zone to the north, produce strong contrasts between the different areas of the region. According to the classical definition of Koppen [22a], the Mediterranean climate is defined as a moderate climate of mid-latitudes with a dry summer, which can be hot or very hot (in the Koppen classification the two types are classified as Csa and Csb respectively). These two climatic types, however, are representative of only a small portion of the territory, since the contrasts between the northern and southern areas are very accentuated (Figure 15). In fact,

there are permanent glaciers in the Alpine humid region north of the Mediterranean, as well as hot and dry desert areas along the southern African coast. Furthermore, a large portion of the territory to the north is characterized by a humid continental climate (Cfa and Cfb).

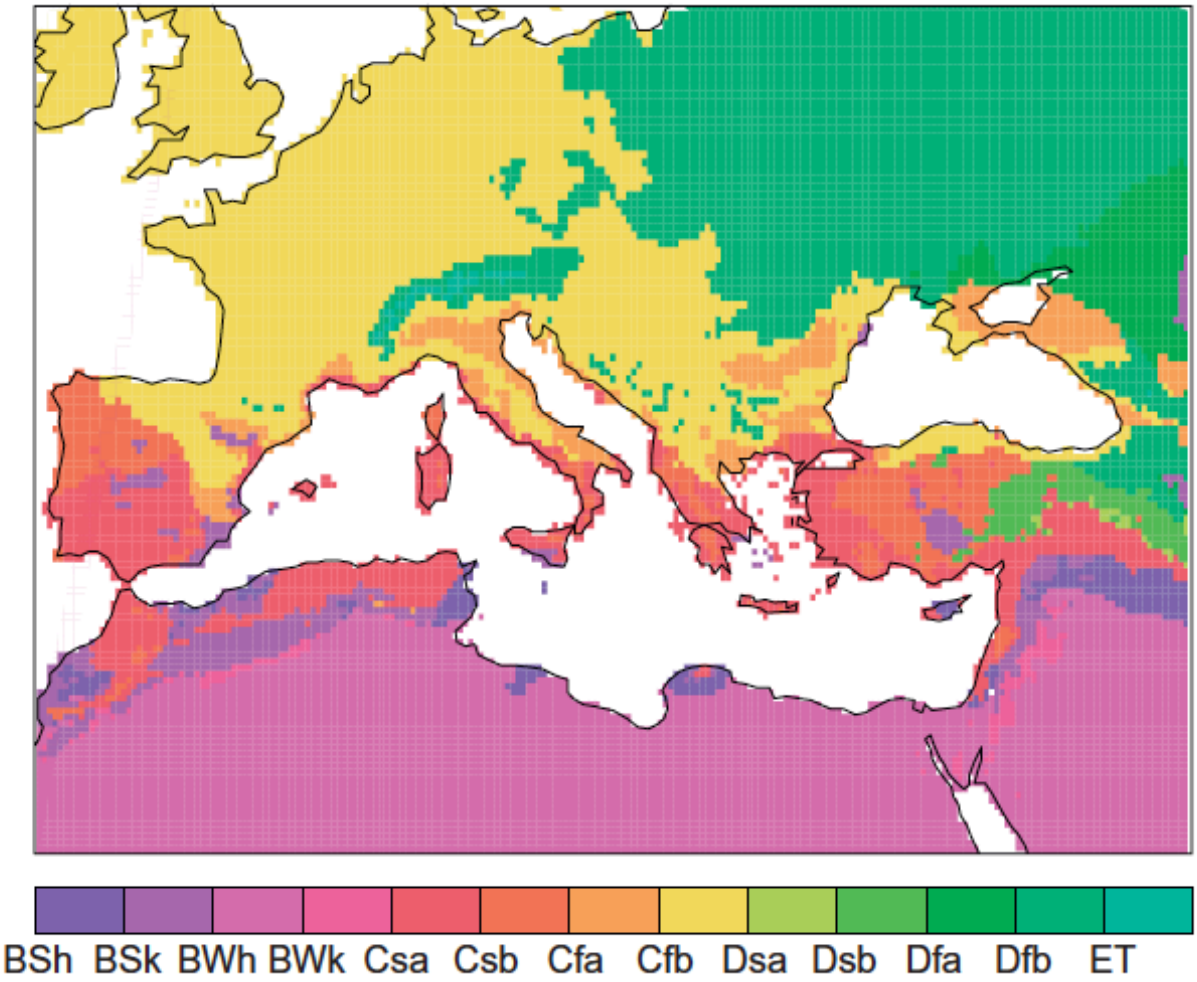

Fig. 15 Köppen climate types in the Mediterranean region: subtropical steppe (BSh), midlatitude steppe (BSk), subtropical desert (BWh), midlatitude desert (BWk), Mediterranean climate with hot/warm summer (Csa/b), humid subtropical with no dry season (Cfa), maritime temperate (Cfb), humid continental with hot/warm summer (Dfa/b), continental with dry hot/warm summer (Dsa/b), and tundra (ET). This figure is based on Climatic Research Unit (CRU) temperature and precipitation gridded data[23]

Its geographical location in a transition zone between the subtropical and mid-latitude regimes influences another important factor: spatial and temporal climatic variability. Although it can not be considered a rigorous distinction, there is still a difference between the south-east and north-western areas of the basin. The northern Mediterranean area is strongly linked to the variability of the mid-latitudes, characterized by the North-Atlantic oscillation

(NAO) [24] [25] [26]. The southern part of the basin is under the influence of the descending branch of Hadley's cell for most of the year and is exposed to the Asian monsoon in the summer. The effects of El Nino Southern Oscillation (ENSO) have been found to vary over time, especially on precipitation [27] [28].

4.1 The climate in Historical Times

A particularity of the Mediterranean region is the strong anthropic action on the environment exercised since the onset of the earlier civilizations in this region. Humans have strongly influenced and modified the Mediterranean environment to such an extent that their impact may obscure the climatic signal, mainly regarding vegetation, forest, and fire regimes. Land use, for instance, is a significant parameter for modifying regional climate in the Mediterranean, and it is an extremely important indicator of changing environments and landscapes [29][30][31]. The climate over the Mediterranean during the past 2000 years has experienced a sequence of humid/dry and warm/cold periods that have produced effects on environmental conditions [32][33]. Two main periods identified in the recent climate evolution are the Medieval Climate Anomaly (MCA) and the Little Ice Age (LIA) [34][35](Fig.16). The LIA is conventionally defined as a cold period extending from the sixteenth (initial date is controversial) to the nineteenth centuries, which in Europe was characterized as a period of glacier expansion in alpine regions—recorded not only in glacial features dated by geologic techniques but also in historical documents, such as field sketches, land values, and weather records. The MCA denotes a period from the tenth to the fourteenth century when evidence suggests that Europe, Greenland, and Asia experienced relative warmth. However, characterizations of the LIA and MCA are not uniform across the Mediterranean area.

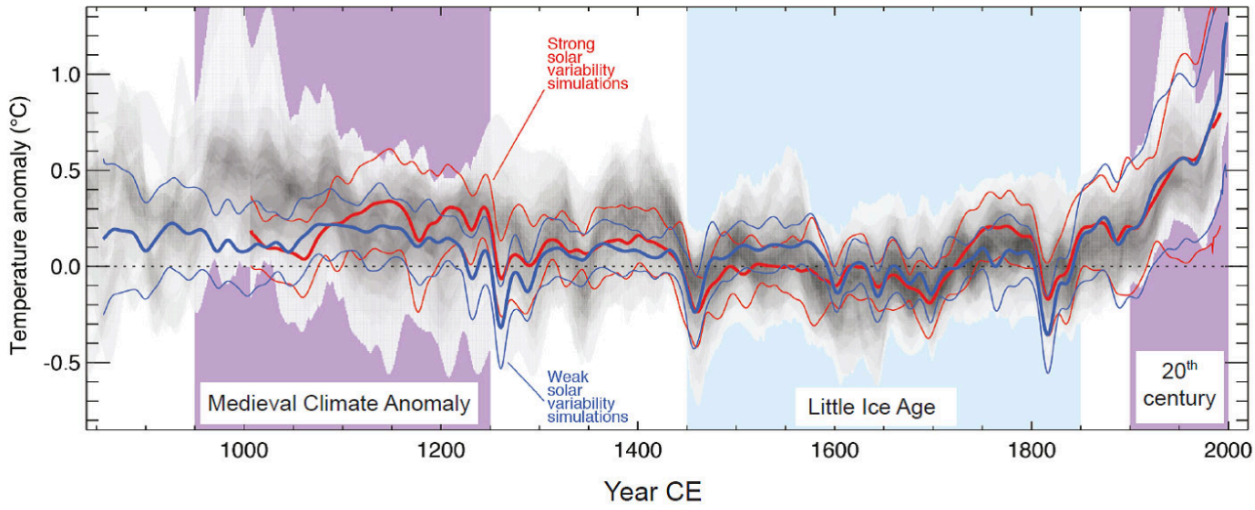

Fig. 16 Comparisons of simulated and reconstructed Mediterranean temperature changes. Simulations are shown by coloured lines, thick lines showing the mean of multiple model simulations and thin lines showing the 90% confidence range of this mean. Red lines show models forced by stronger solar variability and blue lines show models forced by weaker solar variability. Reconstructed temperatures are shown by grey shading. All data are expressed as anomalies from their 1500–1850 mean and smoothed with a 30-year filter. (Source: Intergovernmental Panel on Climate Change Fifth Assessment Report).

For precipitation, the large variability at many timescales prevents drawing any conclusion; however, data available at present from a limited number of proxies provide no evidence in the past of a fast temperature increase in the Mediterranean such as that observed in the last decades of the twentieth century.

4.2 Analysis of present climate

The knowledge of present climate conditions could represent a problem because information is often too sparse and irregular in time. In the Mediterranean region, meteorological stations with long reliable time series are not uniformly distributed, and there is a strong contrast among different areas on the density of data and periods covered. The northwestern areas have the best coverage of records available in public archives while the northern Africa has only few sufficiently long time series. In order to be used for regional-scale climate analysis, observed data need to be transferred to regular grids and statistical methods used to compensate for the variable density of the meteorological stations and for periods with no

data in the single time series. The results are gridded data sets that are, on the basis of the available information, optimally homogeneous in the quality of the time and space coverage.

In Figure 16 are shown the seasonal values of average temperature and accumulated precipitation of the CRU data sets at 0.5° resolution [36]. The panels represent the average values for the period 1961–1990. The effects of orography and complicated land–sea patterns, alter the background temperature gradient along the meridians. The main mountain ridges determine a cool signature in all seasons. With this exception, summer is warm or hot in the whole region. In general, July is the warmest month, with average maximum temperatures above 35°C in many locations. The spatial distribution of precipitation decreases from wet areas in the northwest to arid and semi-arid areas in the southeast. Mountain ridges are evidently associated with local precipitation maxima connected with orographic precipitation. The dominant westward atmospheric circulation, which transports the moisture from the Atlantic and the Mediterranean Sea itself toward the coasts, is responsible for the maxima especially along the western coasts of peninsulas and main islands. Note that summer is generally drier than the rest of the year over most of the Mediterranean region. A notable exception is the Alpine region, where precipitation actually has a maximum in summer. Figure 17 shows the present rate of change of the temperature (°C per decade) and precipitation (mm per decade), versus the seasonal climatology that is shown in Figure 18. It is based on CRU data and refers to the period 1951–2005. Only areas where trends are significant at the 90% confidence level are plotted. All statistically significant temperature trends are positive. Trends are particularly large in summer over the whole western Mediterranean and in spring in its central part. The situation is less unequivocal for precipitation, whose intrinsic and high interannual variability prevents the identification of significant trends over large areas. The main observed feature for precipitation is its winter decrease over small areas in the Balkan and Italian peninsulas, in the southern Anatolian coast, and in a part of northwest Africa.

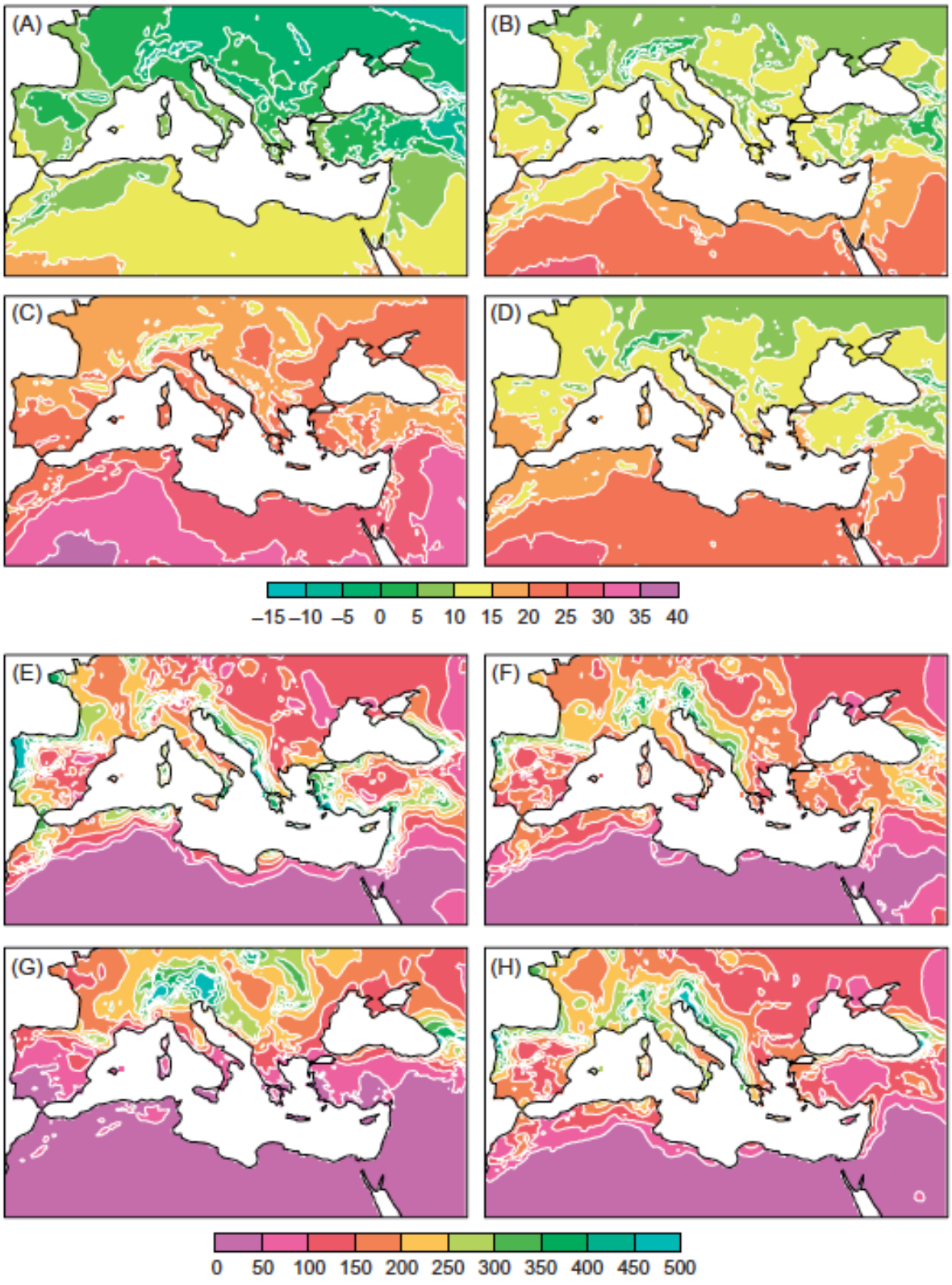

Fig.17 Seasonal (winter: December–January–February; spring: March–April–May; summer: June–July–August; autumn: September–October–November) mean temperature (°C, panels A–D) and total precipitation (mm per season, panels E–H) maps for the period 1961–1990 based on CRU data.

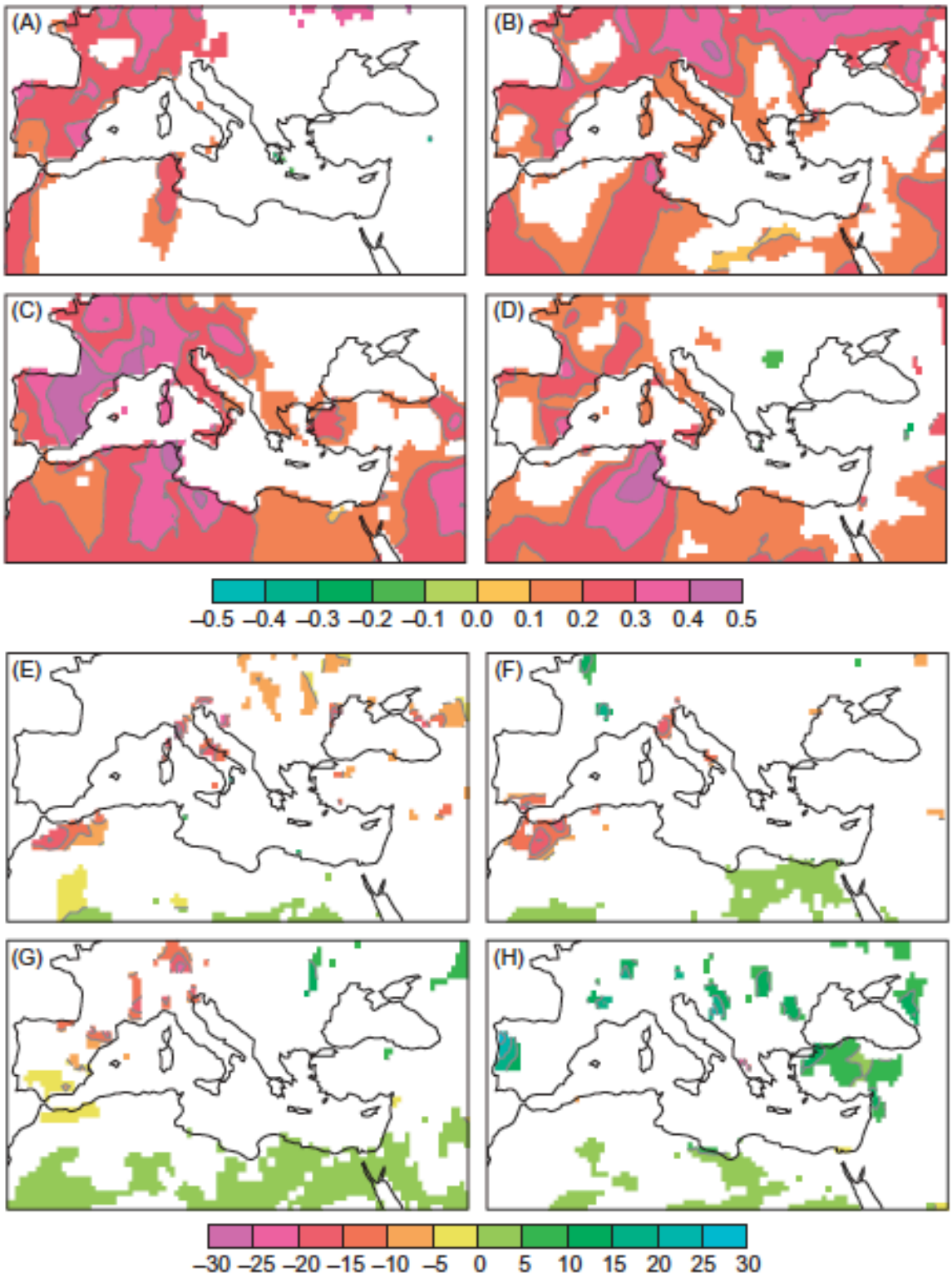

Fig.18 Trends of the seasonal (winter: December–January–February; spring: March–April–May; summer: June–July–August; autumn: September–October–November) mean temperature (°C per decade, panels A–D) and total precipitation (mm per decade, panels E–H) for the period 1951–2005 based on CRU data. Only significant trends at the 90% level are plotted.

4.3 Future climate of Mediterranean area

Future climate change over the Mediterranean is investigated by means of climate model simulations covering the XXI century. These simulations follow different emission scenarios of gases that are connected to human activities and are known to have an influence on climate through the greenhouse radiative effect (CO_2, CH_4, N_2O, and other trace gases). Moreover, the scenarios take into account the emission of aerosols that influence the climate through reflection and absorption of solar radiation and by changing cloud radiative properties (see Chapter 2). Emission scenarios are images of possible future developments, but they are not predictions, since they are based on many aspects of social systems that are unpredictable at a multi-decadal timescale (e.g., population growth, socioeconomic development, and technological progress). The climate-change simulations are first performed with general circulation models (GCMs), coupling the atmosphere, land areas, and the ocean at the global scale (also designated as AOGCMs). These models may include other components of the climate system (e.g., sea-ice and continental hydrology) and some biogeochemical processes (e.g., stratospheric ozone and carbon cycle). Starting from initial conditions for the atmosphere and the ocean that are representative of the present climate, each model is integrated to calculate climate evolution until the end of twenty-first century. For the analysis of regional climate change, the AOGCM simulations may be downscaled dynamically by means of limited area regional climate models (RCMs) and varying resolution atmospheric general circulation models (AGCMs) or statistically using appropriate techniques. Over the Mediterranean domain, RCMs may be only atmospheric models (ARCMs) or atmospheric models coupled with a high resolution Mediterranean Sea model (AORCMs).

4.3.1 Projection of Global Climate Model

The global models issued by IPCC cast different scenarios for the Region, but all of them agreed on a clear trend in the pattern of some climatic parameters. In particular, with regard to air temperatures, most climate models suggest that during the 21st century, the Mediterranean area will experience a period of warming. The average temperature increase is expected to be + 3.2 ° C, which is higher than the global average (2.6 ° C). The warming is expected to be greater in summer than in winter. It is also expected that the highest average temperatures will occur in summer in the Iberian Peninsula, the Balkans and Anatolia, where the temperature increase is likely to reach +5 °C by the end of this century. As a consequence, the number of heat wave episodes should triple by 2025, with three warm events expected every four years, against a hot event every four years.

Regarding rainfall (rain and snow), it is expected that they will decrease by 25% in summer (according to scenario A1B1) and by 10% in winter by 2100. The biggest decreasing in summer rainfall (over 60%) of this century could occur in the same areas as those affected by the most significant warming (Iberian Peninsula, Anatolia, Balkan Peninsula). In winter, the most important water supply season, is expected a light modification in precipitation only in the northern Mediterranean (where there may even be a slight increase), while significant decreases are expected in the southern Mediterranean. Although the demarcation between these two opposite trends is uncertain, climate models agree that the southern Mediterranean countries (North Africa and the Middle East), where water resources are already scarce, will suffer a further reduction in rainfall by 2100 (approximately -20 % in winter and -35% in summer).

Consequently, climate-change impacts on the Mediterranean environment will affect particularly the availability and quality of water resources, via a change in its cycle due to a rise in evaporation and a reduction in rainfall. This water issue will be a core concern in the sustainability challenge of the whole region. Land degradation and desertification will also be exacerbated, and animal and plant biodiversity will be at risk because of a displacement of species natural ranges toward the north and toward higher altitudes, the extinction of less mobile or more climate-change sensitive species, and the appearance or even invasions of new species. Forests will most probably experience an increase in fire and parasitic risks. These forcings will amplify the already existing pressures on the natural environment related to anthropogenic activities; in fact, a whole range of local meteorological and physical risks already affecting the Mediterranean area will have their impacts aggravated by rapid coastal urbanization and global change [37]. Giorgi and Lionello [38] made a review of climate-change projections over the Mediterranean region based on a large ensemble of 17 global climate-change simulations extracted from the MGME (Multi Global Model Ensemble) stored at the Program for Climate Model Diagnosis and Inter-comparison (PCMDI; http://wwwpcmdi.llnl.gov).

A robust and large warming is projected, with a maximum in the summer season. Figure 19 (top) shows the ensemble temperature increase of the 2071–2100 period with respect to the 1961–2100 period and (bottom) the ensemble change of precipitation for the same periods and scenario as for temperature. Both signals in precipitation and temperature are projected to become progressively more severe during the twenty-first century.

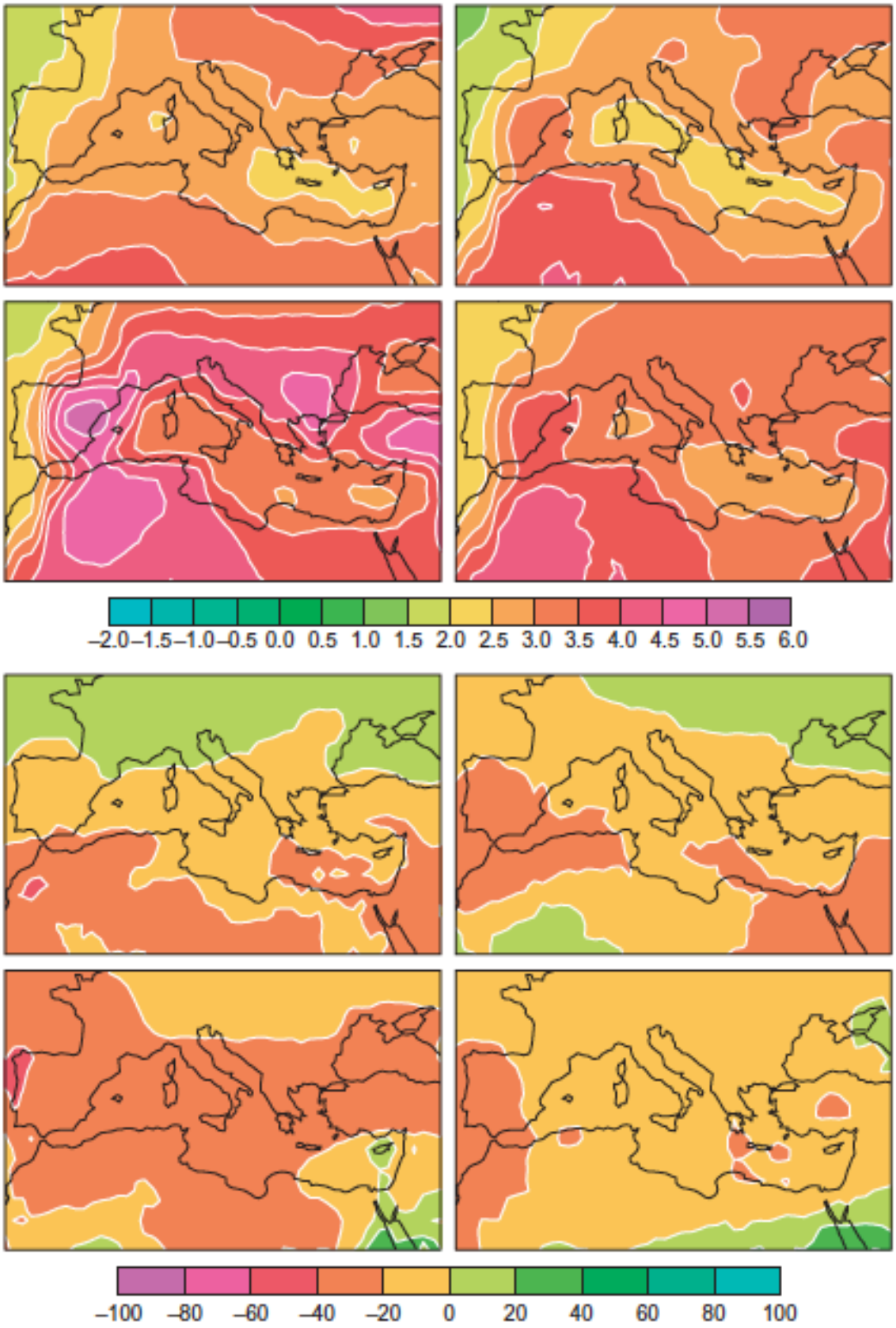

Fig. 19 Seasonal (DJF, MAM, JJA, SON) map of temperature (K, top panels) and precipitation signal (percent of the value in the reference period) climate change as resulting from an ensemble of GCMs. The maps show the differences between the 2071–2100 period of the A1B scenario and the reference period 1961–1990.
Source: Adapted from Giorgi and Lionello (2008).

4.3.2 Projection of Regional Climate Model

A substantial consensus exists among climate simulations carried out with both RCMs and GCMs, as well as between the more recent analysis and previous generations of model projections. In figure 20 and 21 are shown the results of simulation obtained with an ensemble or RCM simulations for temperature and precipitation.

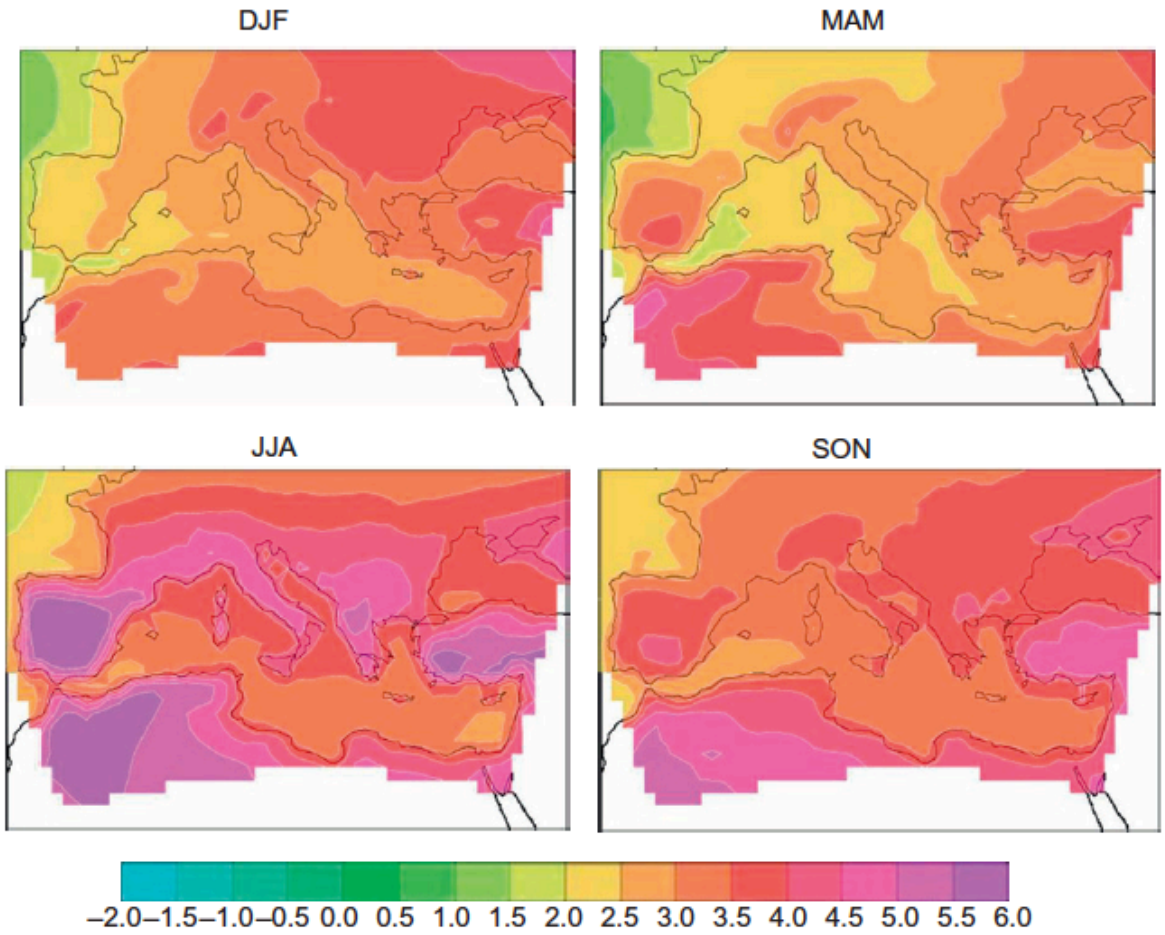

Fig. 20 Seasonal (DJF, MAM, JJA, SON) map of temperature climate change (K) as resulting from an ensemble of RCMs. The maps show the differences between the 2071–2100 period of the A1B scenario and the reference period 1961–1990. (Source: Giorgi – The climate of the Mediterranean region in future climate projections)

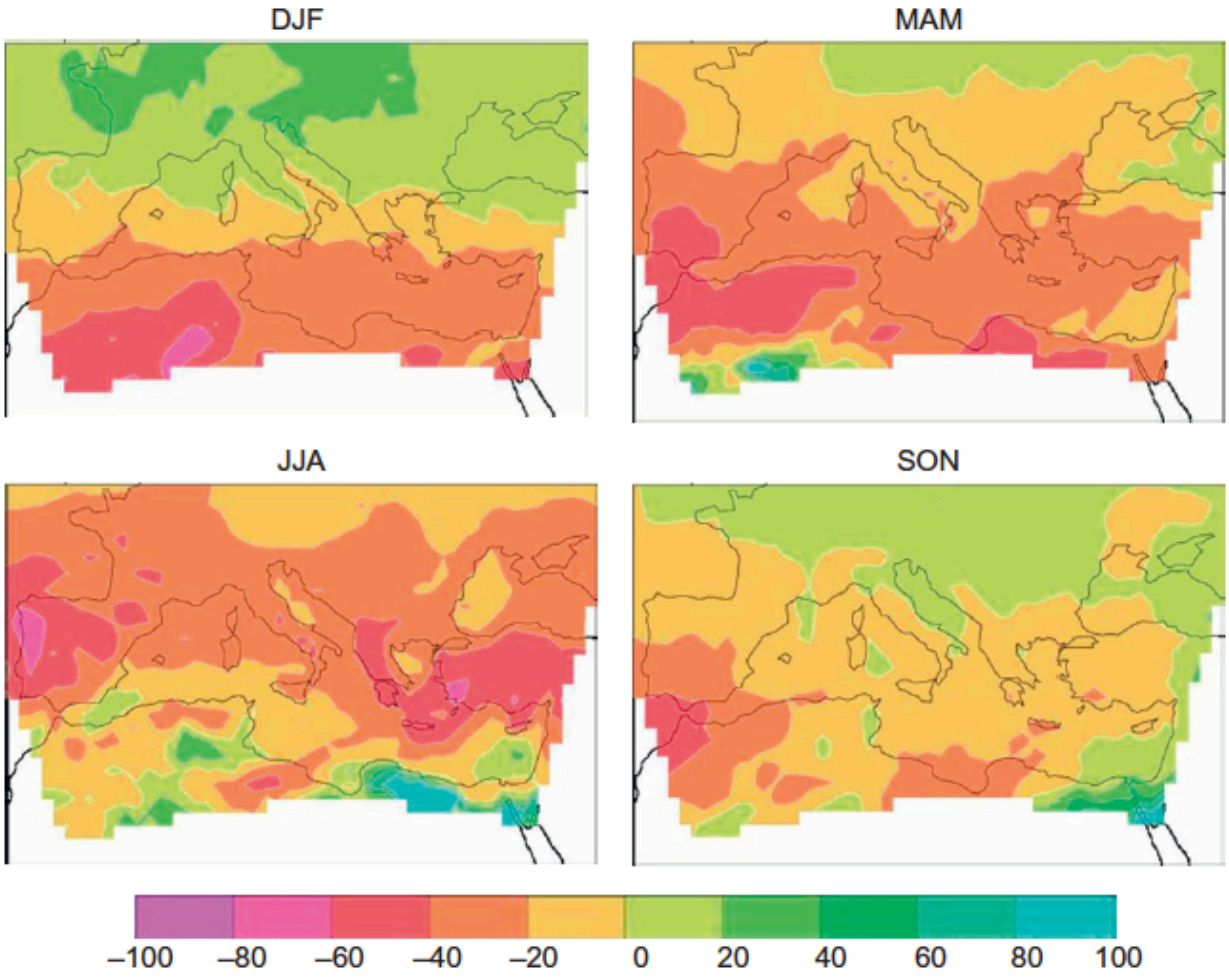

Fig. 21 Seasonal (DJF, MAM, JJA, SON) map of precipitation change (percent) as resulting from an ensemble of RCMs. The maps show the differences between the 2071–2100 period of the A1B scenario and the reference period 1961–1990. (Source: Giorgi – The climate of the Mediterranean region in future climate projections)

There are general similarities between temperature and precipitation changes simulated by GCMs (Figure 19) and by the ENSEMBLES RCMs (Figures 20 and 21). Over land, the warming for RCMs is roughly within the range of 2.5–3.5°C in winter and 4–5°C in summer. Over the sea, the warming is roughly within the range of 2–3.5°C with a lower seasonal dependence. Precipitation changes simulated by RCMs also generally agree with those simulated by GCMs, with a substantial future drying in all seasons and areas of the Mediterranean region, except in winter in the northern part. The comparison RCM with GCM clearly shows that warming and drying of the Mediterranean region at the end of the twenty-first century is very likely,

but actual values and their detailed spatial distribution remain uncertain, as they depend on the modelling tools.

5

Mathematical tools for time-series analysis

5.1 Fourier Series

Linear transformations, especially the Fourier and Laplace transforms, are widely used in solving scientific and engineering problems. They represent a versatile tool, used to turn one problem into another of easier solution. According to Fourier's theorem, any function $f(t)$, in which t represents an non-dimensional variable and which satisfies certain conditions, can be expressed as the sum of an infinite number of sinusoidal terms. **Dirichlet** in 1829 formulated the limits within the theorem is valid. The Dirichlet conditions are the follows:

1. $f(t)$ shall be periodic i.e. $f(t) = f(t + 2p)$, where $2p$ is the period.
2. If $f(t)$ is not periodic, but defined within a finite interval, the sum of the sinusoidal terms will converge to $f(t)$ in the definition interval;
3. $f(t)$ it must be at least one tract continuous function, with at most a finite number of discontinuities in a period;
4. $f(t)$ must have a finite number of maximum and minimums in a period;
5. The integral $\int_{-\pi}^{\pi} f(t)\, dt$ must be convergent.

It must be noted that these conditions for $f(t)$ are sufficient but not necessary. This means that the Fourier theorem is valid for a much wider class of functions than those respecting the Dirichlet conditions. According to the Fourier theorem, a function $f(t)$ having a fundamental

period 2π and satisfying the Dirichlet conditions, can be represented by the following Fourier series:

$$f(t) = a_0 + \sum_{N=1}^{\infty} (a_n \cos(nt) + b_n \sin(nt)) \qquad [1]$$

where a_0 , a_n and b_n are constants.

The calculation of the constants is made multiplying the *[1]* for *cos*(*0*), *cos*(*nt*) e *sin*(*nt*) and integrating in a 2*p* period compared to *t*, using the orthogonality properties of the sine and cosine functions:

$$\int_{-\pi}^{\pi} \sin(mt)\sin(nt)\,dt = \int_{-\pi}^{\pi} \cos(mt)\cos(nt)\,dt = p \quad \text{for } m = n \qquad [2]$$

$$= 0 \quad \text{for } m \neq n$$

$$\int_{-\pi}^{\pi} \sin(mt)\cos(nt)\,dt = 0 \quad \text{per tutti gli } m \text{ e } n \text{ interi} \qquad [3]$$

From the integration, it turns to:

$$a_0 = \frac{1}{2\pi} \int_{-\pi}^{\pi} f(t)\,dt \qquad [4]$$

$$a_n = \frac{1}{\pi} \int_{-\pi}^{\pi} f(t)\cos(nt)\,dt \qquad [5]$$

$$b_n = \frac{1}{\pi} \int_{-\pi}^{\pi} f(t)\sin(nt)\,dt \qquad [6]$$

In the general case of a non-dimensional variable, when the fundamental period is T, we have the following expressions:

$$a_0 = \frac{1}{T} \int_{-T/2}^{T/2} f(t)\,dt \qquad [7]$$

$$a_n = \frac{2}{T} \int_{-T/2}^{T/2} f(t)\cos\frac{(2n\pi t)}{T}\,dt \qquad [8]$$

$$b_n = \frac{2}{T}\int_{-T/2}^{T/2} f(t)\,\sin\frac{(2n\pi t)}{T}\,dt \qquad [9]$$

$$f(t) = a_0 + \sum_{N=1}^{\infty} \left(a_n \cos\frac{(2n\pi t)}{T} + b_n \sin\frac{(2n\pi t)}{T}\right) \qquad [10]$$

The coefficients a_n and b_n are called Fourier coefficients and their determination is called Fourier analysis or harmonic analysis. The expression *[1]* is valid for all the types of function $f(t)$ satisfying the Dirichlet conditions, both real or complex; in both cases the Fourier coefficients will be real or complex, respectively. For a physical time series, such as a geophysical record, $f(t)$ is real and coefficients are real.

It was found from *[2]* and *[3]* that a_0 is the mean of $f(t)$ in the integration interval and that a_n and b_n are twice the average of the modulated functions $f(t)\cos(nt)$ and $f(t)\sin(nt)$. The limits of integration - π and π may be replaced by 0 and 2π by virtue of the periodicity of $f(t)$ and the trigonometric theorems. Finally, equations *[2]* and *[3]* are called Cauchy integrals.

5.2 Application of Fourier series development to an analytical function.

Concerning the Fourier series development, we can distinguish two cases:

1. The function to be analyzed is analytical (expressed by a mathematical formula);
2. The function *f(t)* is presented in graphical or numerical format but is not analytical, most frequent cases are in geophysics where *f(t)* is represented by the observed data.

Let's consider the first case and assume, as example a saw-tooth *f(t)* function (Fig.22)

$$f(t) = \frac{t}{a} \qquad per\ -a+2k\pi \le t \le a+2k\pi \qquad [11]$$

$$f(t) = \frac{\pi - t}{\pi - a} \qquad per\ a+2k\pi \le t \le a+(2k+1)p$$

A saw-tooth waveform is symmetrical with reference to the points $t = np$.

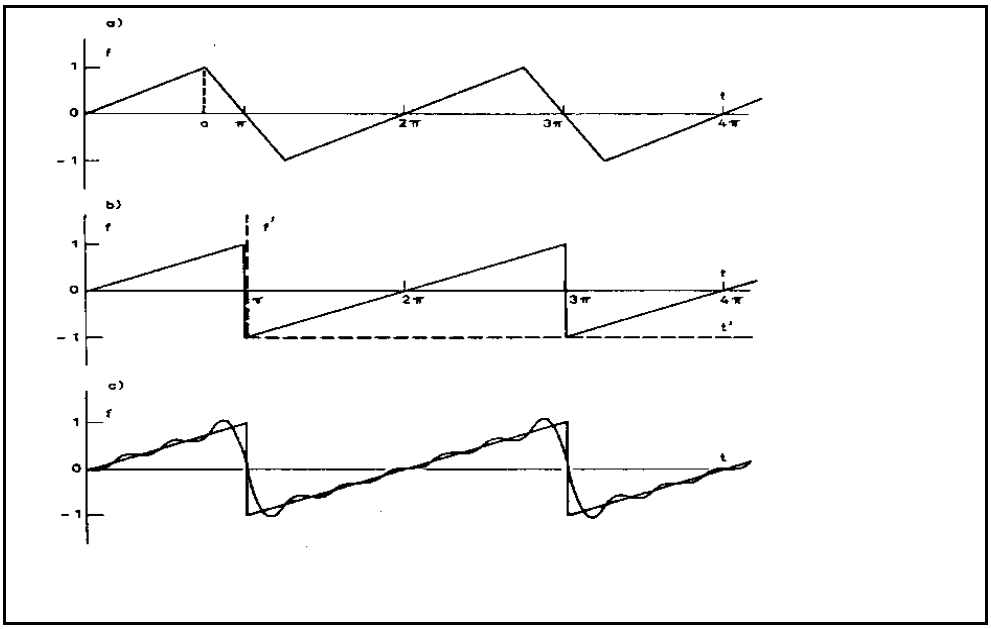

Fig.22 Sawtooth analytical function used for Fourier series development. c) Illustrates the Gibbs phenomenon.

Being it symmetric with reference to the origin, it is called also antisymmetric or odd. Therefore, in the Fourier series development appears sine terms only.

From *[6]* and *[11]*, it is obtained:

$$b_n = \frac{2}{\pi}\int_0^{\pi} f(t)\,\sin(nt)\;dt = \qquad [12]$$

$$= \frac{2}{a\pi}\int_0^{\pi} t\,\sin(nt)\;dt + \frac{2}{(\pi - a)\pi}\int_a^{\pi} (p - t)\,\sin(nt)\;dt = \frac{2}{n^2 a(\pi - a)}\sin(na)$$

In a special case where $a = p$ the expression *[12]* for b_n becomes 0/0. Computing the limit with the Hospital theorem, it is:

$$b_n = -\frac{2}{n\pi}\cos(np) \qquad [13]$$

and therefore: $b_n = \frac{2}{n\pi}$ per n dispari

$b_n = -\frac{2}{n\pi}$ per n pari

Obviously, the amplitude b_n decreases as $\frac{1}{n}$ while *n* grows.

It can be demonstrate that this is a general property of functions with simple discontinuities.

From *[1],* the development in Fourier series becomes:

$$f(t) = \frac{2}{\pi}\left(\frac{sin(t)}{1} - \frac{sin(2t)}{2} + \frac{sin(3t)}{3} - \ldots\ldots\right) \qquad [14]$$

In another coordinate system, *f'* and *t'*, tied to *f* and *t* by

$$f' = \frac{f}{2} + \frac{1}{2} \qquad [15]$$

$$t' = t - p$$

the development in series becomes:

$$f(t) = \frac{1}{2} + \frac{1}{\pi}\left(\frac{sin(t)}{1} + \frac{sin(2t)}{2} + \frac{sin(3t)}{3} + \ldots\ldots\right) \qquad [16]$$

Figure 21 shows the *f(t)* drawing obtained from the *[16]* including the terms up to 6*t*/6. As it can be seen, the approximation to the saw-tooth curve is poor at the discontinuities of *f*(*t*), in *t* = (*2n+1)p*. This is a characteristic known as Gibbs phenomenon. The error due to the inclusion in *f*(*t*) of a finite number of *n* terms is as follows:

$$\text{Error} = f_n(t) - f(t) = \frac{1}{2} - \frac{1}{\pi} Si\left(n + \frac{1}{2}\right)t \qquad [17]$$

where $Si(x) = \int_0^x \frac{sin(x)}{x} dx$

and the integral $\int_0^\infty \frac{sin(x)}{x} dx = \frac{\pi}{2}$

Therefore the error depends from da $(n + \frac{1}{2})t$ only. This means that for a given value of $(n + \frac{1}{2})t$, e.g. corresponding to the maximum error, this will not lower while *n* increases. Only *t* will be smaller at the increase of *n*, keeping $(n + \frac{1}{2})t$ and the error constant. For the saw-tooth function,

this constant error is about 9% of the step. If instead, keeping *t* constant and increase *n* indefinitely, the error will clearly tend to zero.

5.3 Application of Fourier series development to an empirical function.

As already mentioned, the observed data harmonic analysis or Fourier series development played an important role in the investigation of the periodicity of natural phenomena. Numerous developments in geophysical series are made using the mean values of the measured quantities in fixed time intervals. This means that the measured amplitudes of a phenomenon variable over time are smaller than those that would be obtained by using a large number of observations obtained as averages in smaller time intervals (Fig.23).

The relationship between the amplitude *An* of a sine wave with *N* equally-spaced observations within the whole cycle, and the *A* true amplitude is obtained by comparing the areas under the curve:

$$A = An \frac{\pi / N}{sin(\pi / N)} = An \frac{1}{sinc(1/N)} \qquad [18]$$

For N=12 (e.g. monthly average values for annual variations) the correction factor is of 1.01152;

for N = 24 (e.g. hourly average values for daily variations) it is 1.00286 and for N = ∞ it is 1.

If there is one observation only within the entire N = 1 interval the factor becomes ∞.

Obviously N = 2 is the minimum number of observations within the period and then the factor is p/2 = 1.57080. The formula [18] applies when are used the average values, in both the Fourier series development and the transform.

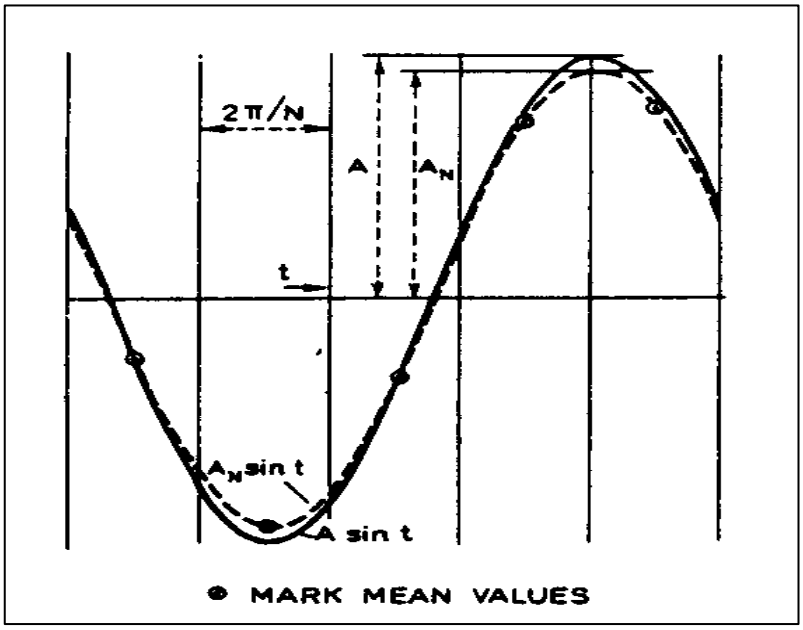

Fig.23 The example shows how for a sinusoidal wave, using the average values are obtained smaller amplitudes.

5.4 Fourier Integral and Fourier Transform

Substituting the argument *t* of the integral *[7]* with the variable λ and replacing the constants a_0, a_n and b_n expressed by *[7], [8]* and *[9]* in the original Fourier series, we have:

$$f(t) = \frac{1}{T}\int_{-T/2}^{T/2} f(\lambda)d\lambda +$$

$$+\sum_{n=1}^{\infty}\left[\left\{\frac{2}{T}\int_{-T/2}^{T/2} f(\lambda)\cos\frac{2n\pi\lambda}{T}d\lambda\right\}\cos\frac{2n\pi t}{T} + \left\{\frac{2}{T}\int_{-T/2}^{T/2} f(\lambda)sin\frac{2n\pi\lambda}{T}d\lambda\right\}sin\frac{2n\pi t}{T}\right]$$

Reducing it is obtained

$$f(t) = \frac{1}{T}\int_{-T/2}^{T/2} f(\lambda)d\lambda + \sum_{n=1}^{\infty}\frac{T}{2}\int_{-T/2}^{T/2} f(\lambda)\cos\left[\frac{2n\pi}{T}(t-\lambda)\right]dt \qquad [20]$$

The factor $cos\left(\frac{2n\pi}{T}\right)(t-\lambda)$ which appears in the second integral is called nucleus of Dirichlet.

Established that

$w_n = \frac{2n\pi}{T}$

$w_{n-1} = \frac{2(n-1)\pi}{T}$

$w_n - w_{n-1} = \frac{2\pi}{T} = Dw$

and replacing in the *[20]* it is obtained:

$$f(t) = \frac{\Delta\omega}{2\pi}\int_{-T/2}^{T/2} f(\lambda)d\lambda + \sum_{n=1}^{\infty}\frac{\Delta\omega}{\pi}\int_{-T/2}^{T/2} f(\lambda)\cos\left[\omega_n(t-\lambda)\right]d\lambda \qquad [21]$$

If now let T tends to infinity:

1. The integral $\frac{1}{T}\int_{-T/2}^{T/2} f(\lambda)d\lambda$ is nil since $\int_{-T/2}^{T/2} f(\lambda)d\lambda$

   it is convergent if $f(\lambda)$ satisfies the Dirichlet conditions;

2. The increment $\Delta\omega$ becomes very small and can be represented by $d\omega$

3. the sum is converted into an integral with limits 0 and ∞.

As result, the *[21]* becomes:

$$f(t) = \frac{1}{\pi}\int_0^{\infty} d\omega\int_0^{\infty} f(\lambda)\cos\left[\omega(t-\lambda)\right]d\lambda \qquad [22]$$

that is the Fourier integral.

Introducing the sine and cosine transforms, using the following definitions:

$$a(\omega) = \int_{-\infty}^{\infty} f(\lambda)\cos(\omega\lambda)d\lambda \qquad [23]$$

$$b(\omega) = \int_{-\infty}^{\infty} f(\lambda)sin(\omega\lambda)d\lambda$$

and defining the function $\Phi(\omega)$ with the equation

$$sin\ \Phi(\omega) = \frac{-b(\omega)}{\left[a^2(\omega)+b^2(\omega)\right]^{1/2}}$$

which implies:

$$\cos \Phi(\omega) = \frac{a(\omega)}{\left[a^2(\omega) + b^2(\omega)\right]^{1/2}}$$

from *[22]* expanding the cosine function under the integral and introducing *a(ω)* e *b(ω)* it is obtained:

$$f(t) = \frac{1}{2\pi}\int_{-\infty}^{\infty} F(\omega)e^{i\omega t}\,d\omega \qquad [24]$$

where

$$F(\omega) = |F(\omega)|e^{i\,\Phi(\omega)} = a(\omega) - ib(\omega) = \int_{-\infty}^{\infty} f(t)e^{-i\omega t}\,dt \qquad [25]$$

Therefore, from the previous formulas we have derived an important set of formulas:

1) Fourier transform

$$F(\omega) = \int_{-\infty}^{\infty} f(t)e^{-i\omega t}\,dt \qquad [26]$$

$$F(\omega) = a(\omega) - ib(\omega) = |F(\omega)|e^{i\,\Phi(\omega)} \qquad [27]$$

$$|F(\omega)| = \left[a^2(\omega) + b^2(\omega)\right]^{1/2} \quad \text{is the spectrum amplitude} \qquad [28]$$

$$\Phi(\omega) = \tan^{-1}\left[\frac{-b(\omega)}{a(\omega)}\right] + 2\pi n \quad \text{is the spectrum phase}$$

$$n = 0, \pm 1, \pm 2, \ldots.$$

2) Inverse Fourier transform

$$f(t) = \frac{1}{2\pi}\int_{-\infty}^{\infty} F(\omega)e^{i\omega t}\,d\omega \qquad [29]$$

Equation *[26]* expresses the Fourier analysis of *f*(*t*) and *[29]* expresses the Fourier synthesis of *f(t)* (the synthesis of the various spectral components F (ω)). The functions *f(t)* and *F(ω)* form a pair of Fourier and their binding is represented as $f(t) \longleftrightarrow F(\omega)$. Equations [26] and *[29]* express a biunique correspondence between these two functions and are valid for any type of function that satisfies the Dirichlet conditions. From *[26], F (ω)* corresponds to a

mean of $f(t)\ e^{-iwt}$ in the integration interval. In a series of observations, this interval is necessarily limited in extension.

By virtue of the trigonometric functions orthogonality properties, the factor e^{-iwt} behaves like an operator that selects in $f(t)$ only the components with frequency ω.

In other words, $F(\omega)$ is an average of the $f(t)$ components with frequency ω. When $F(\omega)$ is referred to a unit frequency range, this quantity is called density or more specifically spectral density for $F(\omega)$ and amplitude density for $|F(\omega)|$.

From the dimensional point of view, $F(\omega)$ has the same dimensions as $f(t)$. For example if $f(t)$ has the dimensions of a length, also $F(\omega)$ has the dimensions of a length and $|F(\omega)|^2$ has the dimensions of (length)^2. Alternatively, it is possible to refer the spectral density to units of time instead of frequency. This is done by multiplying $F(\omega)$ by the number of cycles per second (ν) o any proportional quantity such as ω. Hence $\omega F(\omega)$ is the spectral density referred to the unit of time.

5.5 Correlation functions.

Autocorrelation

The autocorrelation function definition is as follows:

$$C_{11}(\tau) = \int_{-\infty}^{\infty} f_1(t) f_1(t+\tau) dt = \int_{-\infty}^{\infty} f_1(t) f_1(t-\tau) dt \qquad [30]$$

With a simple substitution we find that autocorrelation is an even function, that is

$C_{11}(\tau) = C_{11}(-\tau)$ and has its maximum for $\tau = 0$.

In case of observed data, since the interval is limited, we can write the autocorrelation function as follows:

$$C_{11}(\tau) = \lim_{T \longrightarrow \infty} \frac{1}{T} \int_{-T/2}^{T/2} f_1(t) f_1(t+\tau) dt \qquad [31]$$

For $f_1(t)$ stationary that is statistically independent of time, averages such as those expressed in *[31]* will be clearly independent from the length of record T. From a strictly mathematical point of view, the indefinite integral in *[30]* should correspond to the limit in *[31]* less the 1/T factor in front of the integral. The expression *[31]* will tend to 0 for $f1(t)$ that satisfies the Dirichlet conditions. However, in practical applications, integration must always be limited to a T finite interval, and therefore *[31]* represents the mean of $f1(t).f1(t+\tau)$ on the T record length. The inclusion of 1/T factor serves as a normalization factor, especially necessary when comparing series of different T length, since the value of *[31]* is statistically independent from T, as well as *[31].*

Cross-correlation

The cross-correlation function definition is as follows:

$$C_{12}(\tau) = \int_{-\infty}^{\infty} f_1(t) f_2(t+\tau) dt = \int_{-\infty}^{\infty} f_1(t-\tau) f_2(t) dt \qquad [32]$$

The fact that the two expressions are equivalent can be seen with a simple substitution of the integration variable, which means that

$C_{12}(\tau) = C_{21}(-\tau)$

Generalizations of the cross-correlation function may be made to functions of several variables and to sets of more than two functions. The auto and cross - correlation functions are useful for the calculation of power spectrum and for detection of weak signals with high noise.

Convolution

The convolution definition is as follows:

$$f_1(t) * f_2(t) = \int_{-\infty}^{\infty} f_1(\tau) f_2(t-\tau) d\tau = \int_{-\infty}^{\infty} f_1(t-\tau) f_2(\tau) d\tau \qquad [33]$$

or in equivalent manner:

$$f_1(t) * f_2(t) = \int_{-\infty}^{\infty} f_1(t) f_2(\tau - t) dt = \int_{-\infty}^{\infty} f_1(\tau - t) f_2(t) dt$$

The parts to the right of the expressions, obtained by replacing t - τ with τ in the first expression and τ- t with t in the second, demonstrate the commutative property. Distributive and associative properties are also valid for the convolution. Combining the formulas *[30]* and *[32]* and convolution *[33]* is obtained:

$C_{11}(\tau) = C_{11}(-\tau) = f_1(\tau) * f_1(-\tau)$

$C_{12}(\tau) = C_{21}(-\tau) = f_1(-\tau) * f_2(\tau)$

$C_{12}(-\tau) = C_{21}(\tau) = f_1(\tau) * f_2(-\tau)$

As in the case of correlation, the convolution integral can be extended to the multidimensional case.

Convolution Theorem

If $f_1(t) \leftrightarrow F_1(\omega)$ and $f_2(t) \leftrightarrow F_2(\omega)$ then $f_1(t).f_2(t) \leftrightarrow {}^{1}\!/_{2\pi}.F_1(\omega) * F_2(\omega)$ and

$f_1(t) * f_2(t) \leftrightarrow F_1(\omega).F_2(\omega)$.

It is demonstrated that the Fourier transform of $f_1(t).f_2(t)$ it is for the [26]:

$$\int_{-\infty}^{\infty} f_1(t) f_2(t) e^{-i\omega t} dt = \int_{-\infty}^{\infty} f_2(t) e^{-i\omega t} [\frac{1}{2\pi} \int_{-\infty}^{\infty} F_1(\lambda) e^{i\lambda t} d\lambda] dt =$$

$$= \frac{1}{2\pi} \int_{-\infty}^{\infty} F_1(\lambda) d\lambda \int_{-\infty}^{\infty} f_2(t) e^{-i(\omega-\lambda)t} dt = \frac{1}{2\pi} \int_{-\infty}^{\infty} F_1(\lambda) F_2(\omega - \lambda) d\lambda =$$

$$= {}^{1}\!/_{2\pi}.F_1(\omega) * F_2(\omega)$$

where λ it is an integration variable. Therefore, it results that:

$$f_1(t).f_2(t) \leftrightarrow {}^{1}\!/_{2\pi}.F_1(\omega) * F_2(\omega) \qquad [34]$$

Similarly, by using [29], it is demonstrated that:

$$F_1(\omega).F_2(\omega) \leftrightarrow f_1(t) * f_2(t) \qquad [35]$$

As above, changing the order of integration it is allowed only if the signal has a finite energy. Verification for all physical signals comes naturally. Thus, the product of two functions spectrum is the convolution of their individual spectra, and the signal corresponding to the product of the two spectra is the convolution of the single signals. The theorem is extendable to a finite number of signals. The convolution derivative theorem also applies:

if $f_1(t) \leftrightarrow F_1(\omega)$ e $f_2(t) \leftrightarrow F_2(\omega)$ then

$$[[f_1(t) * f_2(t)]' = f_1'(t) * f_2'(t) = f_1(t) * f_2'(t) \longleftrightarrow i\varpi F_1(\varpi) \bullet F_2(\varpi)$$

Power Spectra

In the time domain, the below expression defines the average power of any real function f(t):

$$\lim_{T \longrightarrow \infty} \frac{1}{T} \int_{-T/2}^{T/2} |f(t)|^2 \, dt$$

$|f(t)|^2$ it is called instantaneous power of *f(t)* and the integral $\int_{-\infty}^{\infty} |f(t)|^2 \, dt$

is the total energy of *f(t)*, when it is convergent. In general *f(t)* may indicate any signal (such as speed of a particle, acceleration, temperature) depending on the physical variable *t* (time, spatial coordinate or other).

Parseval Theorem

We will now derive the relationship between the signal strength *f*(*t*) and its spectrum $F(\omega)$. Suppose that both $f_1(t)$ and $f_2(t)$ are two signals whose spectra are $F_1(\omega)$ and $F_2(\omega)$, and we consider the integral:

$$\int_{-\infty}^{\infty} f_1(t) f_2(t) dt = \int_{-\infty}^{\infty} f_1(t) [\frac{1}{2\pi} \int_{-\infty}^{\infty} F_2(\omega) e^{i\omega t} d\omega] dt$$

$$= \frac{1}{2\pi}\int_{-\infty}^{\infty} F_2(\varpi)d\omega \int_{-\infty}^{\infty} f_1(t)e^{i\omega t}dt = \frac{1}{2\pi}\int_{-\infty}^{\infty} F_2(\omega)F_1(-\omega)d\omega$$

$$= \frac{1}{2\pi}\int_{-\infty}^{\infty} F_2(\omega)F^*{}_1(\omega)d\omega \qquad [36]$$

The equation *[36]* expresses the theorem of power.

Now, if $f_1(t) = f_2(t) = f(t)$, then also $F_1(\omega) = F_2(\omega) = F(\omega)$ and the following relation is valid:

$$\int_{-\infty}^{\infty}|f(t)|^2 dt = \frac{1}{2\pi}\int_{-\infty}^{\infty} F(\omega)F*(\omega)d\omega = \frac{1}{2\pi}\int_{-\infty}^{\infty}|F(\omega)|^2 d\omega = \frac{1}{\pi}\int_{0}^{\infty}|F(\omega)|^2 d\omega \qquad [37]$$

This relationship is defined as a Parseval theorem. The real quantity $|F(\omega)|^2$ is commonly identified as spectra power or spectral energy or more precisely as density of spectral power or spectral energy density. Since the *[37]* contains the square of the absolute value of the spectrum amplitude, no information on the time function spectrum phase is obtainable.

This means that it is impossible to trace the original signal *f*(*t*) if it is given its power only. This also means that signals with identical spectrum amplitude but different phase will have identical spectral powers.

Autocorrelation and power spectrum

Applying the definition *[30]* as autocorrelation function to the *[36],* the result is the Wiener-Khintchine relation:

$$C_{11}(\tau) = \int_{-\infty}^{\infty} f_1(t)f_1(t+\tau)dt = \frac{1}{2\pi}\int_{-\infty}^{\infty}|f_1(\omega)|^2 e^{i\omega\tau}d\omega \quad =$$

$$= \frac{1}{2\pi}\int_{-\infty}^{\infty} E_{11}(\omega)e^{i\omega\tau}d(\omega) \qquad [37a]$$

and:

$$E_{11}(\omega) = \int_{-\infty}^{\infty} C_{11}(\tau) e^{-i\omega\tau} d(\tau) \qquad [37b]$$

Given that $C_{11}(\tau)$ is real and even, the formula [37b] can be expressed as:

$$E_{11}(\omega) = 2\int_{0}^{\infty} C_{11}(\tau)\cos(\omega\tau) d(\tau) \qquad [37c]$$

From the *[37a]* is obtained also:

$$C_{11}(0) = \int_{-\infty}^{\infty} [f_1(t)]^2 d(t) = \frac{1}{2\pi}\int_{-\infty}^{\infty} E_{11}(\omega) d(\omega) = \frac{1}{2\pi}\int_{-\infty}^{\infty} |F_1(\omega)|^2 d(\omega)$$

5.6 Observed spectra data (fundamental problems)

The main differences between an analytical and an observed series are the following:

Condition	**Analytical function *f(t)***	**Observed empirical curve *f(t)***
Dirichlet conditions	It is necessary to check that they are verified in any case	Automatically verified for each practical case[6]
Infinite integration interval	Generally it does not present difficulties	Impossible in the series of observations

The fact of having data contained in a limited time window actually makes it impossible to obtain a correct spectrum. We can see it in the following way:

1. Let's take in account the hypothetical case of an infinitely long time window that is able to contain the whole signal. In this case the time window will be $w(t)$ =1 for each t and we will have:

[6] *The condition for the Fourier integral is that* $\int_{-\infty}^{\infty} |f(t)|\ dt$ is finite; it is verified for the curves of observation within the finite intervals.

$$f(t)W(t) = f(t) \longleftrightarrow \frac{1}{2\pi} F(\omega) * 2\pi\delta(\omega) = F(\omega) * \delta(\omega)$$

$$= \int_{-\infty}^{\infty} F(\varpi)\delta(\omega - \varpi)d\varpi = F(\omega)$$

Which means that we will have the real spectrum $F(\omega)$

2. If we take in account an interval of finite time T, of the rectangular window type, we will obtain:

$$f(t)w(t) = f(t)\prod(\frac{t}{T}) \longleftrightarrow \frac{T}{2\pi} F(\omega) * \frac{sin(\omega T/2)}{\omega T/2} =$$

$$= \frac{T}{2\pi}\int_{-\infty}^{\infty} F(\omega)\frac{sin(\omega - \varpi)T/2}{(\omega - \varpi)T/2}d\omega \neq F(\omega)$$

In this case we will not have the true spectrum F (ω), ma the convolution integral, which represents an approximation to the correct F (ω).

The degree of approximation depends on the T window interval, so that, the smaller the T, the rougher the approximation will be. The spectrum thus calculated is therefore called the average or weighted spectrum [39], naturally, both the amplitude and the phase will be distorted. The window T distortion holds an important role on the characteristic of the calculated spectrum; in fact (Fig.24)

1) A great T produces more accurate detail, that is better resolution in the calculated spectrum;
2) A small T produces a better stability and a better spectrum reliability compared to a great T;
3) The type of record in use may produce limitations on the T choice. For example, in a seismic recording with a sequence of different wave arrivals, the time window must be chosen so that only the waves subject to study are included and not others.

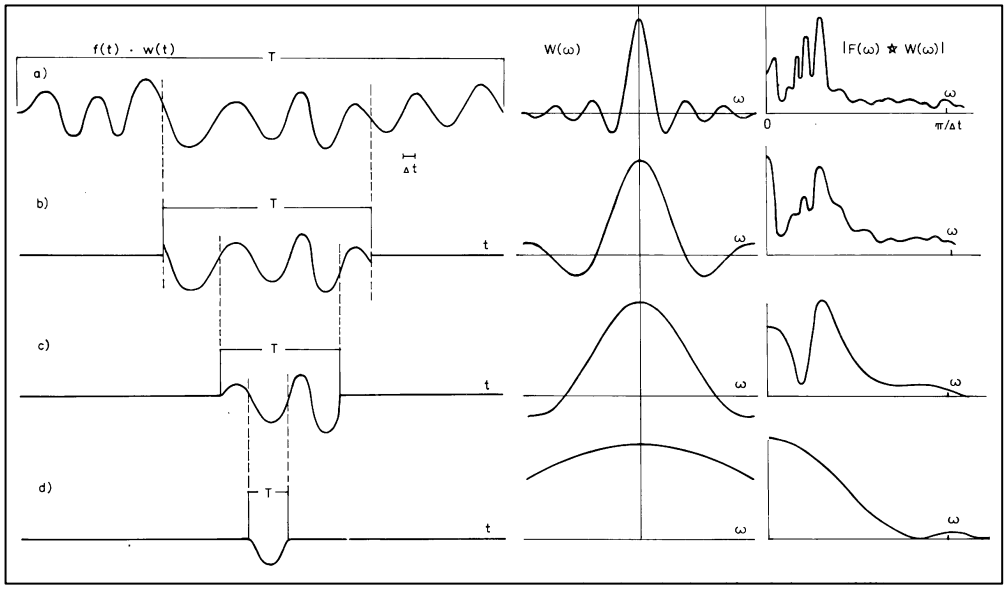

Fig24 Window width influence on the spectral resolution.

An infinite T, practically impossible to realize, will return a correct spectrum, while a very small T, tending to zero, will return a white spectrum or no resolution. In any real case, the choice, in the choice of the appropriate T time window we must make a proper compromise keeping in mind the various considerations.

A T time window defines the fundamental period and its upper harmonics 1/T, 2/T, 3/T etc.…

A 2T window will similarly give the frequencies 1/2T, 2/2T, 3/2T, etc..

In any case, the width of the T window must be chosen by means of an accurate analysis and the degree of representativeness must be judged by the comparison of spectra of recordings of different duration; it should however include many wavelengths.

In addition to the "smoothing" effect, it must be considered that the W (ω) window frequency extreme lobes induces undesirable effects. The negative extreme lobes induces a spectral loss. The ideal is to have a narrow central lobe and insignificant extremes lobes.

Improvements in the quality of the W (ω) spectral window, can be obtained by modifying the data window shape w(t), even if the effect cannot be completely removed. Below is the summary of the effects of data windows:

1) Widen the spectral lines,

2) Insert spurious spectral lines.

If the record limited length is one of the major differences between the observed and the analytical signals, the other is surely the signal representation. In fact, while the exact mathematical formulas represent analytical signals, for the observed data this is not possible. Hence, there are two different ways of proceeding:

1) Use the record directly as data that is in analogic form;
2) Reformulate the record in mathematical format, and then use it as an analytic function. The second method, since it does not require special tools for the construction of the spectrum, is generally the most used. It only requires the availability of a Personal Computer. To represent the record in a format equivalent to an analytic function, it is necessary to determine its numerical values in points generally equidistant along the time axis. The process of determination is called record digitization.

The record is subsequently transformed into analytical form, using a polynomial, a Fourier series or any other function that adapts to the digitized values. By including a sufficiently large number of terms in analytic development, it is possible to obtain the record desired degree of approximation. As previously seen, we then proceed in analytical format. This process of transformation in analytical format is avoidable and it is possible to use digital values directly to calculate the spectrum and other related functions. For this reason it is necessary to reformulate the expressions already provided, transforming them from continuous to discrete. Summaries will replace integrals. Digital spectra always comes out from this procedure calculation. Summarizing, we can therefore say that the spectrum of observed records differs from that of analytical functions for two very important aspects:

1) The use of time windows of finite extension;
2) The record digital format.

5.7 Analog and digital data

Digitalization effects

We have seen that the record of length T defines the fundamental period or the lowest frequency recognizable in the signal. The sampling interval Δt defines the highest resolvable frequency. By intuition is understood that at least 3 points, that is two 2Δt time intervals are the minimum of information necessary to define a period (Fig.25). This means that the smallest period that can be determined is 2 Δt, and that the highest resolvable frequency is $\frac{1}{2\Delta t}$. This frequency limit, for the calculated spectrum is named "Nyquist frequency". It is equivalent to half the sampling rate.

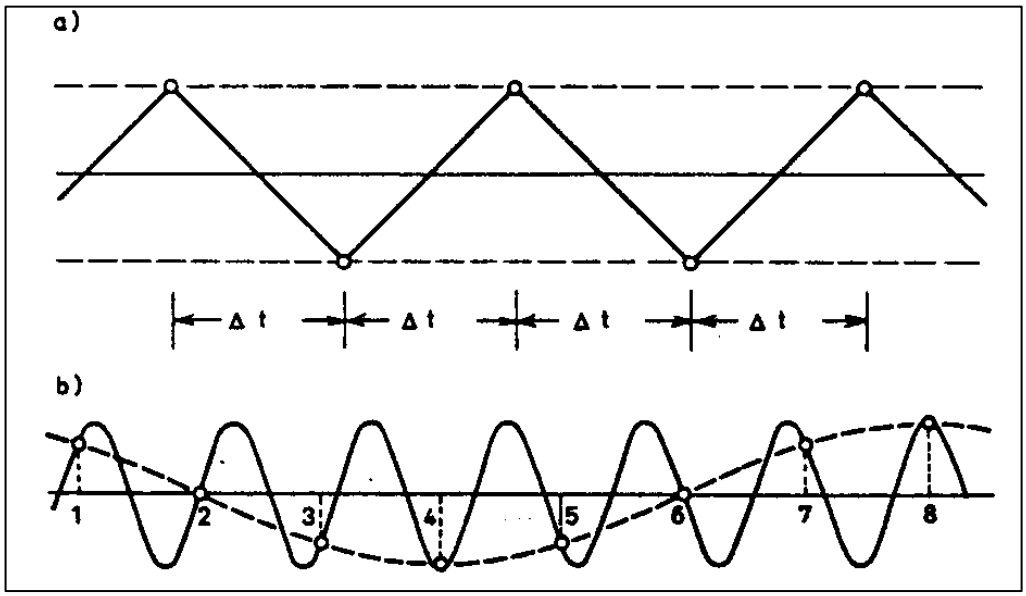

Fig.25 Digital sampling. a) the example that intuitively shows that at least two points per period are needed. b) the example shows the aliasing effect. By varying the sampling interval and the point of origin, it is easily visible that different results will be obtained for both amplitude and frequency and phase.

Spectrum frequency limitations.

The rules for the spectrum frequency limits are as follows:

1) The record T length defines the lowest frequency within the spectrum $\nu_1 = \frac{1}{T}$;

2) The digitization interval or sampling interval Δt defines the frequencies upper limit in the spectrum $\nu_n = \frac{1}{2\Delta t} = \frac{N}{2T}$ where N+1 is the number of samples. Contaminations of calculated spectra due to higher frequencies of ν_n in the signal are due to the phenomenon known by the term "aliasing".

3) The resolving power, that is, the difference between successive frequencies analyzed is $\Delta\nu = \frac{1}{T}$. It is called Nyquist co-interval.

From rules 1 and 2 comes out

$\frac{1}{T} \leq \nu \leq \frac{N}{2T}$ or $\nu = \frac{m}{2T}$ where m = 2,3,.....N.

The lowest frequency (fundamental) that defines the spectral resolution, that is the interval between successive frequencies, is equal to 1/record length.

For a recording of length T, the range of the variable τ in C11 (τ) is obviously 2T. The frequencies limits are correlated by equation $(\frac{N}{2})\nu_1 = \nu_n$.

For simplicity, we consider the development of $f(t)$ in a Fourier series from its N+1 data.

We will then be able to obtain N+1 linear equations with N+1 unknowns a_0, a_n and b_n. Thus $f(t)$ allows to determine the coefficients a_n and b_n up to N/2 harmonics. If N is even, the highest harmonic is N/2, while if it is odd it is of order (N+1)/2. This result, derived from *f(t)* is equally applicable to F(ω) by virtue of the Fourier transform. The result confirms the deduction regarding the Nyquist frequency, obtained graphically above.

Summarizing:

Number of intervals	N
Number of data	N+1
Number of significant harmonics	n = N/2 for N even (N+1)/2 for N odd

Aliasing

By aliasing it is meant the phenomenon according to which the spectral components with higher frequencies of ν_n, contained in a signal, disturb the spectral components with frequencies lower than ν_n. This contamination operates in such a way that the components with symmetrical frequency with respect to the frequency of Nyquist, ν_n, disturb each other. Aliasing is therefore a special type of spectral contamination. It is the result of the use of discrete formulas, rather than continuous, and is a direct consequence of the digitization of a record. Tested several methods to eliminate this unwanted effect:

1) A digitizing interval equal to zero is naturally impossible in geophysics, but choosing Δt as small as possible, it gets very close. However, decreasing Δt also means increasing the frequency of Nyquist and this causes an increase in the frequency range affected by the aliasing. In general, the higher the frequency of Nyquist, the smaller the effect of aliasing. The aliasing maximum effect occurs near the Nyquist frequency. So, if a calculated spectrum shows an increase near this frequency, it is preferable to exclude this part, and study it later. Of course, the major drawback of having a small Δt is the increase in requests in terms of memory utilization and calculation time.
2) The aliasing schematic illustration (Fig. 25) shows that an alternative method to avoid aliasing could be sampling the record in randomly chosen non-equidistant points. This can

be verified mathematically and the result is that a statistical sampling (e.g. Poisson distribution) is free from aliasing [40][41].

3) A third method to avoid aliasing effects, often used, is to filter the record before further analysis. A well-defined low-pass filter serves well the purpose. However, if the filter is not carefully selected, undesirable effects may occur. On the one hand, the filters lead to a partial elimination of aliasing, on the other side, undesirable effects can occur in the spectrum.

5.8 Discrete formulas

Fourier coefficients

With a digitization process, a polygon replaces a continuous curve y(x) which is much more accurate the more Δx is small. For a series of N+1 equally spaced discrete observations and with $\nu = 1, 2, \ldots N$, the formulas of the summation for the Fourier coefficients are the following:

$$a_0 = \frac{1}{N}\sum_{\nu=1}^{N} f(\nu)$$

$$a_n = \frac{2}{N}\sum_{\nu=1}^{N} f(\nu)\cos\frac{2n\pi}{N}\nu \qquad [38]$$

$$b_n = \frac{2}{N}\sum_{\nu=1}^{N} f(\nu)sin\frac{2n\pi}{N}\nu$$

and the discrete Fourier series development becomes:

$$f(\nu) = a_0 + \sum_{n=1}^{N/2} a_n \cos\frac{2n\pi}{N}\nu + \sum_{n=1}^{N/2} b_n sin\frac{2n\pi}{N}\nu \qquad [39]$$

The symmetry properties of the sine and cosine functions allows rewriting the formulas for the coefficients a_n and b_n as follows:

$$a_n = \frac{2}{N}\sum_{\nu=1}^{N/2}[f(\nu)+(-1)^n f(\frac{N}{2}+\nu)]\frac{\cos 2n\pi}{N}\nu \qquad [40]$$

$$b_n = \frac{2}{N}\sum_{\nu=1}^{N/2}[f(\nu)+(-1)^n f(\frac{N}{2}+\nu)]\frac{sin2n\pi}{N}\nu$$

It is clear that the point $\nu = \frac{N}{2}$ represents the Nyquist point along the sequence of ν values.

The *Fourier transform*

The Fourier transform in the discrete case becomes:

$$F_\omega = \int_{-\infty}^{\infty} f(t)e^{-i\omega t}dt \Rightarrow \frac{1}{N}\sum_{\nu=1}^{N} f(t_n)e^{-i\omega t_n} \qquad [41]$$

Rewriting of this formula fits best to the discrete case:

$$F(n) = |F(n)|e^{i\phi(n)} = \frac{1}{N}\sum_{\nu=1}^{N} f(\nu)e^{-i(2\pi n/N)\nu} \qquad [42]$$

This is the discrete Fourier transform (DFT) of the time series

$f(1), f(2)$……..f(N) that is of N data all equally spaced.

This equation immediately results also from the *[38]:*

$F(n) = \frac{1}{2}(a_n - ib_n)$ where a_n e b_n are the Fourier coefficients in discrete format.

The Nyquist frequency is N/2 for N even and (N+1)/2 for N odd. Therefore, *F(n)* shall be computed for n=1, 2, 3….. up to the Nyquist frequency that is N/2 or (N+1)/2 respectively.

It is clear that with N quantity $f(\nu)$ is possible to determine only other N, a_n and b_n and therefore for each F(n) there are two unknown variable that are the F(n) amplitude and phase. The *[42]* can be rewritten as follows:

$$F(n) = \frac{1}{N}\sum_{\nu=1}^{N/2}[f(\nu)+(-1)^n f(\frac{N}{2}+\nu)]e^{-i(2\pi n/N)\nu}$$

The *F(n)* (IDFT) inverse discrete Fourier transform is given by the following formula:

$$f(\nu) = \sum_{n=1}^{N} F(n) e^{i(2\pi\nu/N)n} = 2\sum_{n=1}^{N/2} F(n) e^{i(2\pi\nu/N)n}$$

All these formulas for *F(n)* and $f(\nu)$ can be written as polynomials as follows:

$$F(n) = \frac{1}{N}\sum_{\nu=1}^{N} f(\nu) z^{\nu} \qquad [43]$$

where $z = e^{-i(2\pi n/N)}$ and

$$f(\nu) = \sum_{n=1}^{N} \frac{F(n)}{z^n} \qquad [44]$$

where $z = e^{-i(2\pi\nu/N)}$

The expressions *[43]* and *[44],* often found in the geophysical literature, are called -zeta transformed.

Correlation and convolution function.

In the discrete case, the above-seen autocorrelation formula becomes:

$$c_{11}(\tau) = \frac{1}{N-\tau}\sum_{t=1}^{N-\tau} f(t) f(t+\tau) \text{ dove } \tau = 0, 1, 2, \ldots..m \qquad [45]$$

And the given series is *f*(1), *f*(2) ……*f*(N).

Correspondingly, to [45] we can write the cross-correlation formula:

$$c_{12}(\tau) = \frac{1}{N-\tau}\sum_{t=1}^{N-t} f_1(t) f_2(t+\tau) \text{ where } \tau = 0, 1, 2, \ldots.. n \qquad [46]$$

and the given series are $f_1(1), f_1(2), f_1(3)\ldots\ldots f_1(N)$ and

$f_2(1), f_2(2), f_2(3)\ldots\ldots f_2(N)$,

and of the convolution:

$$f_1(t) * f_2(t) = \frac{1}{N-t}\sum_{\tau=1}^{N-t} f_1(\tau) f_2(t-\tau) \text{ dove } t = 0, 1, 2, \ldots\ldots m$$

and the given series are $f_1(1), f_1(2), f_1(3)\ldots\ldots f_1(N)$ and

$f_2(1), f_2(2), f_2(3)\ldots\ldots f_2(N)$.

5.9 Description of some methods of spectral analysis

Both deterministic and stochastic processes can, in principle, be characterized by a function of frequency (rather than time) called the power spectrum. Thus, for example, a very irregular movement (e.g. noise) has a flat, continuous and regular spectrum, which indicates that all the frequencies contained in a very wide band of frequencies are excited by this process.

On the other hand, in the frequency domain a single line or a set consisting of a few lines, having a considerably greater amplitude than all subsequent spectral lines, may generally characterize a purely periodic or quasi-periodic process. Between these two extremes, deterministic nonlinear processes may have spectral peaks superimposed on a continuous and regular background.

The calculation of the power spectrum of a random process is essentially a reverse problem badly put [42]. For example, the simple calculation of the discrete Fourier transform of a random time series (with continuous spectral density), will give a spectral estimate whose variance is equal to the estimate itself. The following are some methods to reduce this variance, used for climate time series spectral analysis.

5.9.1 Blackman e Tukey

The Blackman-Tukey method is the classic method for performing spectral analysis. The algorithm first computes the data autocorrelation, then applies a window, and finally performs a Fourier transform to calculate the spectrum. It is a very effective method, which unfortunately has spurious spectral characteristics.

The Blackman-Tukey method [39] gives an estimate of the power spectrum that reduces the variance of the spectral estimates of a given real signal X and attenuates the loss effects due to

the finiteness of the window in which the data are sampled [43]. The starting point of this method is the Wiener-Khintchine identity, which establishes that the power spectrum

$P_x = |F(\omega)|^2$ is equal to the Fourier transform of the self-correlation function $\emptyset X = C_{11}(\tau)$ [44].

It follows that the power spectrum can be approximated by a discretized version of this identity, through the first M + 1 self-correlation coefficients.

$$P_x(\omega) \approx \sum_{k=0}^{M} \emptyset X(k) e^{i\omega k} \qquad [47]$$

This operation called (periodogram) diagram of a period smooths the spectrum and reduces the variance of spectral estimates. In this formula, the choice of M is linked to a compromise between the frequency resolution (large values of M) and the variance of the estimates that is proportional to M/N, where N is the number of experimental data.

Therefore, an acceptable general rule is to take M smaller than N/5 or N/10 to avoid spurious results due to the estimates high variances. Furthermore, a window or taper is applied to the data to reduce the spectral loss, by attenuating the side lobes of the step function transform. These windows are empirically chosen as modified cosine functions or cubic functions, etc. [43].

Confidence levels on a pure red noise can be calculated [44], but the spectral resolution is generally poor if the number of experimental data is low.

5.9.2 Maximum Entropy.

The Maximum Entropy (MEM) method is particularly powerful for estimating the frequency lines in self-regressive time series. Exhaustive details are available in Burg [45], Childers [46] or Haykin [47].

In short, it starts with a stationary time series X of mean zero, with M + 1 coefficients of self-correlation *{ØX(k)}, k = 0 ... M:X*

$$ØX(k)=\frac{1}{N+1-k}\sum_{t=0}^{N-k}X(t)X(t+k) \qquad [48]$$

The aim is to determine the spectral density Px which corresponds to the most random or unpredictable process described by the same autocorrelation coefficients. In terms of information theory, this constitutes the notion of maximum entropy: hence the origin of the name of the method.

Entropy h measures unpredictability for a Gaussian process:

$$h=\int_{-1/2}^{1/2}\log Px(\omega)d\omega \qquad [49]$$

The functional *[49]* is maximized with reference to the ØX autocorrelation coefficients obtained from the Wiener-Khintchin report [47]. M Lagrange multipliers $\{a_k\}$ resolve this optimization problem. These Lagrange multipliers correspond to the coefficients of a self-regressive chronological series (AR): Ξ (t) whose autocorrelation coefficients are ØX:

$$\Xi(t+M+)=\sum_{k=1}^{M}a_k\Xi(t-M+k)+\xi \qquad [50]$$

where ξ it is a residual blank noise. An estimate of the spectral density of Fourier Px power of this AR process is given by:

$$Px(\omega)=\frac{a_0}{\left|1+\sum_{k=1}^{M}a_k e^{ik\omega}\right|^2} \qquad [51]$$

Where a_0 it is the variance of the noise ξ. Therefore, the knowledge of the coefficients $\{a_k\}$, k = 0 ... M directly provides an estimate power spectrum of X. The coefficients $\{a_k\}$ can be calculated by solving a system of linear equations *[48] [49],* with a Theoplitz symmetric self-correlation matrix:

$$\begin{bmatrix} Ø0 & Ø & \dots & ØM \\ Ø1 & Ø0 & \dots & ØM-1 \\ . & . & & . \\ . & . & & . \\ . & . & & . \\ ØM & ØM-1 & \dots & Ø0 \end{bmatrix} \begin{bmatrix} 1 \\ a1 \\ . \\ . \\ . \\ aM \end{bmatrix} = \begin{bmatrix} a0 \\ 0 \\ . \\ . \\ . \\ 0 \end{bmatrix} \quad [52]$$

An alternative technique is to take the auto-covariance matrix for the selected M coordinates [50]. The definition of this matrix is positive but it is not of the Toeplitz type. This technique seems to be less sensitive to the phase of the signal and introduces less frequency distortions [50][51].

The method of maximum entropy is very efficient for the detection of the frequency lines for stationary time series. If this hypothesis is not verified, or if the chronological series is not nearly self-regressive, misleading results can be obtained, which cannot be detected except by analysing the chronological series with other techniques.

Furthermore, it is noted that the behaviour of the spectral estimation depends a lot on the choice of the M self-regression order: the number of peaks in the spectrum increases with M regardless of the content of the time series. This means that anomalous results may appear for high values of M. An upper limit for M is generally considered N/2. Empirical criteria have been proposed for the optimization of the value of M, based on the minimization of the residual of a regression with the least squares method between the autoregressive approximation of the data and the original time series.

5.9.3 Multitaper

The Multitaper method offers several interesting features: a high resolution and variance of estimates that are statistically independent of the spectral power (small amplitude oscillations can have a high level of significance). Some cautions are always necessary: the level of statistical confidence assessed for this method is often more optimistic than that given for classical methods.

The purpose of this non-parametric spectral method [42] is to compute a set of independent and significant estimates of the power spectrum, to obtain a better and more reliable estimate than is possible with the single window methods (Blackman -Tukey), in a finite chronological series. A set of optimal tapered windows is calculated so that this spectral estimation technique is less heuristic than traditional ones (e.g. Blackman and Tukey).

Thomson's multi-taper (MTM) method [42] has been applied to various fields of geophysics. This includes Earth science [52][53]; geophysics [54]; climatology on the inter-decennial and secular time scales [55][56]; paleoclimatology, on data related to tree growth rings [57]; data obtained from marine cores [58][59] and data obtained from ice cores [60][61].

Suppose that {X (t)} is a sinusoidal chronological series of angular frequency $\hat{\omega}$, for example, $X(t) = \mu e^{i\hat{\omega}t}$ *per t = 0 ... N - 1*. Then let it be {w (t), t = 0 ... N - 1} a window of length N and that {y(w)} is the Discrete Fourier Transform (DFT) of the windowed signal {X (t) w (t)}:

$$y(\omega) = \sum_{t=0}^{N-1} X(t)w(t)e^{-i\omega t} \qquad [53]$$

Where $\omega = \frac{k}{N}$ is the angular frequency with k = 0, 1, ... N-1.

The primary purpose of the tapered window is to minimize spectral losses, that is to minimize the energy contribution outside a given bandwidth ($\hat{\omega}$ - Ω, $\hat{\omega}$ + Ω) of the windowed signal with angular frequency $\hat{\omega}$, where $|y(\omega)|^2$ it is an estimate of the signal strength.

Therefore, the windowed signal {*X(t)w(t)*} should maintain as much as possible of its energy in the interval ($\hat{\omega}$ - Ω, $\hat{\omega}$ + Ω), relative to the total power covering the whole band (-π,π). Therefore, it is possible to choose a {*w(t)*} window to maximize the functional

$$F(w) = \frac{\int_{\hat{\omega}-\Omega}^{\hat{\omega}+\Omega} |y(\omega)|^2 d\omega}{\int_{-\pi}^{\pi} |y(\omega)|^2 dw} \qquad [54]$$

In maximizing F compared to {*w(t)*} a classic Rayleigh-Ritz problem arises, the solutions of which are given by a problem to auto vectors with Toeplitz matrix [42]. The windows obtained from these auto vectors are called discrete prolate spheroidal sequences (Discrete Prolate Spheroidal Sequences DPSS) [62]. By construction, they are orthogonal; therefore, the associated spectra provide independent estimates of the real spectrum. If we organize the self-vectors by their corresponding self-values

$1 > \lambda 1 > \ldots \lambda N > 0,$

the expression 1 - λk results the fraction of the k° window total energy out of the interval (-$\hat{\omega}$ Ω, $\hat{\omega}$ + Ω). It is clear that the first K = [2N.Ω] self-vectors (where [.] means whole part) have the best spectral properties, since the relative fractions of loss 1 - λk, k = 1 ... K are very close to one [62]. Therefore, a maximum of K = [2NΩ] windows must be taken to obtain an efficient spectral estimate. Slepian [62], Thomson [57] and Rögnvaldsson [63] provide efficient algorithms for DPSS computation.

Below, we will show with $\{y_k(w)\}$ the Fourier Discrete Transform of the windowed signal $\{X(t)w_k(t)\}$.

Once done the windows calculation, estimation of the total power spectrum occurs averaging the individual spectra of each windowed signal. Therefore, if we define $\check{S}_k(\omega) = |Y_k(\omega)|2$ the k° self-spectra of the time series {X(t)}, the estimate of the total spectrum obtained from the first K windows is:

$$\check{S}(\omega)=\frac{1}{K}\sum_{k=0}^{k-1} \check{S}k(\omega) \qquad [55]$$

The resolution is therefore ± Ω, which means that the spectral lines will be detected by peaks or humps of 2Ω width. The advantage of this multi-taper estimate is that the average process on different independent estimates Sk of the real spectrum attenuates spurious irregularities and therefore reduces the variance of the estimate. Further reduction of variance can be done and the error bars can be calculated by applying the so-called "jack-knifing" procedures to the K estimates [63].

The purpose of the harmonic analysis is to determine the spectral lines of a periodic or quasi-periodic signal and the related amplitudes. The Fourier transform of an infinite periodic signal provides a function of the Dirac δ type at the signal frequency that is an infinite height peak.

A simple spectral estimate (from the maximum entropy method, or from the Fourier transform) provides indirect information on the amplitude of a signal at a given frequency, through the area under the peak, which is approximately constant, even if the height of the peak is proportional to the number of points in the time series, and tends to infinity as this number increases. Thus, the purpose of harmonic analysis is to define a way to have direct access to the amplitude of a periodic oscillation.

Now, assuming that the signal {X(t)} is the sum of a sinusoid with angular frequency $\hat{\omega}$ and amplitude μ, and a noise {ξ(t)}, which is the sum of other sinusoids and blank noise. It can be written:

$$X(t) = \mu e^{i\hat{\omega}t} + \xi(t) \qquad [56]$$

In considering the first K DPSS , we will call { $U_k(\omega)$} the Fourier discrete transform {$w_k(t)$}.

A minimum-square regression in the frequency domain provides an estimate $\hat{\mu}$ of the amplitude μ:

$$u(\hat{\omega}) = \frac{\sum_{K=0}^{K-1} U^*_k(0)\, yk(\hat{\omega})}{\sum_{K=0}^{K-1} |U_k(0)|^2} \qquad [57]$$

where the asterisk indicates complex conjugation. A Fisher test lets obtain a statistical reliability measure. This test is roughly based on the relationship between the "explained" variance from the model *[56],* and the residual variance. If you expand the variance of the model, you find that it is the sum of two terms:

$$\theta = \left|\hat{\mu}(\hat{\omega})\right|^2 \sum_{k=0}^{k-1} |U_k(0)|^2 \qquad [58]$$

and

$$\psi = \sum_{k=0}^{k-1} \left| y_k(\hat{\omega}) - \hat{\mu}(\hat{\omega}) U_k(0) \right|^2 \qquad [59]$$

which are the contribution to the "explained" and residual variance.

The random variable

$$F(\hat{\omega}) = (K-1)\frac{\theta}{\psi} \qquad [60]$$

follows a Fisher-Snedecor law with 2 and 2K - 2 degrees of freedom if the signal behaves like Gaussian. The value can be interpreted assuming that μ = 0, that is a "blank" series, and trying to reject this hypothesis with the lowest probability of error.

With this method small amplitude oscillations can be detected in a relatively short chronological series, with a high degree of statistical significance, or discard a large amplitude peak if fails at the F test, because the F value does not depend in first approximation on the value of μ (ω). Practically this means that this test is robust in case of blank noise and still gives reasonably good results with the coloured noise such as that present in many climatic series. Mann and Lees [64] have developed specific tests for red noise.

One of the main assumptions of this harmonic analysis technique is that the signal must provide separate periodic components. Otherwise, a continuous spectrum (in the case of red noise or a chaotic system) will be broken up into spurious lines with arbitrary frequencies and possibly with high F values. This is one of the disadvantages of the method, which can be partially avoided if a raw power spectrum is computed and evidence of spectral lines is detected. It is also very important to vary the bandwidth parameter ΩN and the number of windows, to ensure the stability of the frequency and amplitude estimates. ΩN = 4 is generally taken as an initial ΩN choice, which implies K ≤ 7 windows [52][53]. Subsequently the bandwidth can be modified according to the length of the time series and the frequencies to be investigated.

5.9.4 Wavelet

Most of the observed signals are not stationary and contain transient components that excite a wide frequency range in a small time interval. It seems that the classic Fourier analysis is not adequate for the treatment of these signals since all information on the temporal location of a given frequency is lost in the analytic process. Firstly, this led to the evolutionary spectral

analysis with mobile windows [65] [61] [66] and subsequently to more elaborate time-frequency representations, that is, the wavelet transforms. The wavelet analysis first time utilization independently was in physics by A. Grossmann [67], in geophysics by Morlet and in mathematics by Y. Meyer [68]. Their popularity in data processing is largely due to S. Mallat's work on digital imagery analysis [69]. The Wavelet analysis is a strong mathematical tools that provide a time–frequency representation of an analysed signal in the time domain [70]. Especially in meteorology and climatology, such analysis seems to be advantageous. For instance, in comparison with the Fourier transformation, it is possible to differentiate not only values of particular frequencies in non-stationary series, but also their location in time can be determined. On the other hand, the possibility of time–frequency representation is connected with a problem of resolution. Another advantage of wavelet analysis is that this method, contrary to the other types of transformation providing time–frequency presentation, like the windowed Fourier transformation, solves the dilemma of resolution to a certain extent. Wavelet transforms have been used in many studies, e.g.: to investigate trends in the central England temperature series [71]; to study El Nino–southern oscillation ENSO [72]; to study atmospheric blocking; to analyse, model and compute turbulence; to study hemispheric temperature series and the southern oscillation index [73]; to detect shifts in global temperature [74]; and to analyse variability in European temperatures [75].

The purpose of the wavelet decomposition is to study the time-frequency variations of a time series [75a]. In fact, detection of transient or intermittent components is possible. The main property of wavelets is that the analysing functions (wavelet functions) are localized both with respect to time and frequency that is oscillates in a finite time interval and then disappear, as they do their Fourier transforms, with respect to frequencies. On the other hand, both sine and cosine functions of Fourier transforms are perfectly localized in frequency, but oscillates endlessly over time. Therefore, a classical Fourier analysis will spread the

singularities of a chronological series across the power spectrum, creating staggered peaks or hiding true peaks, unless a time-frequency analysis is performed [75b].

Since Wavelet decomposition uses only dilatations and translations of a single function, it is optimal in the sense of the so-called time-frequency uncertainty principle [76], since the correlation between the duration and the average frequency is respected. However, wavelet transforms should not be in opposition to Fourier transforms: as we will see, these are two complementary instruments, and Fourier transforms are necessary for the calculation and interpretation of wavelet transforms.

Wavelet analysis decomposes a time series into component scales, thus allowing discrimination between fast oscillations that occur in short time scales and other slow ones that occur in longer time scales. More precisely, for a signal X and a given wavelet function ψ, the transform ψ-wavelet of X to a scale *a* and a time *b* is given by:

$$W_\psi X(a,b) = \frac{1}{\sqrt{a}} \int_{-\infty}^{\infty} \psi\left(\frac{t-b}{a}\right) X(t)dt \qquad [61]$$

This integral expresses an analysis of X, located around b and scaled by parameter a. Therefore, a wavelet analysis can be seen as a projection of the X signal on the non-orthogonal family of functions ψ(t - b)/a). Fourier analysis is simply a projection on the harmonic modes given by the sine and cosine functions. Fast and stable estimates of wavelet transforms can be obtained in the Fourier domain if the data are sampled regularly (Combes et al., 1989).

The wavelet decomposition is represented in an expansion plane (scale) - translation (time), with separate representations for the amplitudes and phases. An axis in a logarithmic scale allows better resolution of small-scale components that is high frequencies. In case of a purely monochromatic signal X(t) = A exp(i ω_0 t), the wavelet transform is as follows:

$$W_\psi X(a,b) = A\sqrt{\frac{a}{2\pi}}\,\hat{\psi}(a\omega_0)e^{i\omega_0 b} \qquad [62]$$

From this relation, the module of Wψ X does not depend on the translation time b and the phase of the wavelet transform on a scale a directly gives ω_0.

The amplitude A can be determined by dividing the maximum modulus of the Wavelet Transform:

$(W_\psi X)$ for $\sqrt{\frac{a}{2\pi}}\hat{\psi}(a\omega_0)$ *[63]*

This means that in such a representation, the wavelet transform of a purely periodic signal is a constant-scale peak and the phase increments should indicate exactly the period of oscillation [76].

A practical problem of Wavelet analysis consists of the edge effects in the transform [69], for which no satisfactory correction is applicable. Therefore, the wavelet analysis is truncated at the ends, based on the wavelet function scales that is the larger the scale analysed, the greater the truncation will be.

This adds restrictions on the times and scales analysed and avoid the possibility of occurrence of spurious results. However, with this precaution it is no longer possible to analyse features at a relatively large scale (or low frequencies). For this reason, in order to perform a correct and useful wavelet analysis, it is important to have very long time series.

6

Analysis of historical climatic series in Sicily: an approach using Wavelet analysis

The wavelet analysis represents the powerful instrument to extract information from a time series. It can be used to analyse time series that contain non-stationary power at many different frequencies. In the case of meteorological and climatological series, this type of analysis is particularly appreciated because it is able to extract important information from the signal. For example, if compared to the simple Fourier transform, the wavelets analysis allows to find not only the value of certain frequencies in a non-stationary series, but also to identify the time interval in which these frequencies are present and predominant. A wavelet function is a function having a wave shape and a limited but flexible length with a mean value that is equal to zero, and is localized in both time and frequency domains.

6.1 The Wavelet Transform (WT)

Mathematical transformations are applied to signals to obtain further information from that signal that is not readily available in the raw signal. There are several transformations that can be applied, among which the Fourier transforms are probably by far the most popular. In order to maintain time and frequency localization in a signal analysis, one possibility would be to do a Windowed Fourier Transform (WFT), using a certain window size and sliding it along in time, computing the Fast Fourier Transform (FFT) at each time using only the data within the window. This would solve the frequency localization problem, but would still be

dependent on the window size used. The main problem with the WFT is the inconsistent treatment of different frequencies: at low frequencies there are so few oscillations within the window that the frequency localization is lost, while at high frequencies there are so many oscillations that the time localization is lost. Finally, the WFT relies on the assumption that the signal can be decomposed into sinusoidal components. Thus, to measure the stationarity of a time series is necessary to calculate the running variance using a fixed-width window. Despite the disadvantage of using a fixed-width window, the analysis could be repeated with a variety of window widths. By smoothly varying the window width, a picture of the changes in variance versus both time and window width could be built. The obvious problem with this technique is the simple "boxcar" shape of the window function, which introduces edge effects such as ringing. Using such a black-box-car, there will be no information on what is going on within the box, but only recover the average energy. Wavelet analysis attempts to solve these problems by decomposing or transforming a one-dimensional time series into a diffuse two-dimensional time-frequency image simultaneously. Then, it is possible to get information on both the amplitude of any "periodic" signals within the series, and how this amplitude varies with time. An example of a wave "packet", of finite duration and with a specific frequency, is shown in Fig. 26. Such a shape could be used as a window function for the analysis of variance. This "Wavelet" has the advantage of incorporating a wave of a certain period, as well as being finite in extent. In fact, the wavelet shown in Fig. 26 (called the Morlet wavelet) is nothing more than a Sine wave multiplied by a Gaussian envelope.

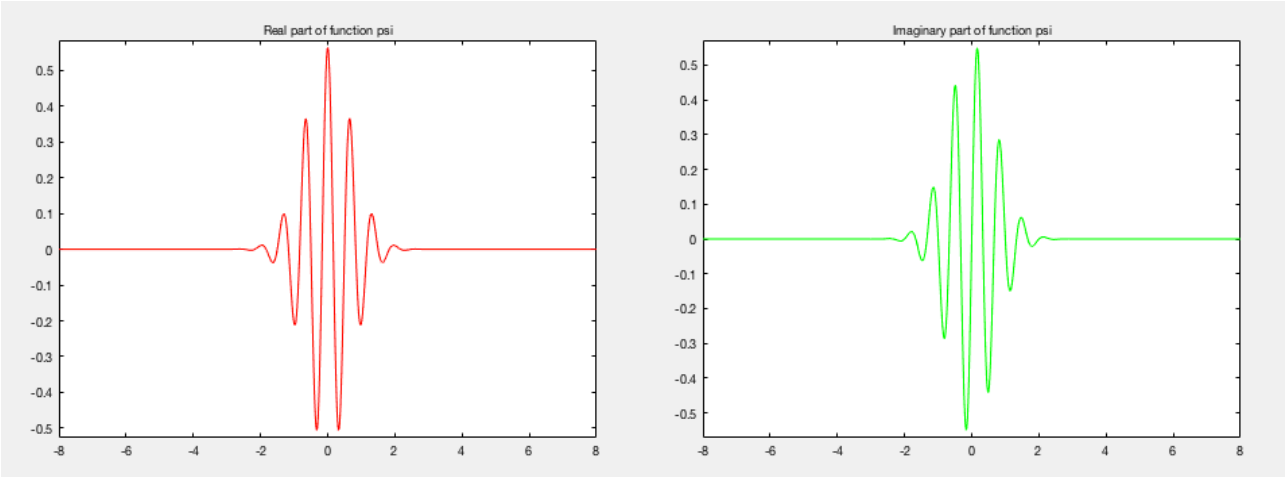

Fig.26 Morlet Wavelet in which the real part is in red and the imaginary in green

Assuming that the total width of this Wavelet is about 10 years, it is possible to find the correlation between this curve and the first 10 years of the time series object of analysis. This single number gives a measure of the projection of this wave packet on the data during the 10 years period. By sliding this wavelet along the time series, a new time series of the projection amplitude versus time can be constructed. Finally, the "scale" of the wavelet can be varied by changing its width. This is the real advantage of Wavelet analysis over a moving Fourier spectrum. For a window of a certain width, the sliding FFT is fitting different numbers of waves; i.e., there can be many high-frequency waves within a window, while the same window can only contain a few (or less than one) low-frequency waves. The wavelet analysis always uses a wavelet of the exact same shape, only the size scales up or down with the size of the window. In addition to the amplitude of any periodic signals, it is worth to get information on the phase. In practice, the Morlet wavelet shown in Fig. 28 is defined as the product of a complex exponential wave and a Gaussian envelope:

$$\Psi_0(\eta) = \pi^{-1/4} e^{\iota\omega_0\eta} e^{-\eta^2/2} \qquad [64]$$

where $\Psi_0(\eta)$ is the wavelet value at non-dimensional time η, and ω_0 is the non-dimensional frequency. This is the basic wavelet function, but it will be now needed some way to change

the overall size as well as slide the entire wavelet along in time. Thus, the "scaled wavelets" are defined as:

$$\Psi\left[\frac{(n'-n)\delta t}{s}\right] = \left(\frac{\delta t}{s}\right)^{1/2}\Psi_0\left[\frac{(n'-n)\delta t}{s}\right] \qquad [65]$$

where *s* is the "dilation" parameter used to change the scale, and *n* is the translation parameter used to slide in time. The factor of $s^{-1/2}$ is a normalization to keep the total energy of the scaled wavelet constant. We are given a time series X, with values of *xn*, at time index *n*. Each value is separated in time by a constant time interval δt. The wavelet transform Wn(s) is just the inner product (or convolution) of the wavelet function with the original time series:

$$W_n(s) = \sum_{n'=0}^{N=1} x_{n'}\Psi * \left[\frac{(n'-n)\delta t}{s}\right] \qquad [66]$$

where the asterisk (*) denotes complex conjugate. The above integral can be evaluated for various values of the scale s (usually taken to be multiples of the lowest possible frequency), as well as all values of n between the start and end dates. A two-dimensional picture of the variability can then be constructed by plotting the wavelet amplitude and phase. Then, a time series can be decomposed into time-frequency phase space using a typical (mother) wavelet. Wavelet transforms involve shifting forward the wavelet in a number of steps along an entire time series, and generating a wavelet coefficient at each step. This measures the level of correlation of the wavelet to the signal in each section. The variation in the coefficients indicates the shifting of similarity of the wavelet with the original signal in time and frequency. This process is then repeated for each scaled version of the wavelet, in order to produce sets of wavelet coefficients at the different scales. The lower scales represent the compressed version of the mother wavelet, and correspond to the rapidly changing features or high-frequency components of the signal. The higher scales are the stretched version of a wavelet, and their wavelet coefficients are identified as slowly changing or low frequency components of the signal. Therefore, wavelet transforms analyse trends in time series by

separating its short, medium, and long-period components [78]. WT can be performed using two approaches: Continuous Wavelet Transform (CWT) and Discrete Wavelet Transform (DWT). CWT operates on smooth continuous functions and can detect and decompose signals on all scales. Examples of mother wavelets used in CWT are the Morlet and Paul wavelets, among others. DWT may use mother functions such as the Mallat or Daubechies, which operate on scales that have discrete numbers. The scales and locations used in DWT are normally based on a dyadic arrangement (i.e. integer powers of two) [79].

6.2 Data set description

The work carried out during the research doctorate consisted mainly in the climatic analysis of the historical series of temperatures and rainfall available for Sicily.

Sicily, due to its geographical position in the centre of the Mediterranean, is a privileged place of observation. Its relative proximity to the African desert coasts and the future climatic projections for the Mediterranean area, make it a very sensitive place to desertification processes and therefore is well suited to the study of climate change.

The databases used were different, as well as the data analysed, different by type of collection, sampling methods and spatial distribution. A first subdivision of the analysed data can be made between data coming directly from meteorological stations and reconstructed data from the main world databases.

In the first case, the data analysed during the research activities comes from some of the meteorological stations of the Italian Air Force belonging to the Sicilian observational synoptic network. Specifically, were used data collected from the stations of Palermo (WMO ID 16405), Messina (WMO ID 16420), Cozzo Spadaro (WMO ID 16480) and Trapani (WMO 16429) (Fig.27 and Table 1) which are four coastal stations located at short distance from the

sea and which altogether represents a significant sample able to describe the characteristics of the Mediterranean climate.

The temperature and precipitation data of Messina and Cozzo Spadaro under analysis were extracted directly from SYNOP messages, while the Palermo and Trapani series were downloaded from the SCIA database (National System for the collection, processing and dissemination of Climatic data of Environmental Interest) of the Institute for Environmental Protection and Research (ISPRA). Palermo data series is the longest under analysis, which ranges between 1861 and 2016, while the others are shorter, having started the observations activity only from the fifties.

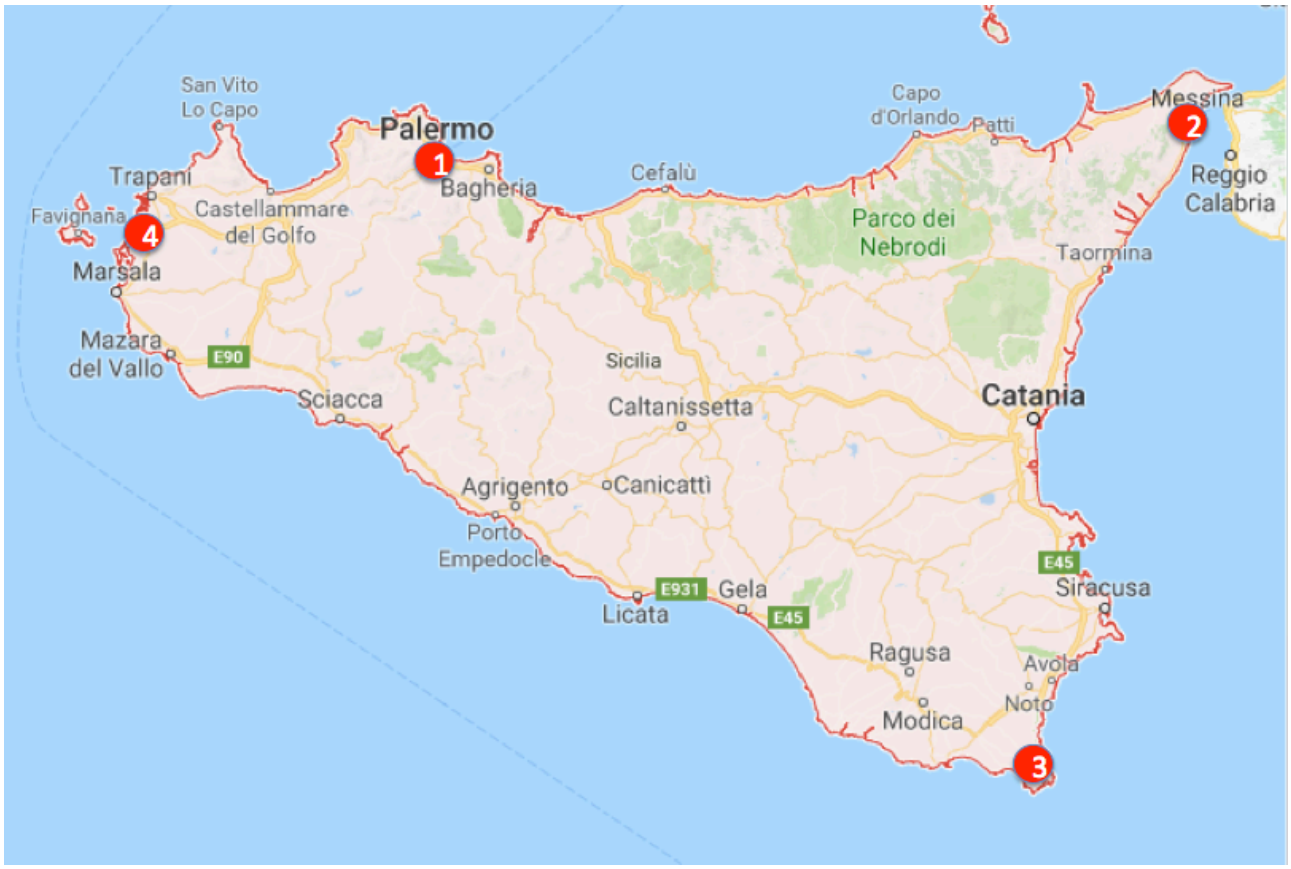

Fig.27 Geographic position of the four weather station analysed

WMO ID	Station Name	Latitude (°)	Longitude (°)	Elevation (m a.s.l.)	Observation Period
16405	Palermo	38°07'00"	13°18'44"	36	1865-2016
16420	Messina	38°12'02"	15°33'11"	54	1962-2016
16480	Cozzo Spadaro	36°41'10"	15°07'57"	44	1952-2016
16429	Trapani-Birgi	37°54'50"	12°29'28"	4	1962-2016

Table 1: Meteorological stations recording temperature and precipitations data used in this study

To make the study as complete as possible and extended to the entire Sicilian territory was added also the analysis of the historical series reconstructed by the Climatic Research Unit (CRU) of the University of East Anglia in Norwich, England [77]. It consists of an updated gridded climate dataset (referred to as CRU TS4.10) from monthly observations at meteorological stations across the world's land areas. Station anomalies (from 1961 to 1990 means) were interpolated into 0.5° latitude/longitude grid cells covering the global land surface (excluding Antarctica), and combined with an existing climatology to obtain absolute monthly values. The dataset includes six mostly independent climate variables (mean temperature, diurnal temperature range, precipitation, wet-day frequency, vapor pressure and cloud cover). This gridded product will be publicly available, including the input station series (http://www.cru.uea.ac.uk/ and http://badc.nerc.ac.uk/data/cru/). For the purposes of the research activities, were taken the temperature and precipitation data between 1901 and 2016 of 8 grid points falling within Sicily and highlighted in figure 28 by purple rectangles (Fig. 28).

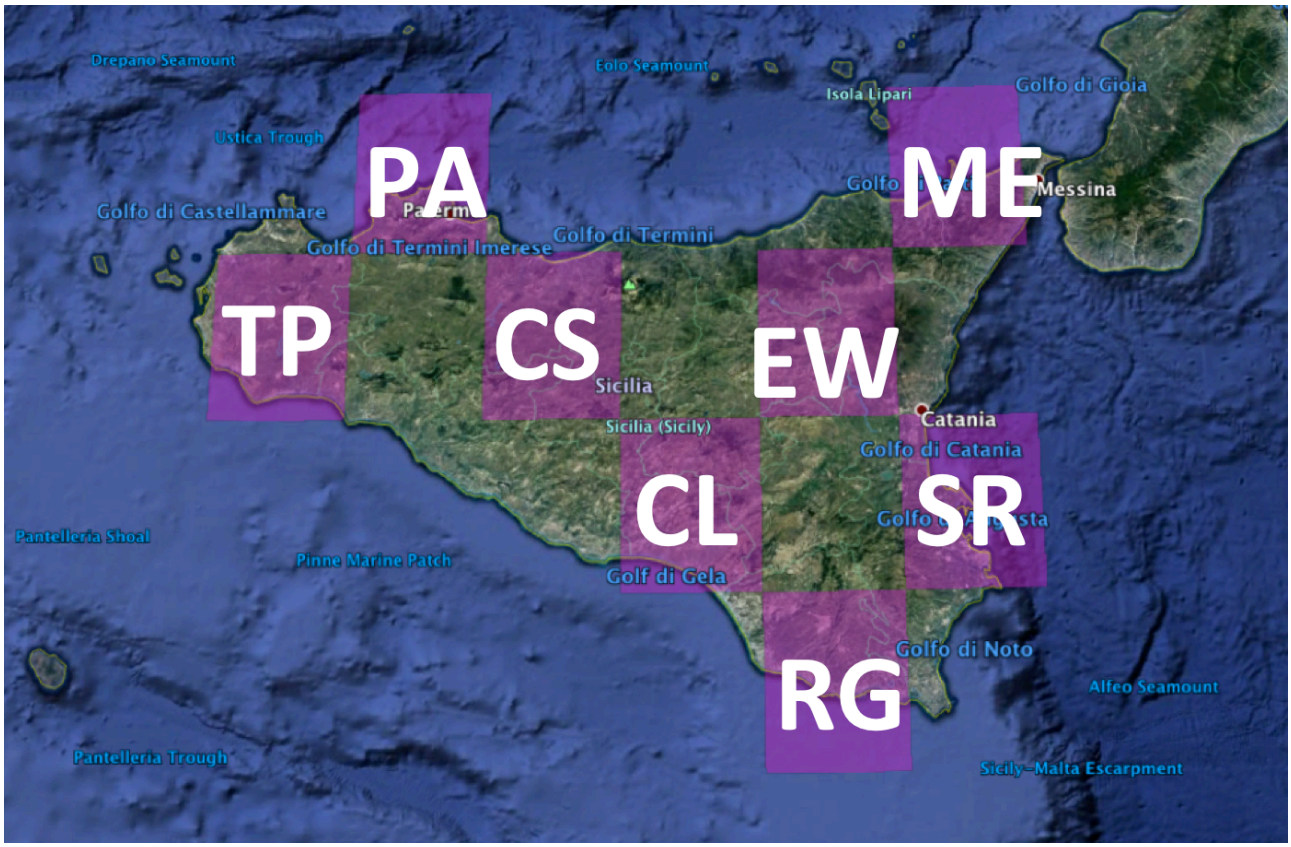

Fig.28 Grid points of CRU TS4.10 dataset.

6.3 Sicilian meteorological data preliminary statistical analysis.

In order to have an overall picture of the climate of Sicily, which can be deduced from the collected data, some classical statistical analyses were carried out on the latter. Data shown in the tables below is organized in observed (Tab. 2 and 3) and reconstructed data.

	Palermo	Trapani	Messina	Cozzo
N	636	636	636	636
Min	9,3	8,7	8,4	9,8
Max	28,3	27,7	30,1	29,1
Sum	11534,5	11271,9	12009,6	11882,9
Mean	18,13601	17,72311	18,88302	18,68381
Std. error	0,199866	0,2052412	0,2195305	0,2080613
Variance	25,40593	26,79082	30,65114	27,53213
Stand. dev	5,04043	5,175985	5,536348	5,247107
Median	17,55	17,15	17,75	17,95
25 prcntil	13,5	13	13,725	13,725
75 prcntil	22,975	22,7	24	23,6
Skewness	0,1634714	0,1755454	0,2281344	0,2123291
Kurtosis	-1,333901	-1,353809	-1,302894	-1,336928
Geom. mean	17,42612	16,95703	18,06799	17,94448
Coeff. var	27,79239	29,20472	29,31919	28,08372

Table 2. Mean monthly temperature summary statistics observed data

	Palermo	Trapani	Messina	Cozzo
N	636	636	636	636
Min	0	0	0	0
Max	294	300	371,3	332,8
Sum	32479,5	25459,8	46045,6	26694,5
Mean	51,0684	40,03113	72,39874	41,97248
Std. error	1,842675	1,617042	2,367882	2,078602
Variance	2159,507	1663,029	3565,967	2747,893
Stand. dev	46,47049	40,78026	59,71572	52,42035
Median	41,15	30,2	61,8	22,8
25 prcntil	11,075	6,325	21,5	3,125
75 prcntil	78,95	64,05	108,6	59,725
Skewness	1,105437	1,582961	1,032682	1,975014
Kurtosis	1,401456	4,216884	1,453632	4,705235
Geom. mean	0	0	0	0
Coeff. var	90,99657	101,8714	82,48171	124,8922

Table 3. Mean monthly precipitations summary statistics observed data

	3825-1525(ME)	3825_1325 (PA)	3775_1275 (TP)	3675_1475 (RG)	3775_1325(CS)	3725_1425(CL)	3725_1525(SR)	3775_1475(EW)
N	1392	1392	1392	1392	1392	1392	1392	1392
Min	7	6,6	8	8,4	6,3	7,5	8	4,6
Max	28,3	27,8	27,7	28,2	26,8	27,6	28,4	25,8
Sum	24035,3	23394,3	24285,5	24641,7	22405,3	23668,2	24550,8	20479,2
Mean	17,26674	16,80625	17,44648	17,70237	16,09576	17,00302	17,63707	14,71207
Std. error	0,1509436	0,1520557	0,1385155	0,1425645	0,1453542	0,1463151	0,1464507	0,1528672
Variance	31,71528	32,18434	26,70765	28,29191	29,40994	29,80008	29,85536	32,52878
Stand. dev	5,631632	5,673124	5,167945	5,319014	5,423093	5,458945	5,464006	5,703401
Median	16,3	16	16,7	17	15,3	16,15	16,9	13,8
25 prcntil	12,2	11,6	12,7	12,8	11,2	12	12,6	9,5
75 prcntil	22,7	22,3	22,5	22,975	21,3	22,375	23	20,2
Skewness	0,2142845	0,1689753	0,1690458	0,1954842	0,202654	0,1909554	0,1760724	0,2124259
Kurtosis	-5,815064	-5,786834	-5,778344	-5,775657	-5,781028	-5,762068	-5,788339	-5,793211
Geom. mean	16,33382	15,81973	16,66747	16,8935	15,16335	16,11074	16,77407	13,56753
Coeff. var	32,61549	33,75604	29,6217	30,0469	33,69268	32,10574	30,98024	38,76682

Table 4. Mean monthly temperature summary statistics CRU database

	3825_1525(ME)	3825_1325(PA)	3775_1275(TP)	3675_1475(RG)	3775_1375(CS)	3725_1425(CL)	3725_1525(SR)	3775_1475(EW)
N	1392	1392	1392	1392	1392	1392	1392	1392
Min	0	0	0	0	0	0	0	0
Max	332,4	204,4	222,6	293,5	220,1	259,4	312,9	297,6
Sum	82165,1	60237,4	58527,6	60192,6	63423,7	60981,5	68122,3	73763,2
Mean	59,02665	43,27399	42,04569	43,24181	45,563	43,80855	48,93843	52,9908
Std. error	1,337693	0,9909383	0,9874176	1,259841	1,074258	1,161008	1,358777	1,251979
Variance	2490,876	1366,887	1357,191	2209,38	1606,41	1876,332	2570,014	2181,893
Stand. dev	49,90868	36,97143	36,84007	47,00404	40,08004	43,31665	50,69531	46,71074
Median	47,05	35,85	34,4	28,5	37,25	32,75	33,9	42,3
25 prcntil	18,9	11,025	10,525	5,425	12,6	9	8,7	16,8
75 prcntil	88,675	65,875	65,65	64,75	68,5	64,125	73,65	78,45
Skewness	1,164974	0,9052645	1,025228	1,577034	1,169984	1,432703	1,54514	1,30013
Kurtosis	-10,81698	-8,788992	-9,626248	-12,74073	-10,34486	-11,89389	-12,67977	-11,47881
Geom. mean	0	0	0	0	0	0	0	0
Coeff. var	84,55278	85,43568	87,61914	108,7004	87,9662	98,87715	103,59	88,14876

Table 5. Mean monthly precipitations summary statistics CRU database

Graphs for each grid point compares the average temperatures and monthly precipitation. These graphs allow an immediate reading and evaluation of both the length and the intensity of the periods of aridity that in the summer season afflict the island. The area obtained from

the intersection of both the precipitations and the temperatures curve represents an index of aridity (Fig. 29).

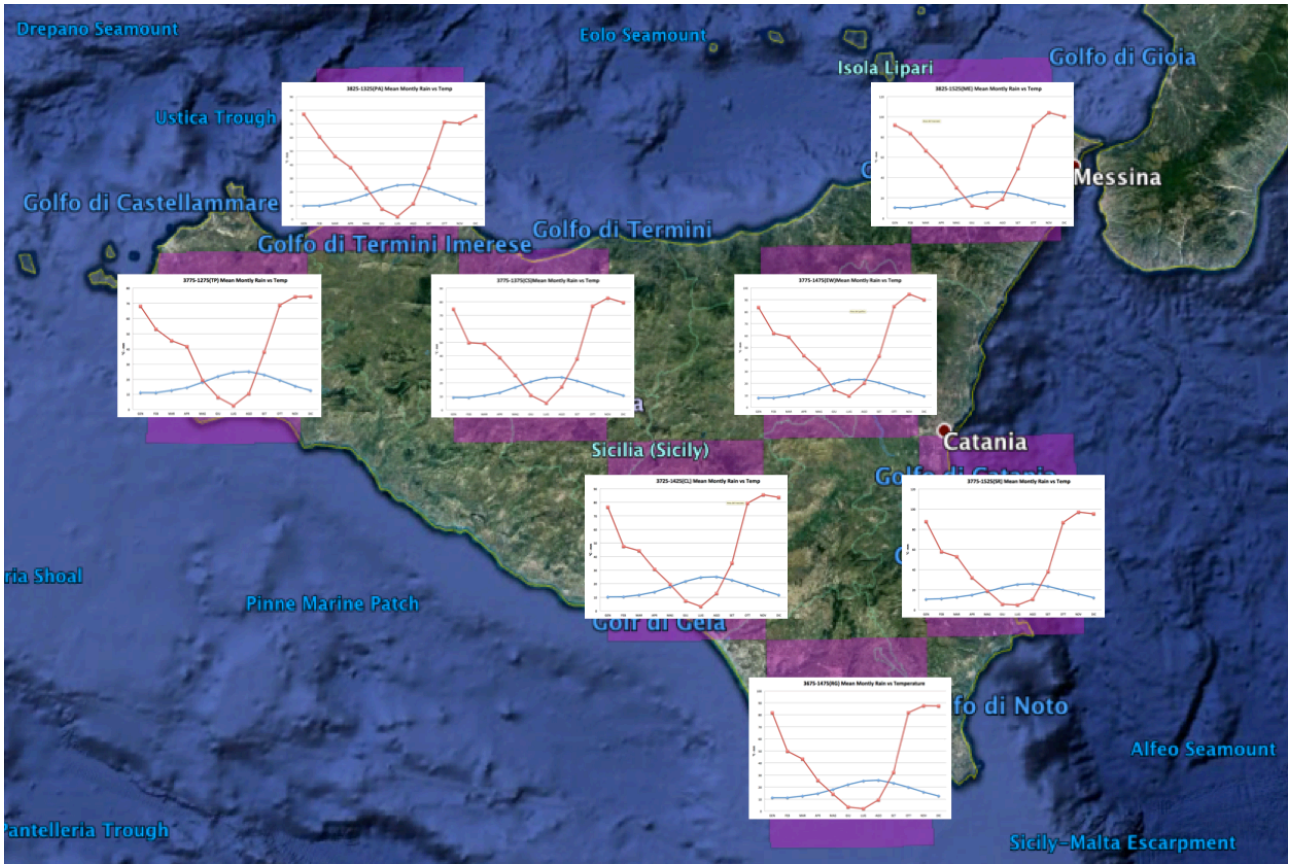

Fig. 29 Temperature-Precipitation graphs on the CRU data grid points.

A careful analysis of Fig. 29 shows that the southern coast of Sicily is the one most subject to longer periods of aridity, being the intersection of the curves between May and mid-September. The northeastern area is the richest in precipitation as shown by the sectors EW and ME graphs holding the lowest intersection areas. Further evidence that emerges from the figure, which shows a "step" in the precipitation graph between the months of March and April that is absent in the most northern latitude areas facing the Tyrrhenian Sea.

It is possible to justify this trend according to two synoptic schemes. The first considers a precipitation contribution from the southern sectors during the spring months, which are absent along the northern belt. The second one considers that the first spring rainfall coming from the North Atlantic in the months of February and March, reaches mainly the Tyrrhenian

belt not reaching the rest of the island because of the Apennine chain that is a real orographic block. In the following months, between March and April, these perturbations grows intensity allowing going beyond the northern Apennine range raining over the whole island.

6.4 Wavelet analysis of rainfall

The conventional discrete wavelet analysis of signals was performed on each precipitation time series using the multilevel 1-D wavelet decomposition function in MATLAB (MATLAB Wavelet Toolbox). This produces the wavelet transform of the input data at all dyadic scales. The DWT relies more on down-sampling, which is excellent for de-noising signals [80]. Decomposing the signals using specified filters (wavelet and scaling functions) produces two types of coefficients: the approximation or residual, and detail vectors [81]. These coefficients resulted from the convolution of the original signal with a low-pass filter and a high-pass filter. The low-pass filter is the scaling function and the high-pass filter is the wavelet function. The convolutions of signals with the low-pass filter produced the approximation coefficients, which represent low-frequency components of the original signal. Convolutions with the high-pass filter produced the detail coefficients, which represent the high-frequency components [82]. The process of signal decomposition was repeated multiple times, decomposing the original signal into several different lower-resolution components. In this study, the Daubechies (db) wavelets were used. They are commonly used for the DWT in hydro-meteorological wavelet-based studies. The numbers of data points used in this study were from the observed and CRU monthly datasets. For the observed data set the number of point is 636, covering the period from 1962 to 2014, while for CRU data set, it cover the period 1900-2016 and there are 1392 data points. In order to avoid unnecessary levels of data decomposition, the number of decomposition levels had to be determined first. This number is based upon the number of data points, as well as the mother wavelet used. The highest

decomposition level should correspond to the data point at which the last subsampling becomes smaller than the filter length [83]. According to [83], if *v* is the number of vanishing moments of a *db* wavelet and *n* is the number of data points in a monthly-based time series, the maximum decomposition level *L* is calculated using the following equation:

$$L = \frac{Log(\frac{n}{2v-1})}{Log(2)} \qquad [67]$$

Using a Daubechies 6 wavelet, which has a 12-point filter length, the resulting maximum level of decomposition is equal to 6 for observed data set and 7 for CRU data set. For this reason, each monthly average total precipitation dataset was decomposed into seven lower resolution levels via the DWT approach. The detail components represent the 2-month periodicity (D1), 4-month (D2), 8-month (D3) till 128-month periodicity (D7). The A7 represents the approximation component at the seven level of decomposition. The results obtained for each grid point of CRU data are shown in the figures from 30 to 37.

GRID POINT 3775-1275 (TP) CRU Dataset Precipitation DWT decomposition

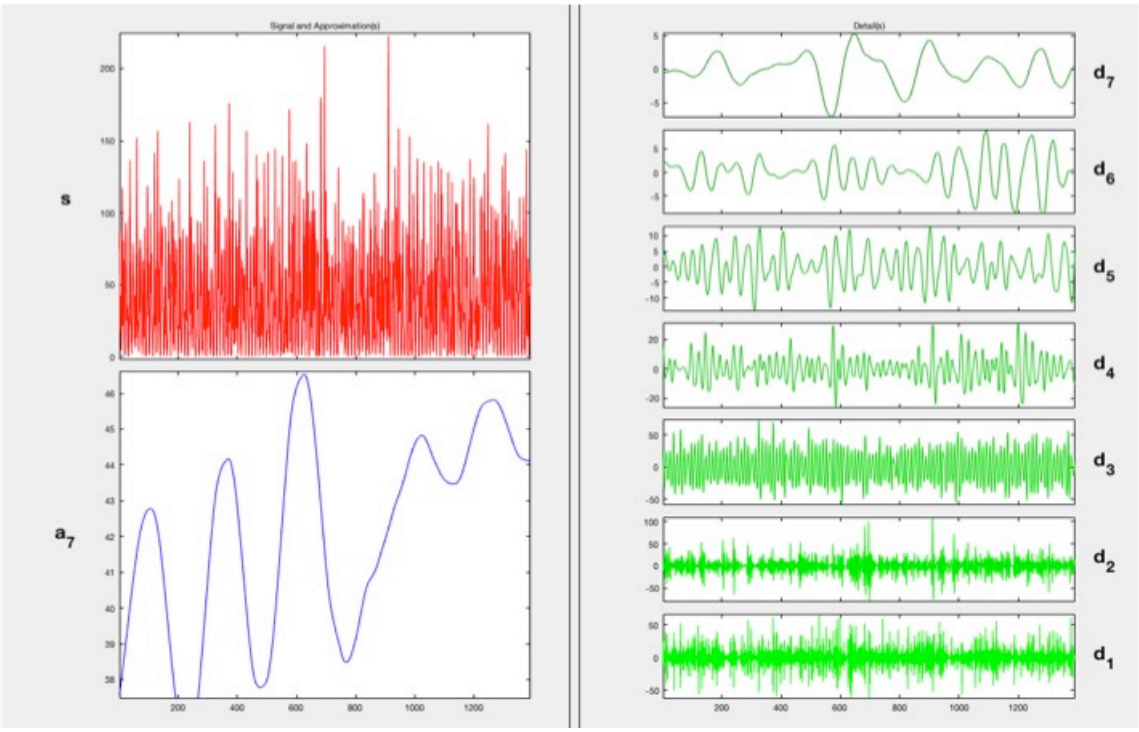

GRID POINT 3775-1275 (TP) CRU Dataset Precipitation DWT decomposition
Signal (RED) and A7 approx. Comp. (BLUE)

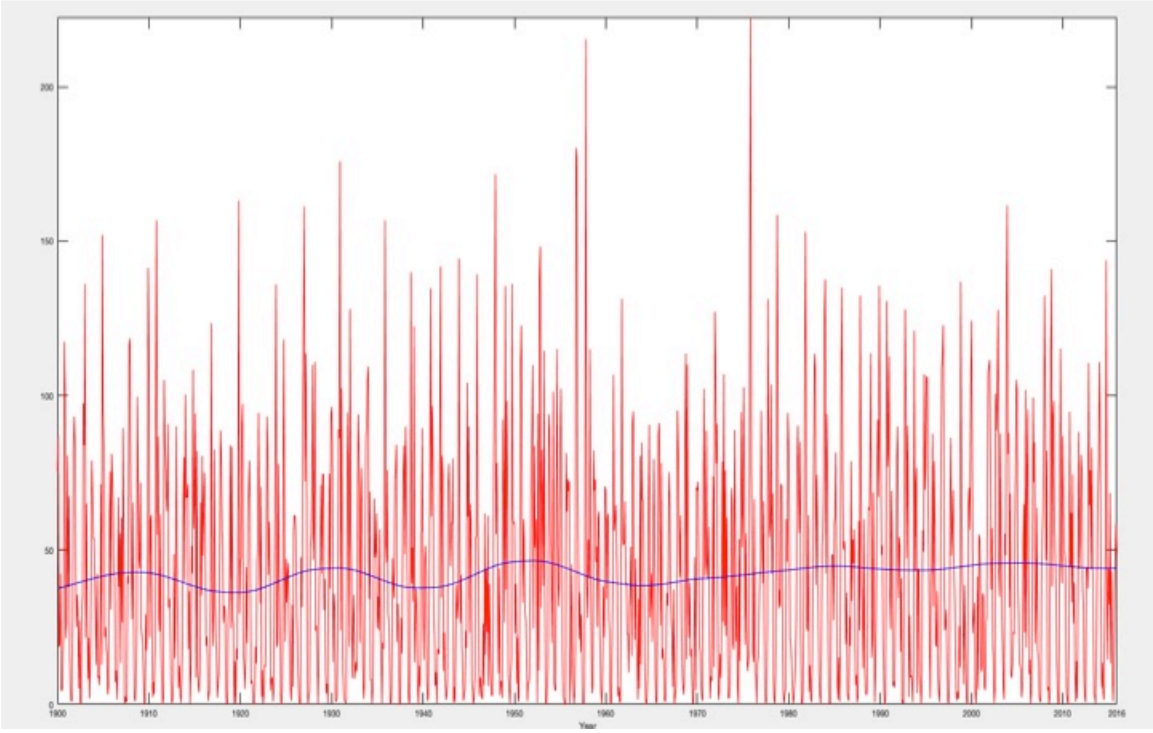

Fig.30 DWT of Mean Monthly Precipitation with db6 at 7 level of decomposition (up) and Signal (red) with over imposed A7 approximation component (blue)

GRID POINT 3725-1525 (SR) CRU Dataset Precipitation DWT decomposition

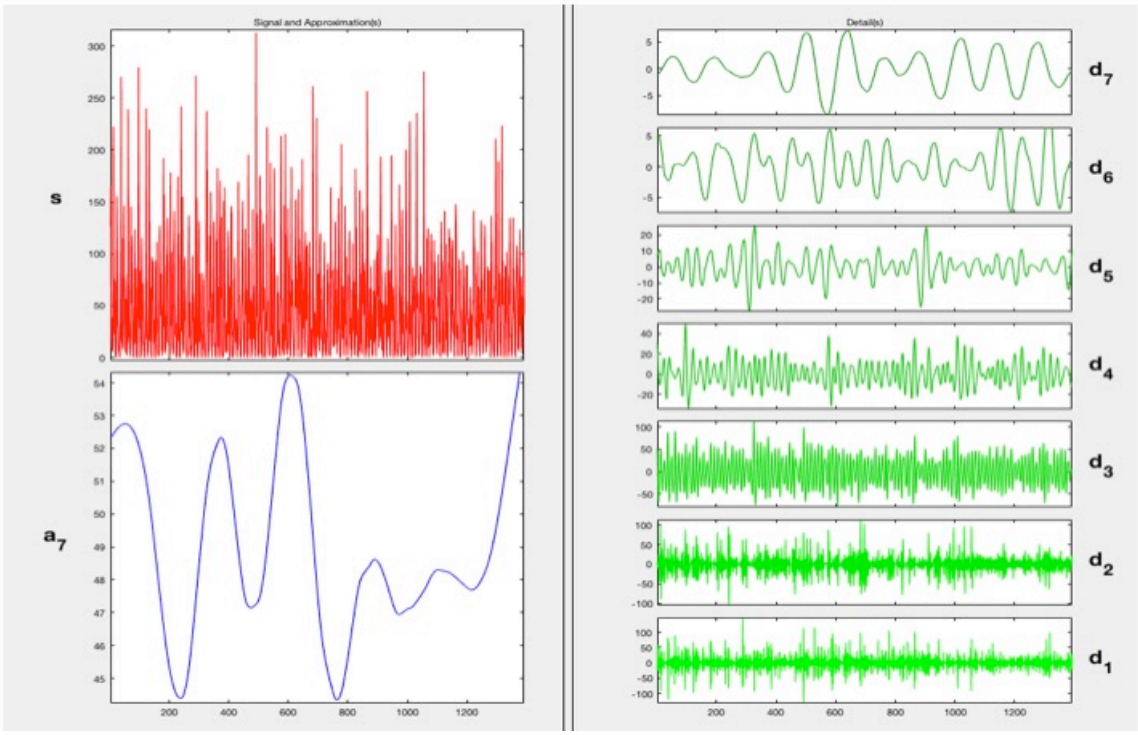

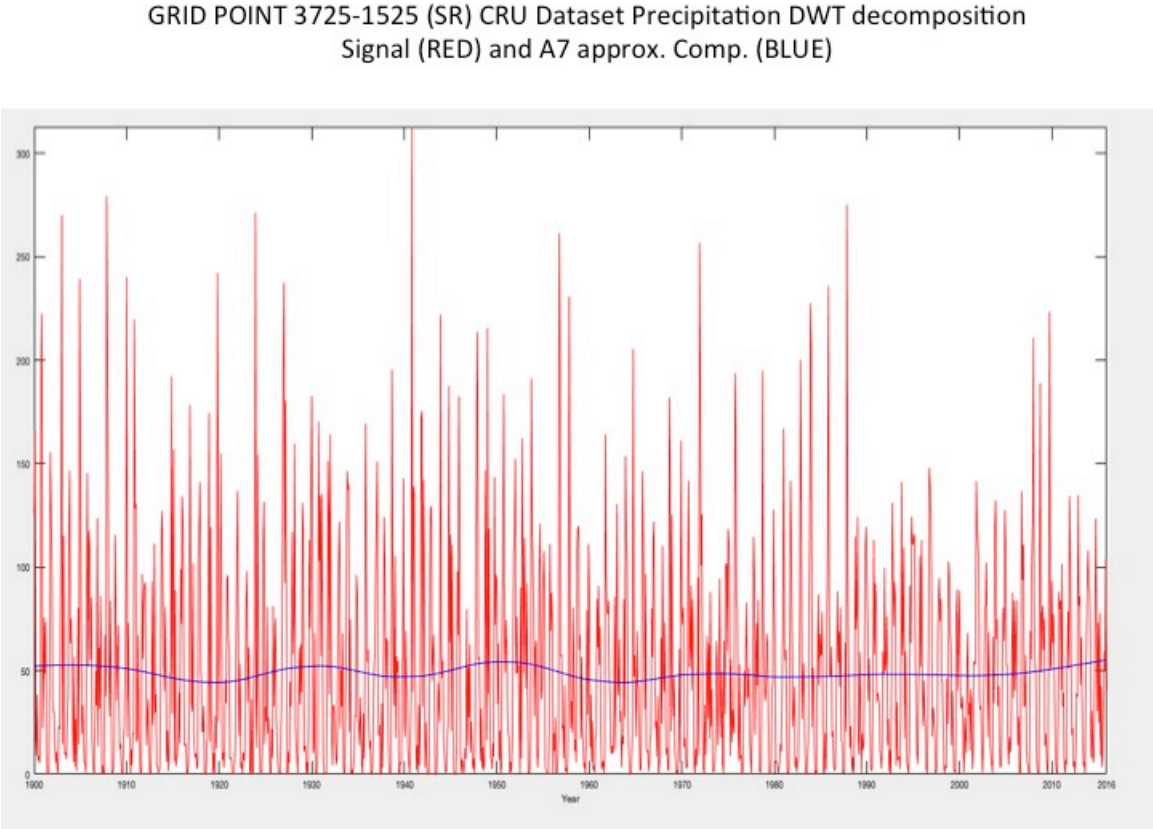

Fig.31 DWT of Mean Monthly Precipitation with db6 at 7 level of decomposition (up) and Signal (red) with over imposed A7 approximation component (blue)

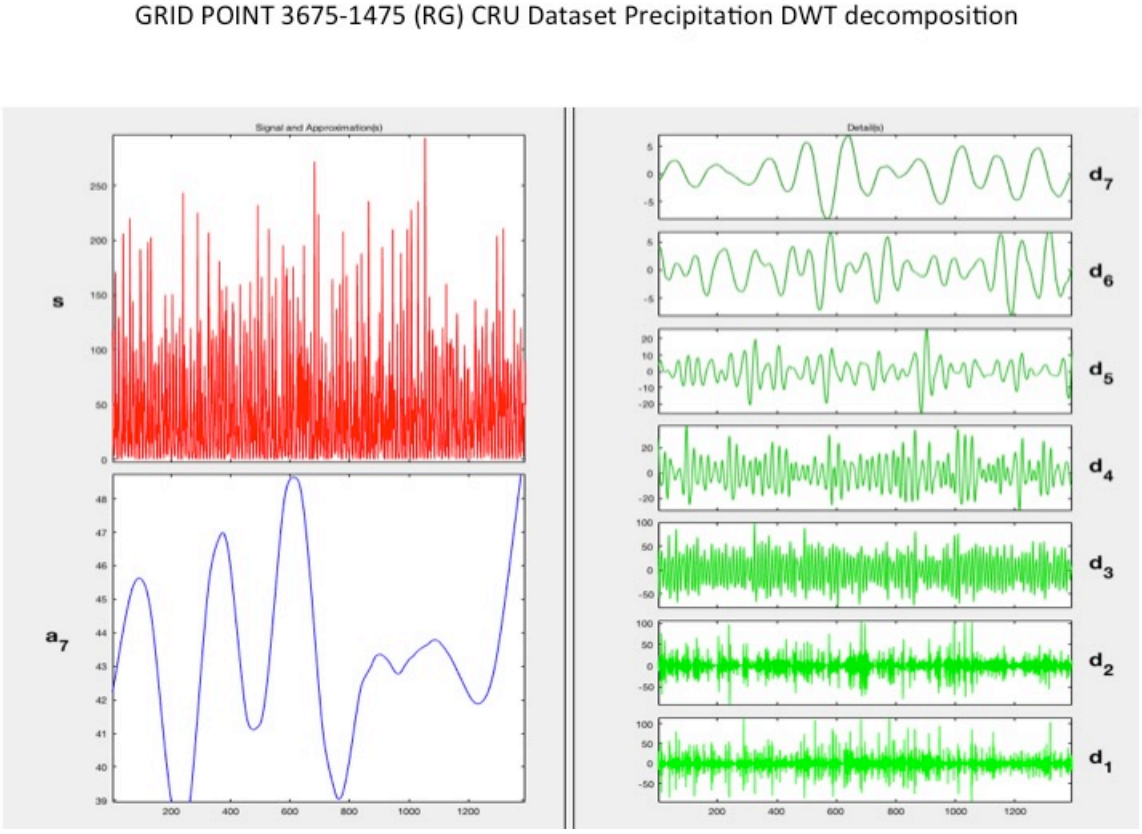

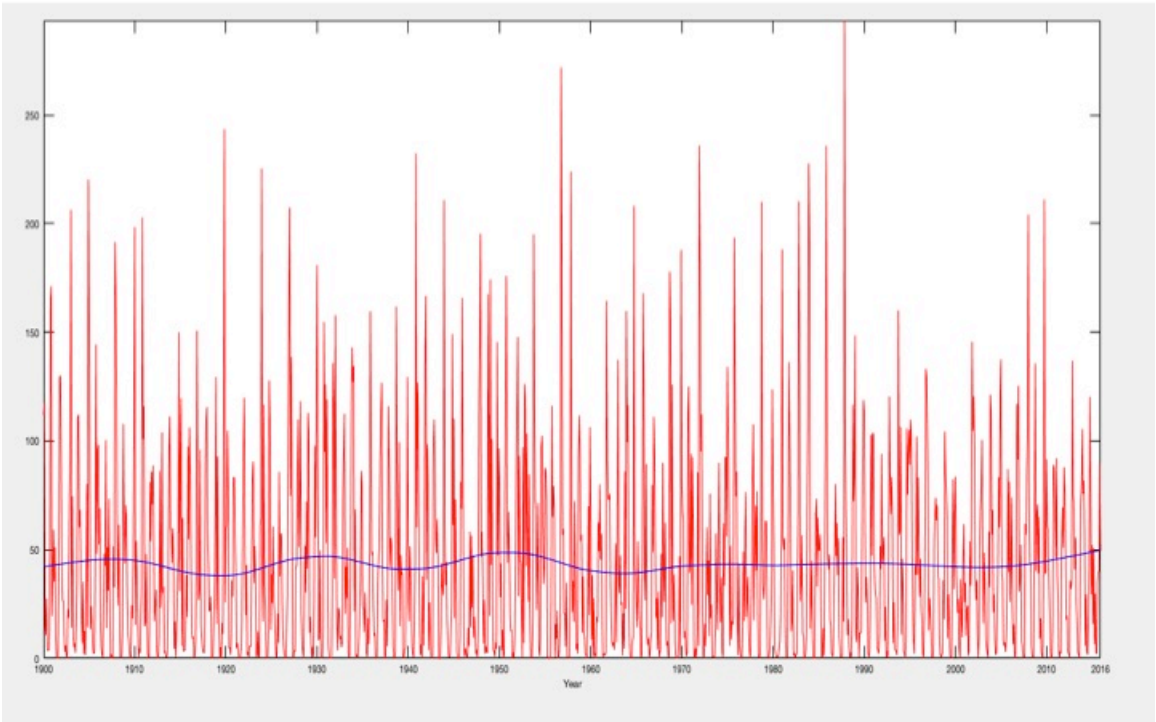

Fig.32 DWT of Mean Monthly Precipitation with db6 at 7 level of decomposition (up) and Signal (red) with over imposed A7 approximation component (blue)

GRID POINT 3825-1325 (PA) CRU Dataset Precipitation DWT decomposition

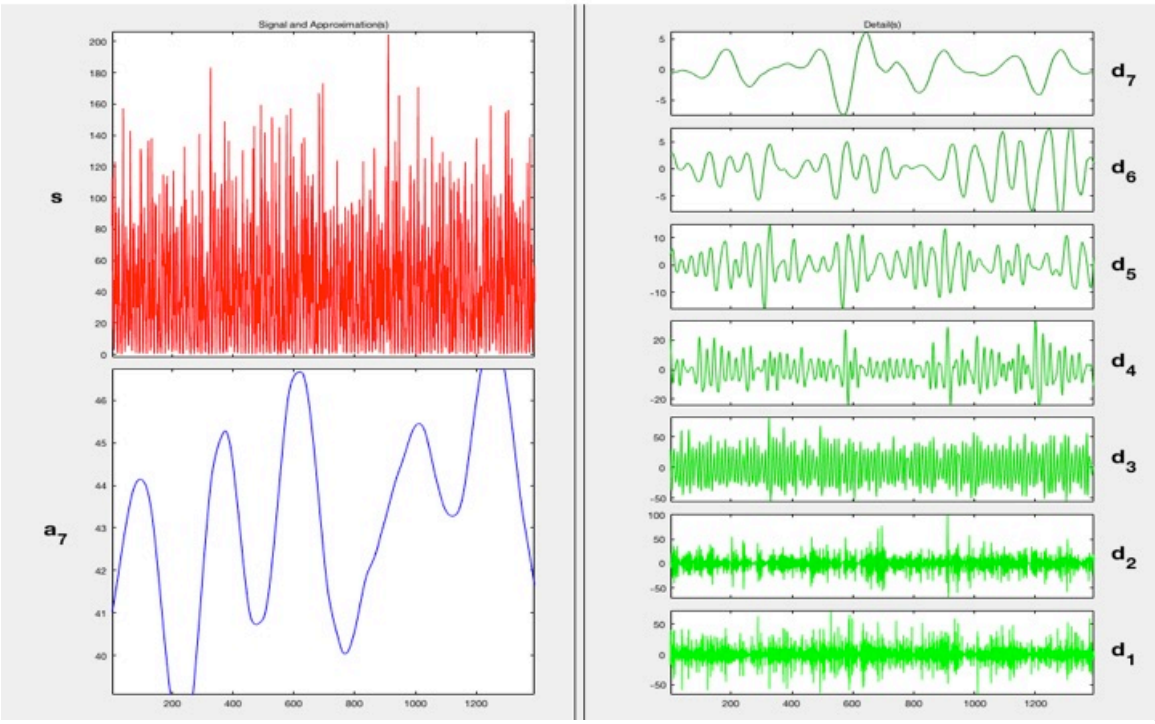

GRID POINT 3825-1325 (RG) CRU Dataset Precipitation DWT decomposition
Signal (RED) and A7 approx. Comp. (BLUE)

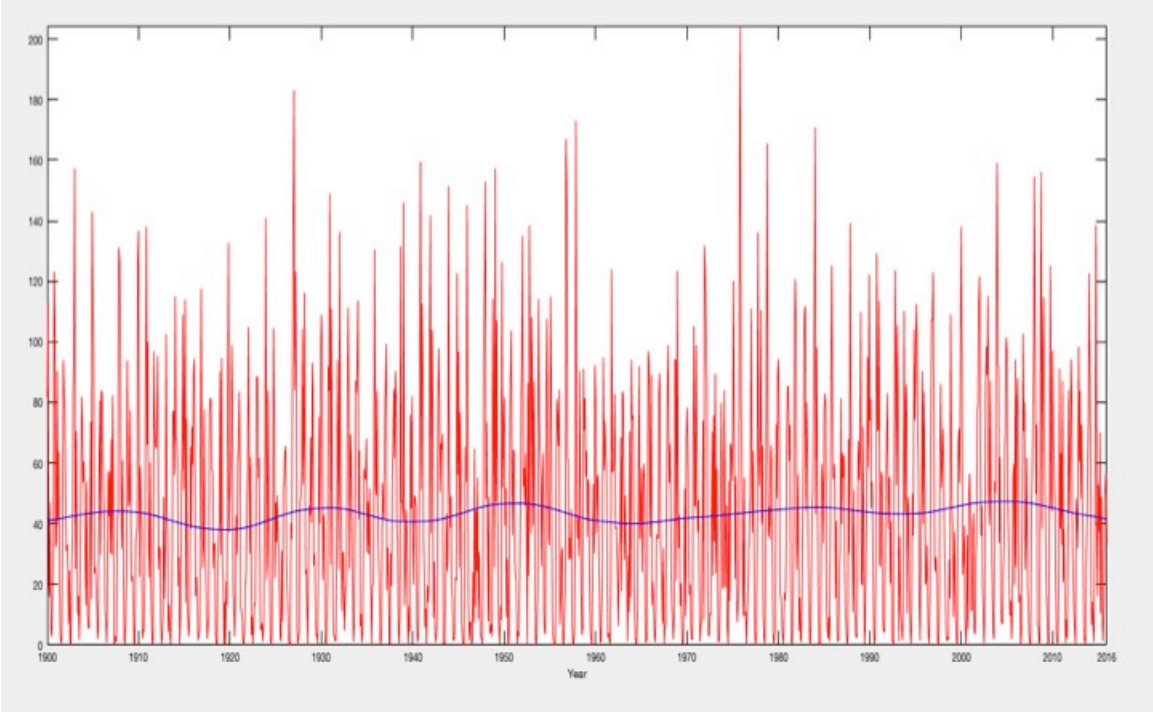

Fig.33 DWT of Mean Monthly Precipitation with db6 at 7 level of decomposition (up) and Signal (red) with over imposed A7 approximation component (blue)

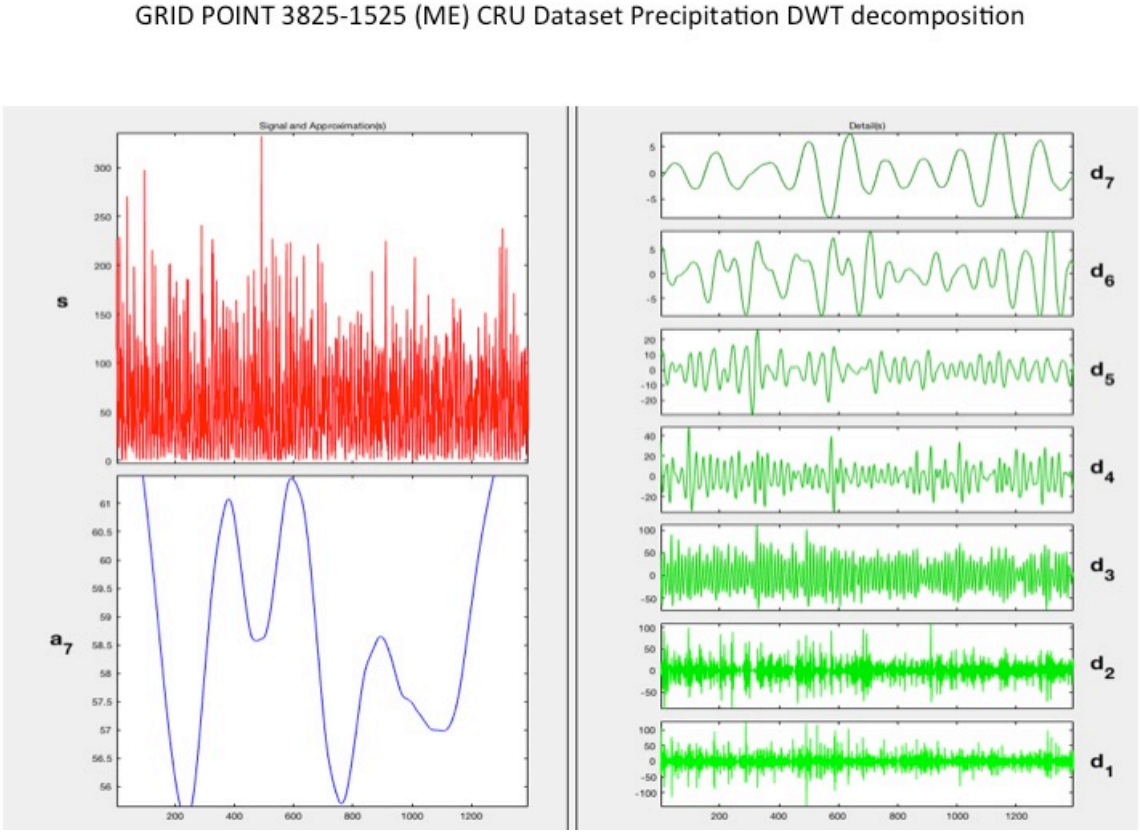

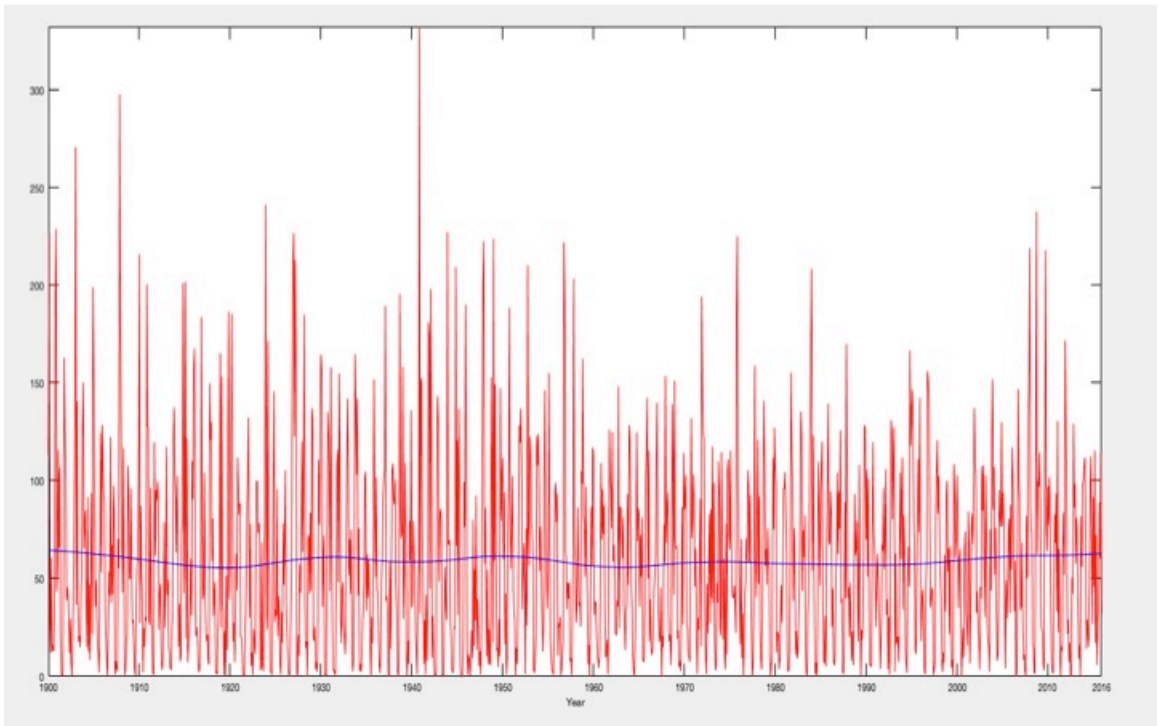

Fig.34 DWT of Mean Monthly Precipitation with db6 at 7 level of decomposition (up) and Signal (red) with over imposed A7 approximation component (blue)

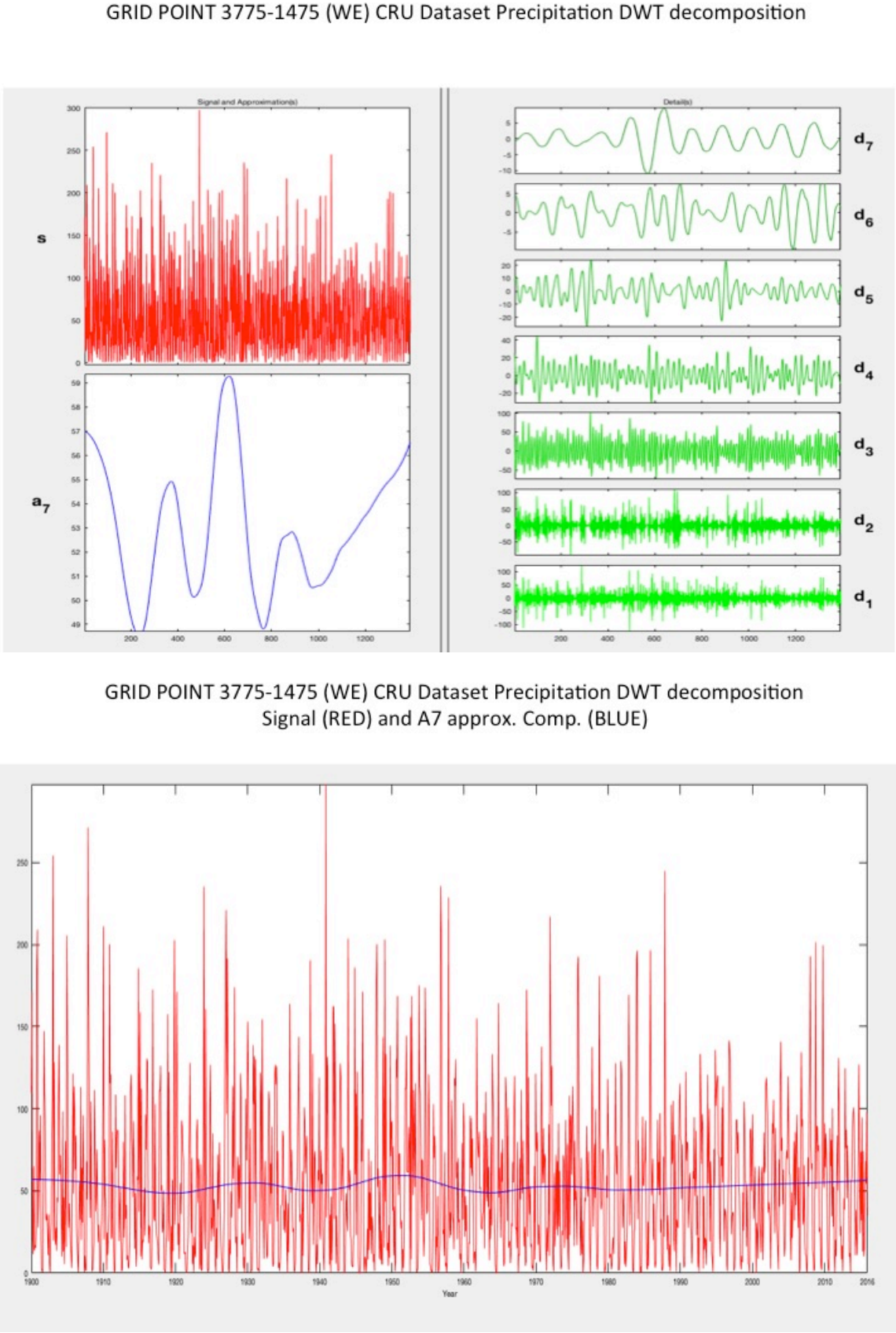

Fig.35 DWT of Mean Monthly Precipitation with db6 at 7 level of decomposition (up) and Signal (red) with over imposed A7 approximation component (blue)

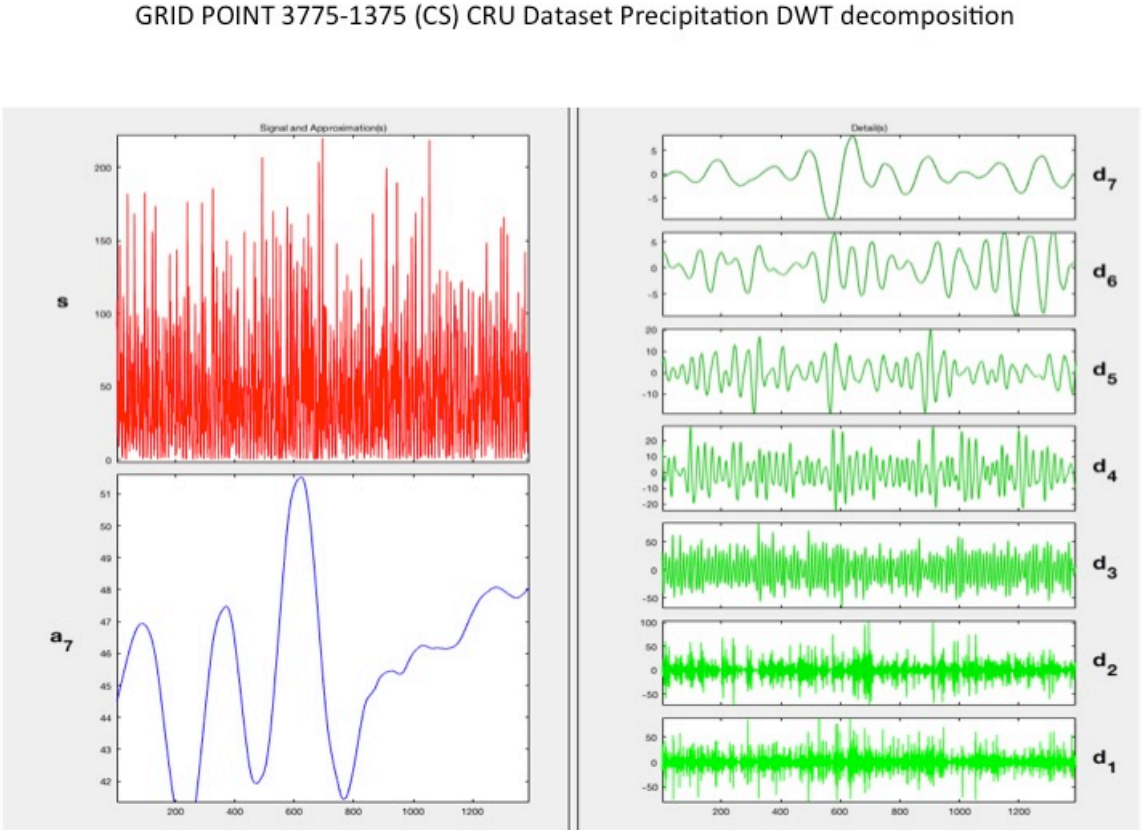

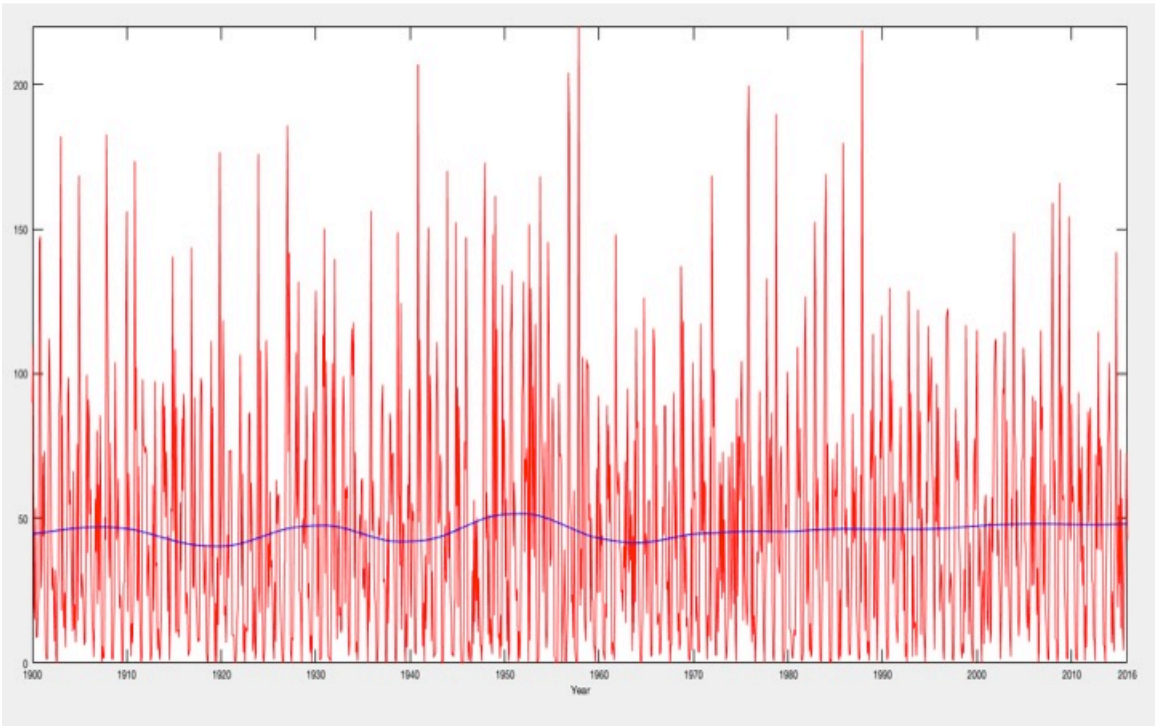

Fig.36 DWT of Mean Monthly Precipitation with db6 at 7 level of decomposition (up) and Signal (red) with over imposed A7 approximation component (blue)

GRID POINT 3725-1425 (CL) CRU Dataset Precipitation DWT decomposition

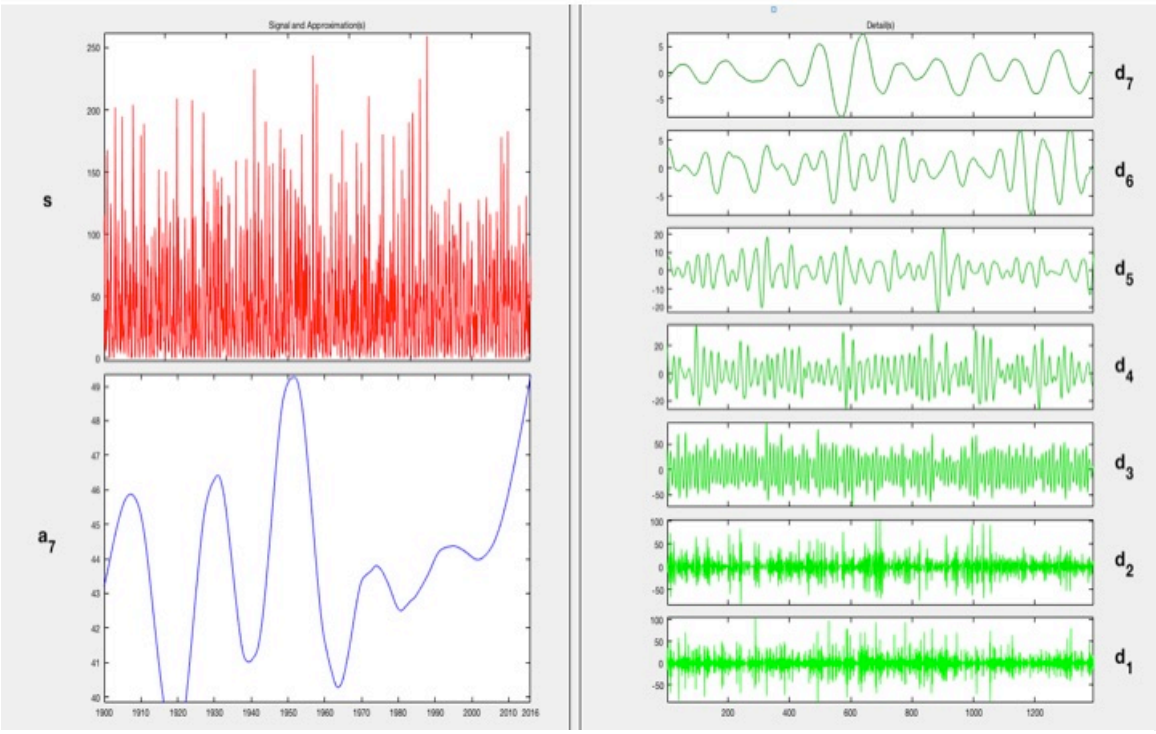

GRID POINT 3725-1425 (CL) CRU Dataset Precipitation DWT decomposition
Signal (RED) and A7 approx. Comp. (BLUE)

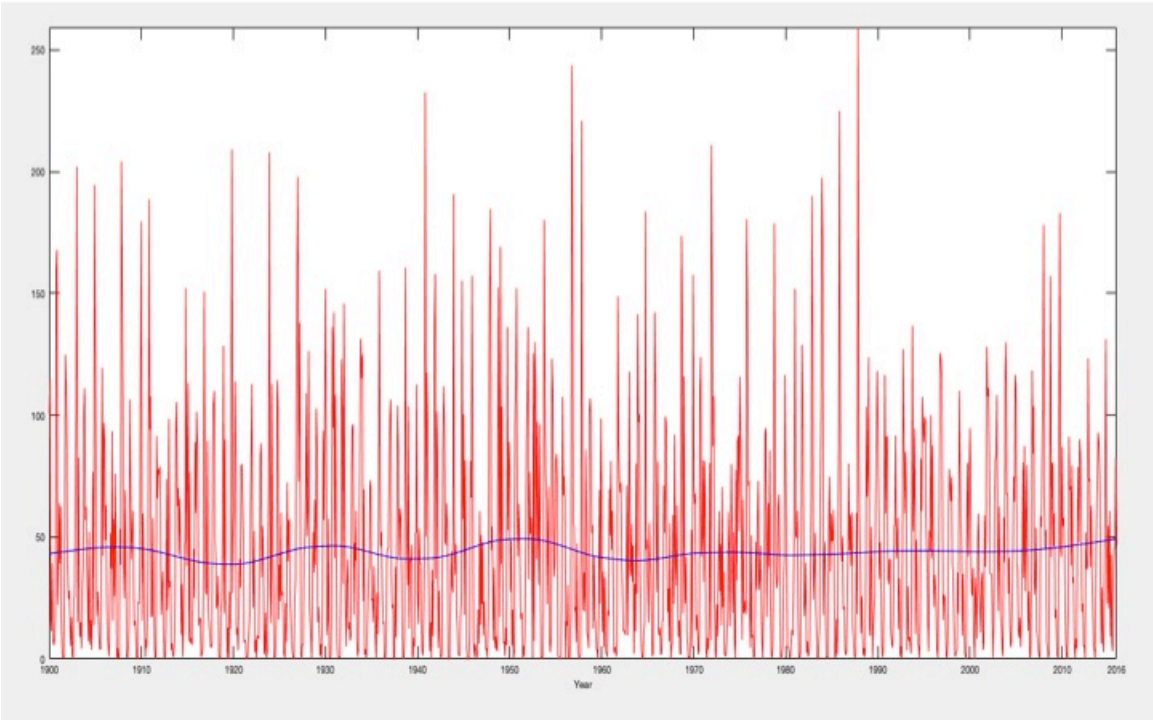

Fig.37 DWT of Mean Monthly Precipitation with db6 at 7 level of decomposition (up) and Signal (red) with over imposed A7 approximation component (blue)

Cozzo Spadaro observed Precipitation DWT decomposition

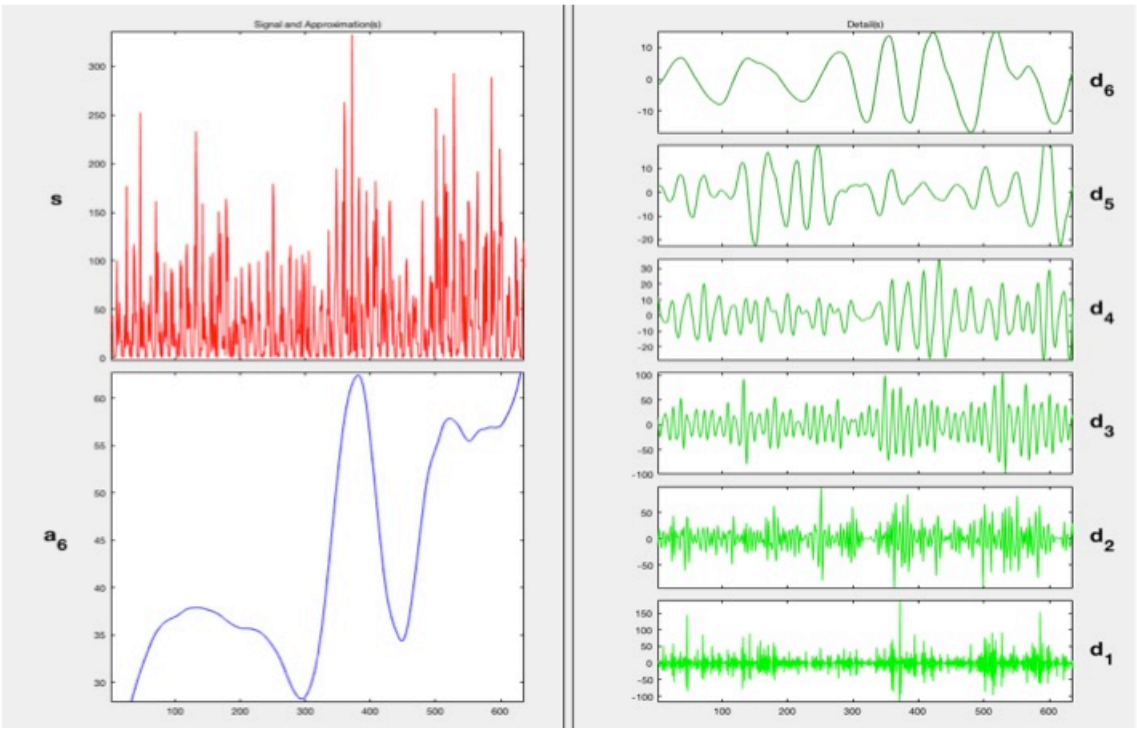

Cozzo Spadaro observed Dataset Precipitation DWT decomposition
Signal (RED) and A6 approx. Comp. (BLUE)

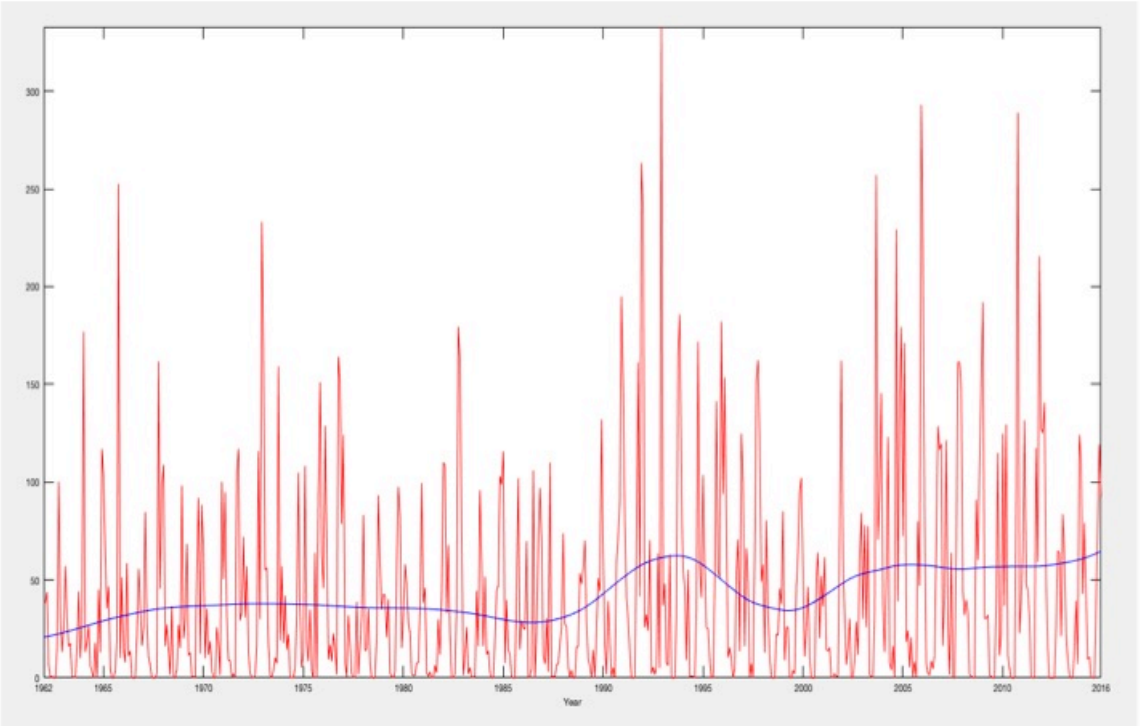

Fig.38 DWT of Mean Monthly Precipitation with db6 at 6 level of decomposition (up) and Signal (red) with over imposed A6 approximation component (blue) for Cozzo Spadaro

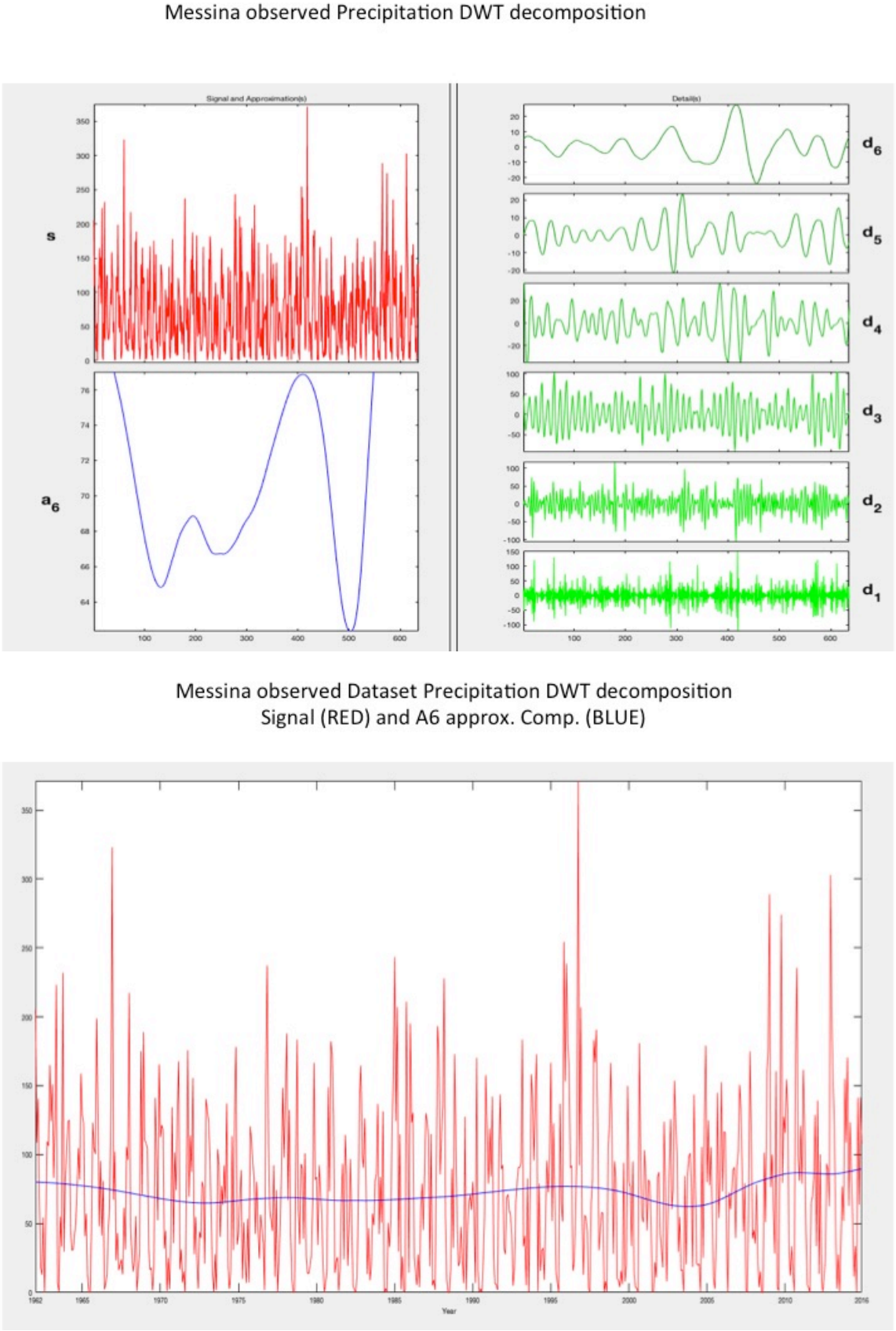

Fig.39 DWT of Mean Monthly Precipitation with db6 at 6 level of decomposition (up) and Signal (red) with over imposed A6 approximation component (blue) for Messina

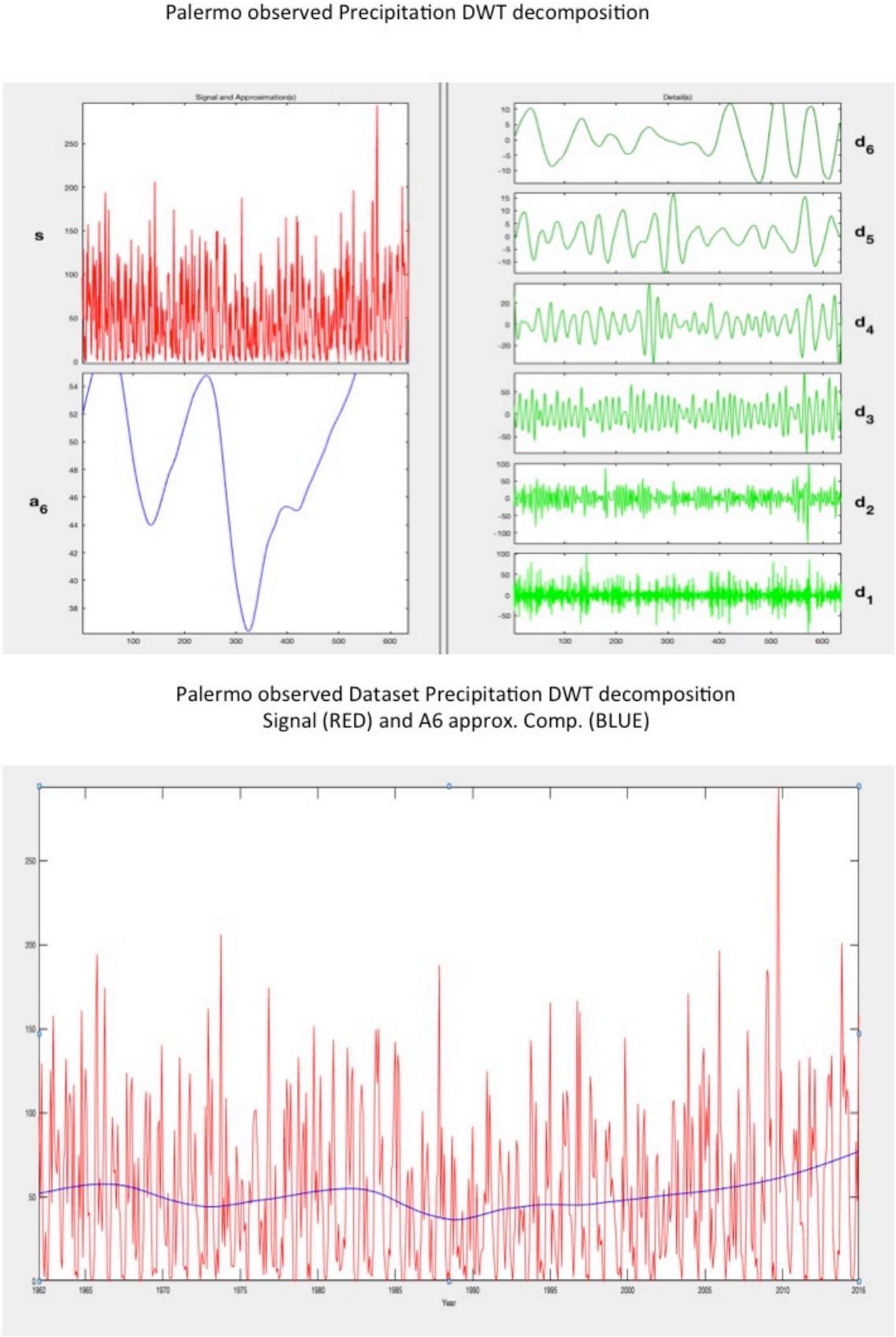

Fig.40 DWT of Mean Monthly Precipitation with db6 at 6 level of decomposition (up) and Signal (red) with over imposed A6 approximation component (blue) for Palermo

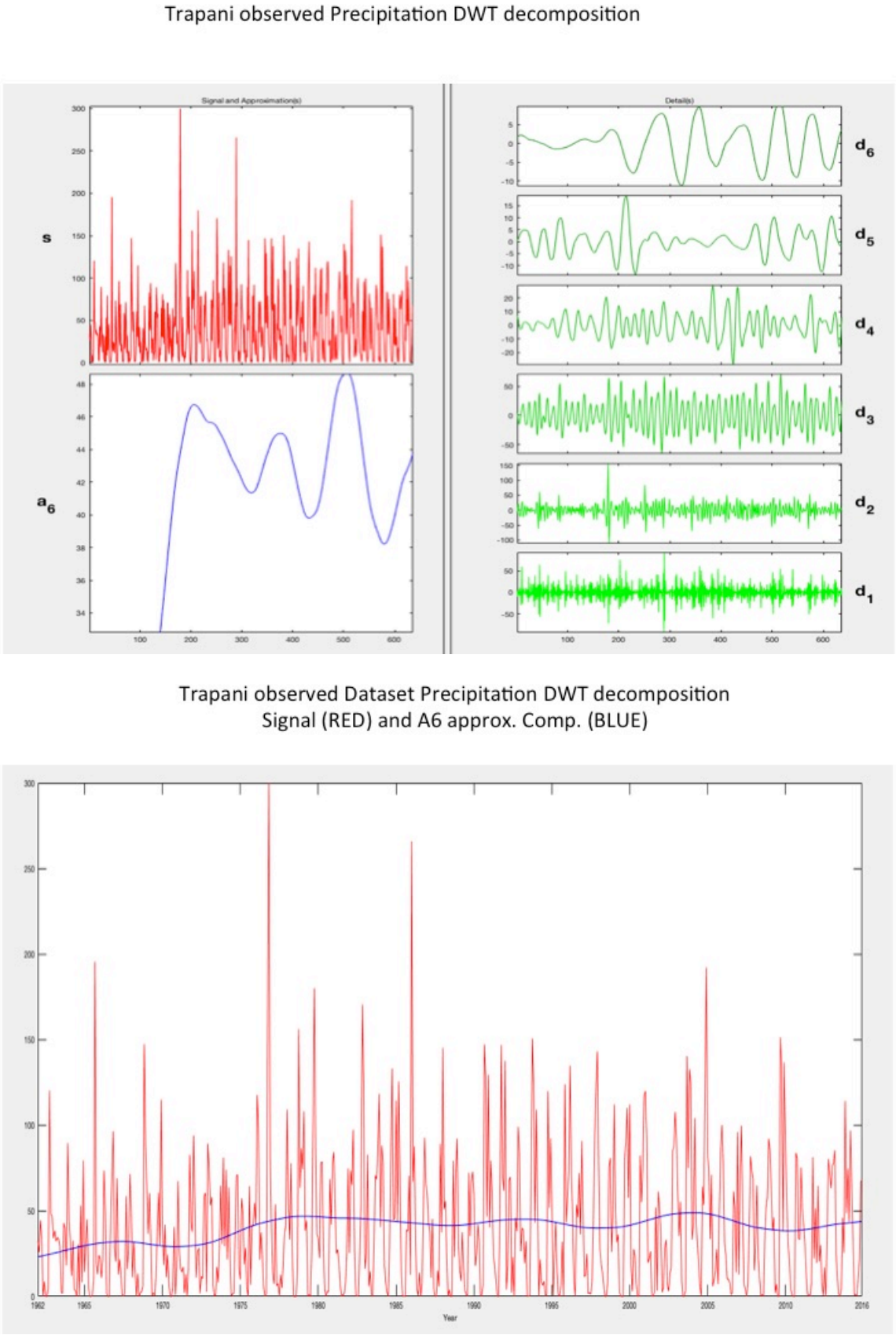

Fig.41 DWT of Mean Monthly Precipitation with db6 at 6 level of decomposition (up) and Signal (red) with over imposed A6 approximation component (blue) for Trapani

The analysis of the results obtained from the decomposition of historical series of precipitation in Sicily with the DWT allows stating that:

- The data obtained from the CRU database, being averaged over the entire grid surface shows very marked similarities, apparently providing similar or not very different results for all the locations;
- Around the 1920s, it is possible to identify a prolonged deficit phase of precipitation, whose duration, deduced by averaging the results of the approximation at level 7 lasted about 4 years. Likewise, it is possible to identify on all the CRU data grid points a maximum that culminated in the 1950s;
- Although climate models predicted a decrease in precipitation over the next few decades; currently the data obtained from the DWT decomposition do not show significant trend on any of the grid points analysed.

Extrapolation from the data observed at the stations of Messina, Palermo Trapani and Cozzo Spadaro brings some additional details. Specifically:

- Cozzo Spadaro station shows a precipitation slight positive trend with a peak in 1994, preceded and followed by two lows coinciding with 1986 and 1999;
- Messina has a virtually regular trend for the entire duration of the measurements, showing only a small minimum around 2004;
- Palermo shows a regular trend until the early 1980s followed by a minimum in 1988 continued by a regular and positive trend.
- Finally, Trapani, after the first decade characterized by low rainfall, since 1977 the trend seems to stabilize and continue without significant differences until the end of the period.

The next step in the research was to perform a power spectrum using a Continuous Wavelet Transform (CWT). In consideration of the analogies of the data coming from the CRU data set, only the 3775-1375 CS data grid, being specific of the central Sicily area, have been used in the

rest of the research. Figures 42, 43, 44 and 45 show the power (absolute square value) of the wavelet transform for monthly precipitation in Messina, Palermo, Trapani and Cozzo Spadaro in the 63 years of observations, while figure 46 refers to the period of 110 years of the grid point CS.

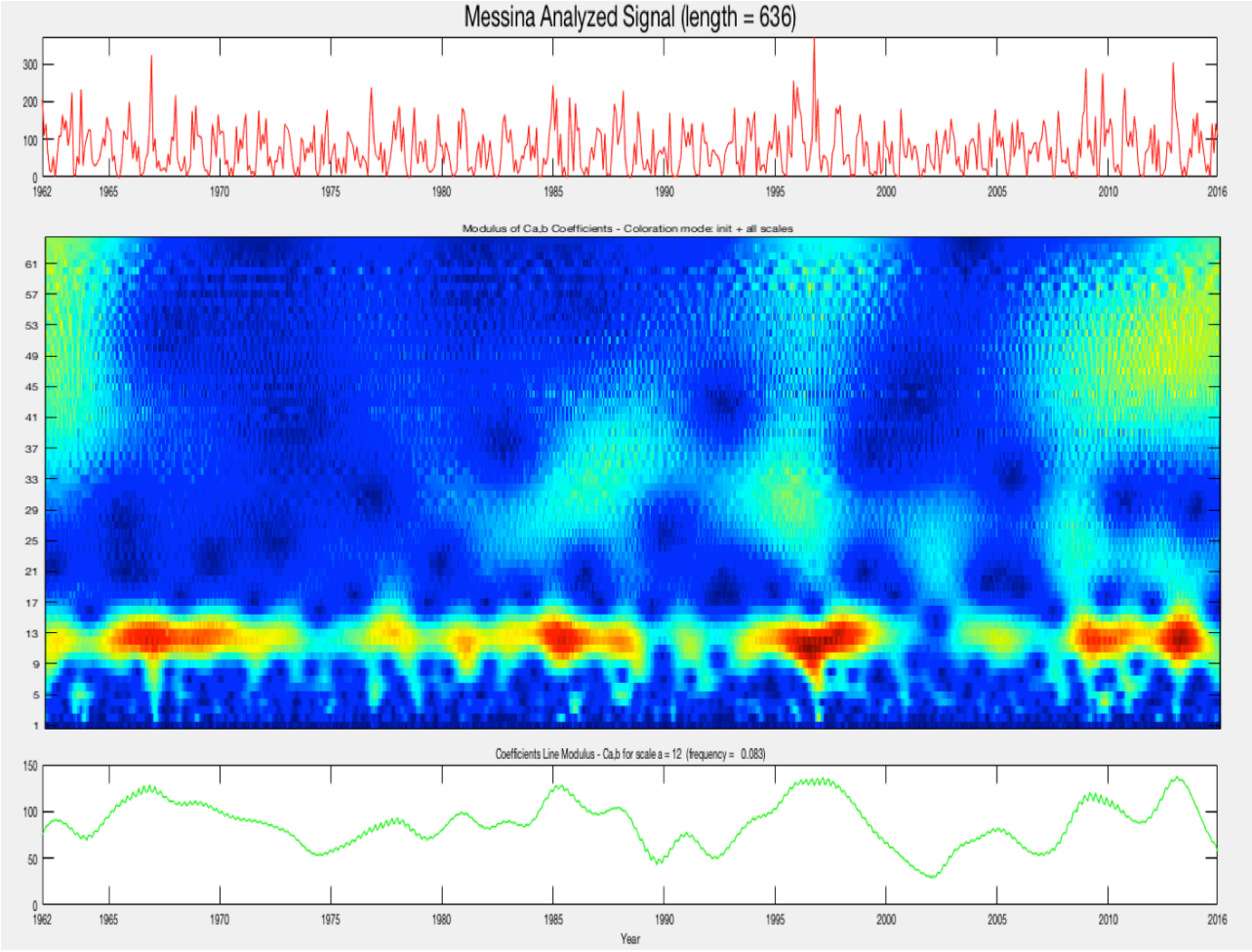

Fig.42 Messina monthly rainfall wavelet power spectrum. The green line at bottom of figure shows the scale-average wavelet power over 12-month band.

The power spectrum provides power information related to certain scales and at certain periods. Observing the figures, it is clear that the highest concentration of power is included in the band between 9 and 15 months, confirming the strong presence of the annual signal in the series.

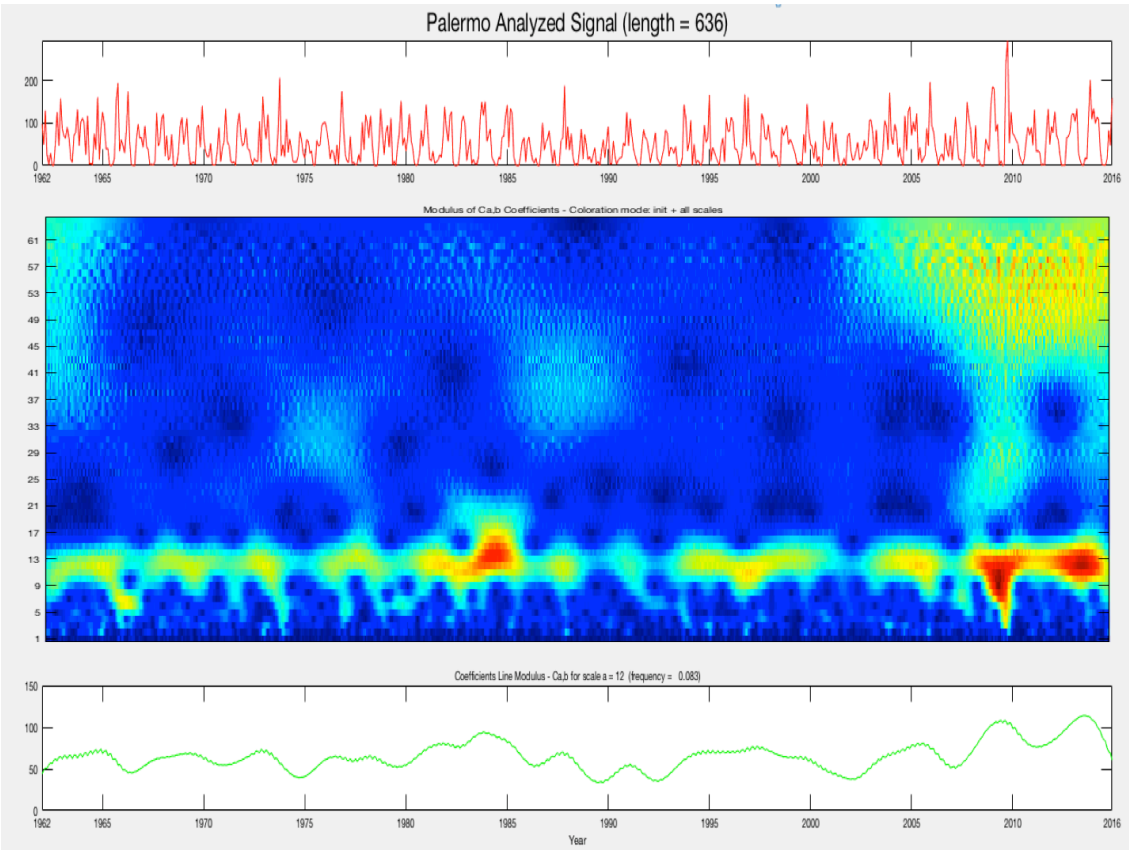

Fig.43 Same as fig 42 in Palermo.

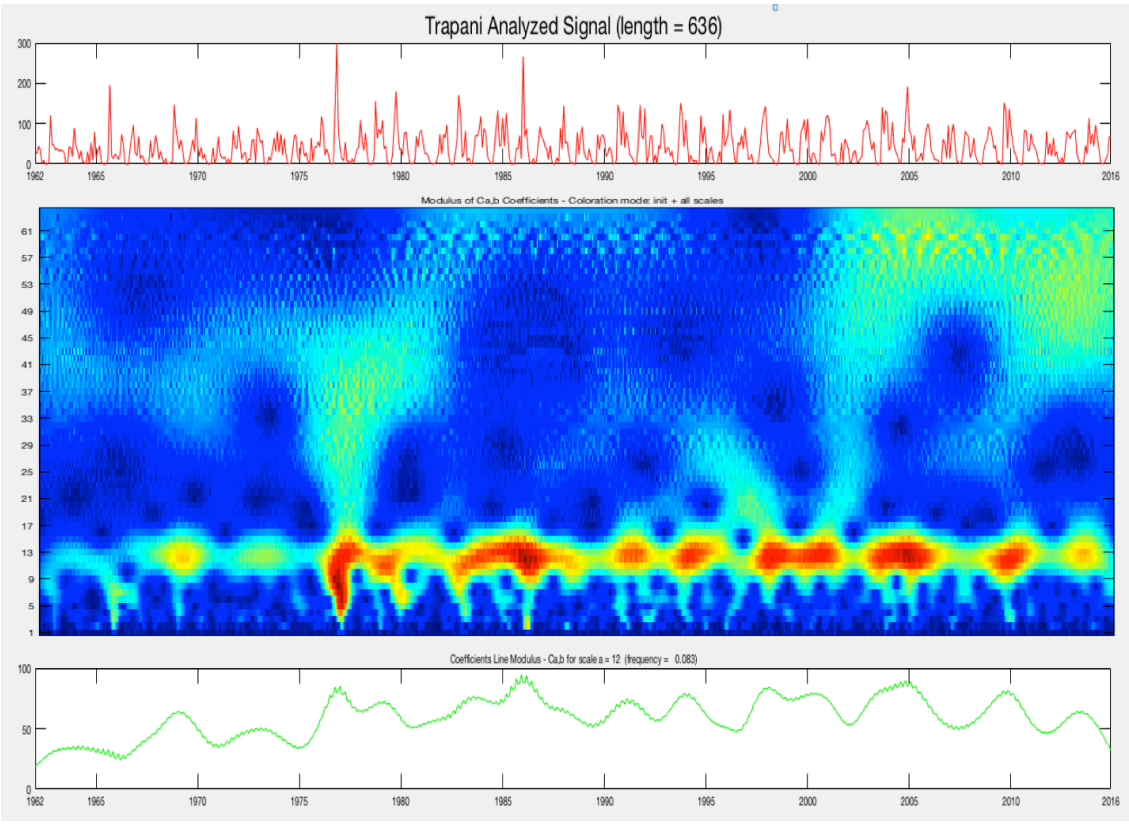

Fig.44 Same as fig 42 in Trapani.

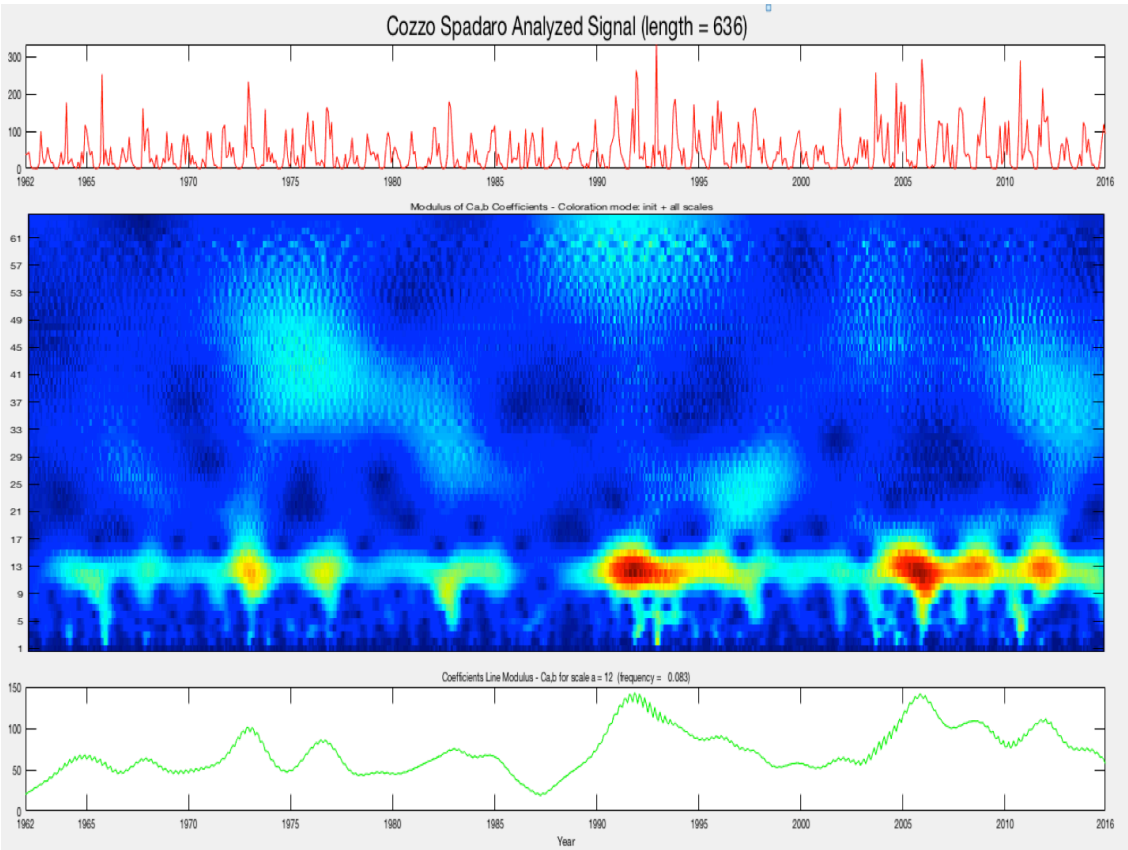

Fig.45 Same as fig 42 in Cozzo Spadaro.

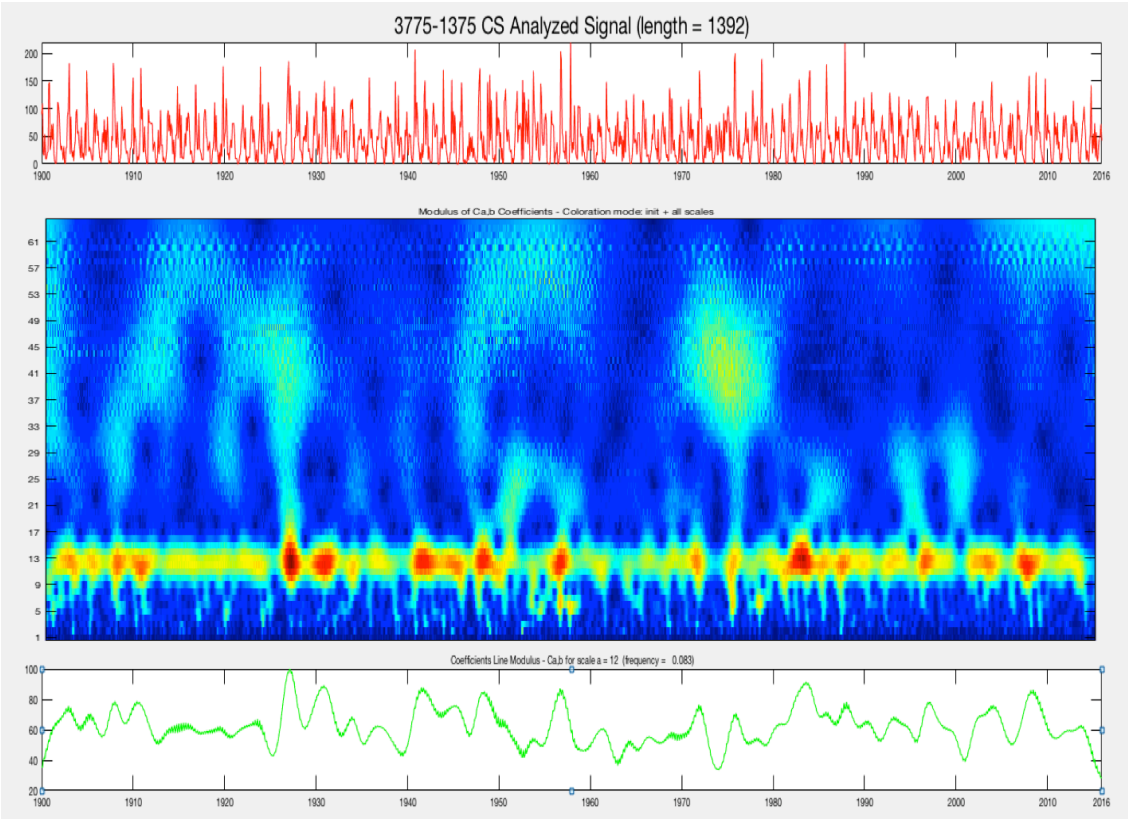

Fig.46 Same as fig 42 in grid point CS for 116 years length signal.

The variance of power in 12-month band, which gives a measure of the average year variance versus time, shows the dry and wet years; i.e., when the power decreases substantially in this band, it means a dry year and when the power is maximum means a wet year. For example, a long dry period can be identified in fig 45, during 1985-1990, or in the long series (Fig 46) during almost 10 years from 1913 to 1925. In the CWT of Messina, Palermo and Cozzo Spadaro (Figures 42, 43 and 45) there are peaks with periods of less than 6 months, concentrated mainly at the end of the observation period between 2005 and 2016. Most of the events characterized by extreme monthly precipitation occurred in the coastal areas of Sicily in the same years. This indicates that the Wavelet analysis allows to highlight even single episodes with powers concentrated in the 2-6 months band. Finally, the spectra of Messina, Palermo and Trapani also show a moderate concentration of power in the band between 45 and 55 months (4-5 years) that occurred after 2005, the significance of which will be explored in other works.

6.5 Wavelet Analysis of temperature

Unlike rainfall, the historical series of reconstructed temperatures are all quite similar and from the analysis do not show sufficient significant differences. Therefore, the analysis is on the reconstructed CS series on the grid point 3775-1375 only. Wavelets analysis conducted on the four historical series of the observed temperatures and on the CS series to determine both the possible trend and to identify the climatic dynamics that may be present and identifiable in the signals.

In order to eliminate the annual periodic signal and let emerge other information, the average values for the period 1971-2000 were subtracted from the temperature data, thus obtaining series of thermal anomalies on which were carried out the subsequent analysis. The first analyses concerned the observed series of Cozzo Spadaro, Palermo, Messina and Trapani

stations. The anomaly signal was initially decomposed by DWT on 6 levels to identify the possible trend. On the signal plot were overlapped both the level of approximation 6, similar to the trend, and the level of approximation 5, of interest since contains a modulation with a period of about 64 months present in all the signals and the meaning of which will be discussed later. Furthermore, for each series has been carried-out a decomposition of the signal with CWT setting a continuous scale up to 128 months.

The joint analysis of the two decompositions, allows highlighting some aspects about the times and the ways in which global warming has occurred on the individual locations studied and more generally on Sicily. Compared to the averages of reference period 1971-2000, Cozzo Spadaro shows the lower temperatures since the beginning of the observation period and until 1978. During this period, there was a negative general trend and the CWT analysis shows only signals with a periodicity of less than 24 months. In 1977, a heat episode seems to mark the start of the warming of the following years. A second heat episode, much more marked than the previous one occurs in 1987. This episode, in addition to the periodicity of 12 months, shows another very marked periodicity around 30 months that extends between 1984 and 1989. In the same period, appears and continues at least until 2012, a singular periodicity of 64 months that seems to drive the late global warming, knowing only a brief pause at the beginning of the nineties, between the eighties and 2014. In 1998 and 2003, the CWT observes two other heat episodes. Finally, an attenuation of the positive trend is clearly visible after the year 2003 coinciding with the exhaustion of the periodicity at 64 months (Fig. 47 and Fig. 48).

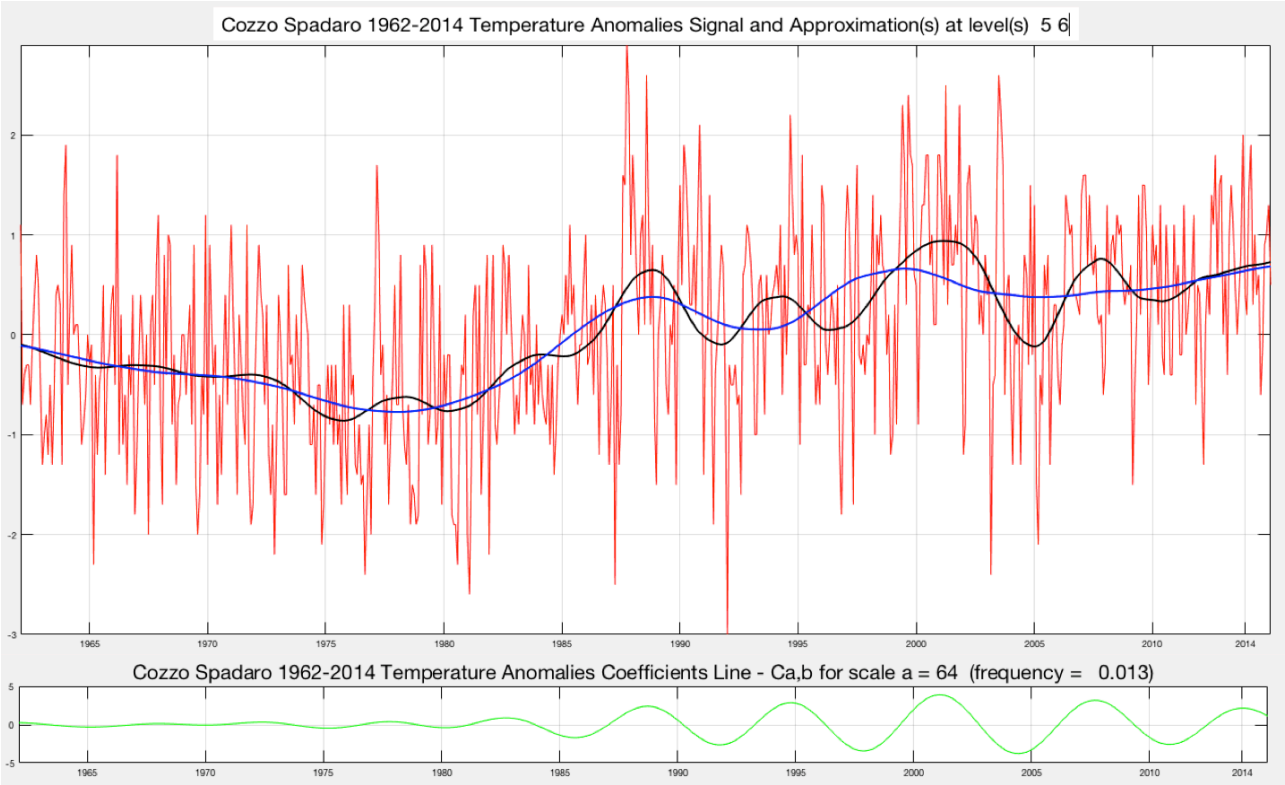

Fig. 47 Cozzo Spadaro 1962-2014 Temperature Anomalies analyzed signal (red) with superimposed DWT approximation level 5 (black) and 6 (blue) and coefficient line for scale 64 months (green).

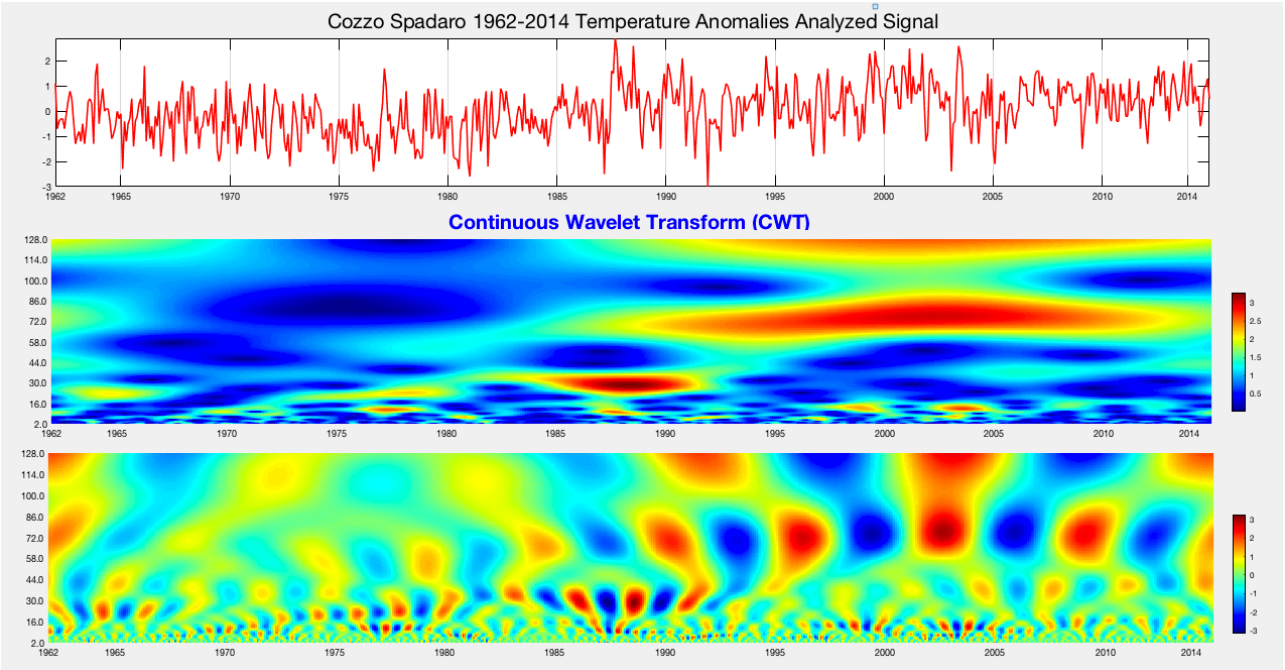

Fig. 48 Cozzo Spadaro 1962-2014 Temperature Anomalies analyzed signal (upper), CWT Modulus (middle) and Real part (bottom).

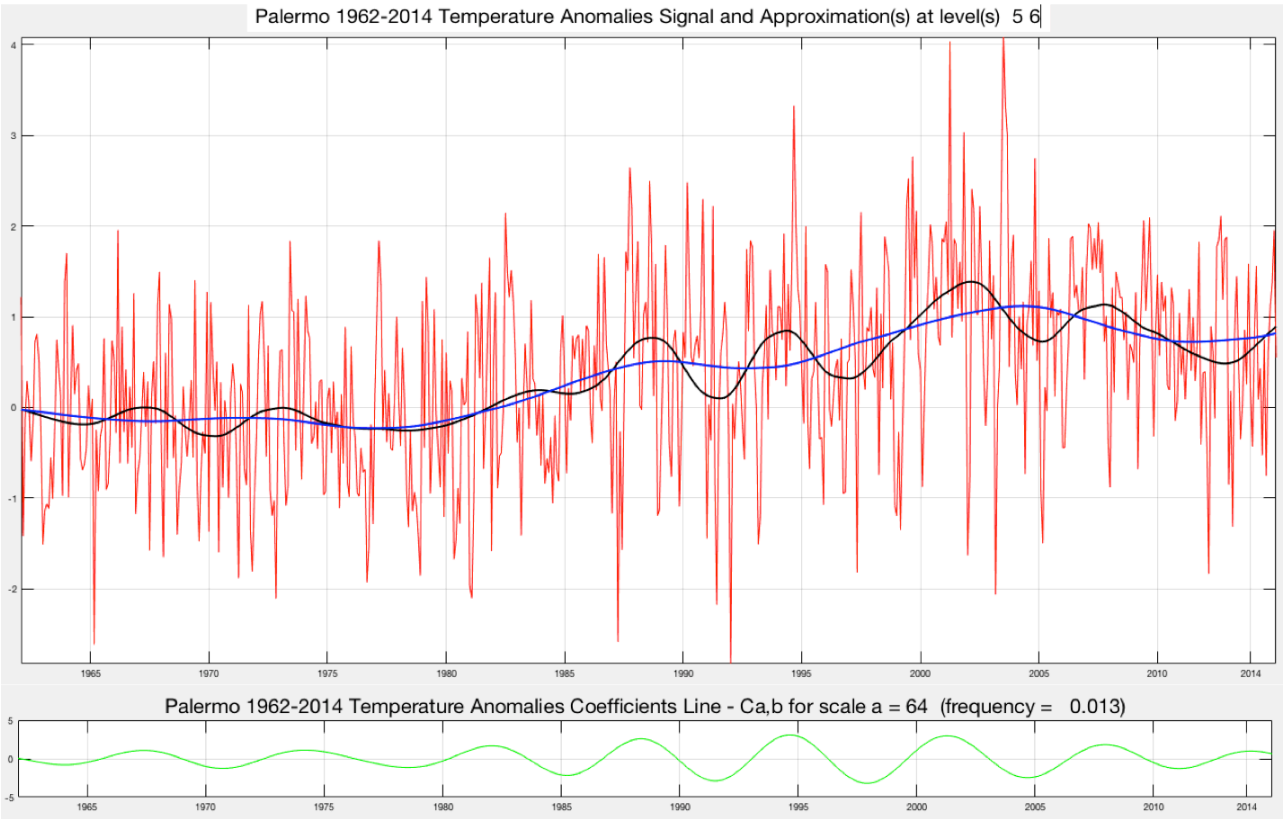

Fig. 49 Palermo 1962-2014 Temperature Anomalies analyzed signal (red) with superimposed DWT approximation level 5 (black) and 6 (blue) and coefficient line for scale 64 months (green).

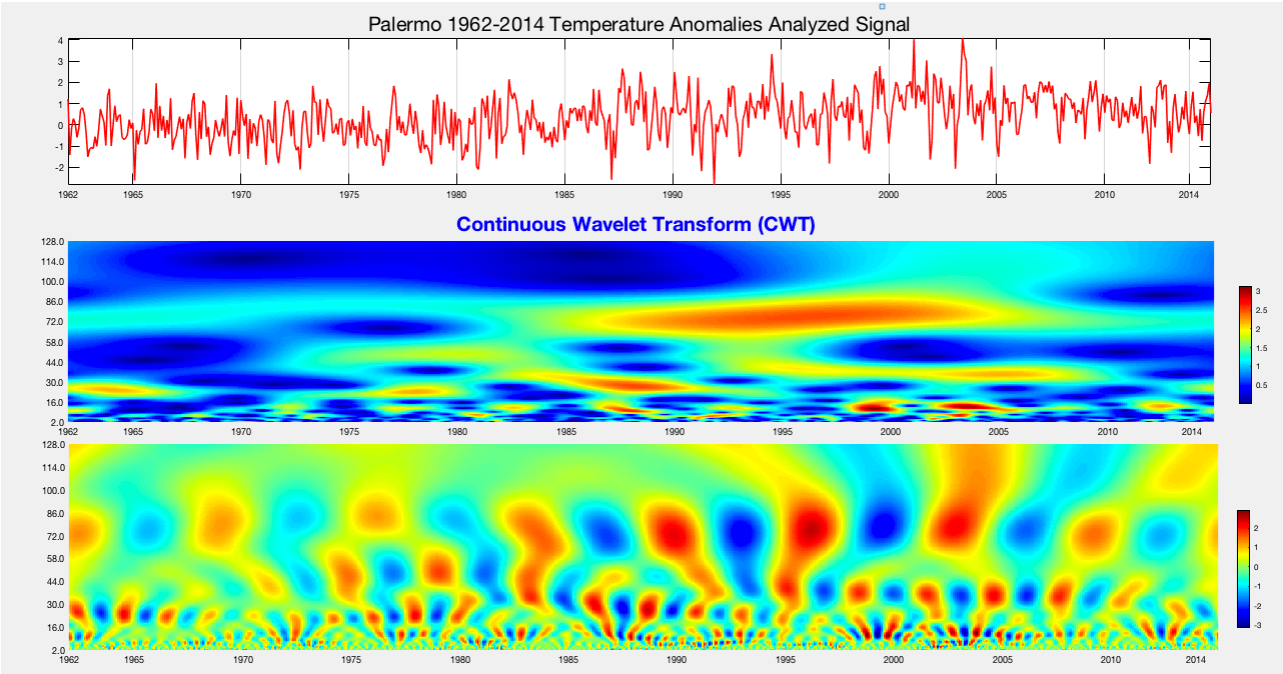

Fig. 50 Palermo 1962-2014 Temperature Anomalies analyzed signal (upper), CWT Modulus (middle) and Real part (bottom).

The comparative analysis of the historical series of Palermo shows a weak negative trend between 1962 and 1978, when the trend is reversed and heating begins. The annual and quasi-biennial periodicity is the one that most appears in this time interval, alongside that of 64 months, which unlike Cozzo Spadaro, here appears throughout the examined period, albeit with a very small amplitude. From 1978 to 2005, the trend is always positive, showing a slight decline between 1990 and 1995. Once again, in conjunction with the period of maximum temperature increase, the signal with a period of 64 months appears very strong, which here overlaps to a period of about 35 months, visible between 1995 and 2008.

Two intense episodes are evident in the CWT in 1998-99 and 2003. Finally, starting from the year 2005 there is a new trend inversion with decreasing temperatures (Fig. 49 and Fig. 50).

The analysis of the temperatures series in Messina shows a quasi-stationary for the entire period covering the years between 1962 and 1980. It appears evident in this period, both the absence of single episodes, and the absence of long periodicity going beyond that quasi-biennial.

Since the early eighties and until the end of 2010, temperatures have grown at an almost regular rate with a short break at the turn of the nineties. Once again, the period of maximum warming is accompanied by the 64-month modulation that appears most clearly between 1983 and 2010. A single and isolated hot episode appears in the CWT in 1981, followed by the very strong one in 2003. In recent years, even for this historical series, there is a weak tendency towards cooling or in any case to stationarity.

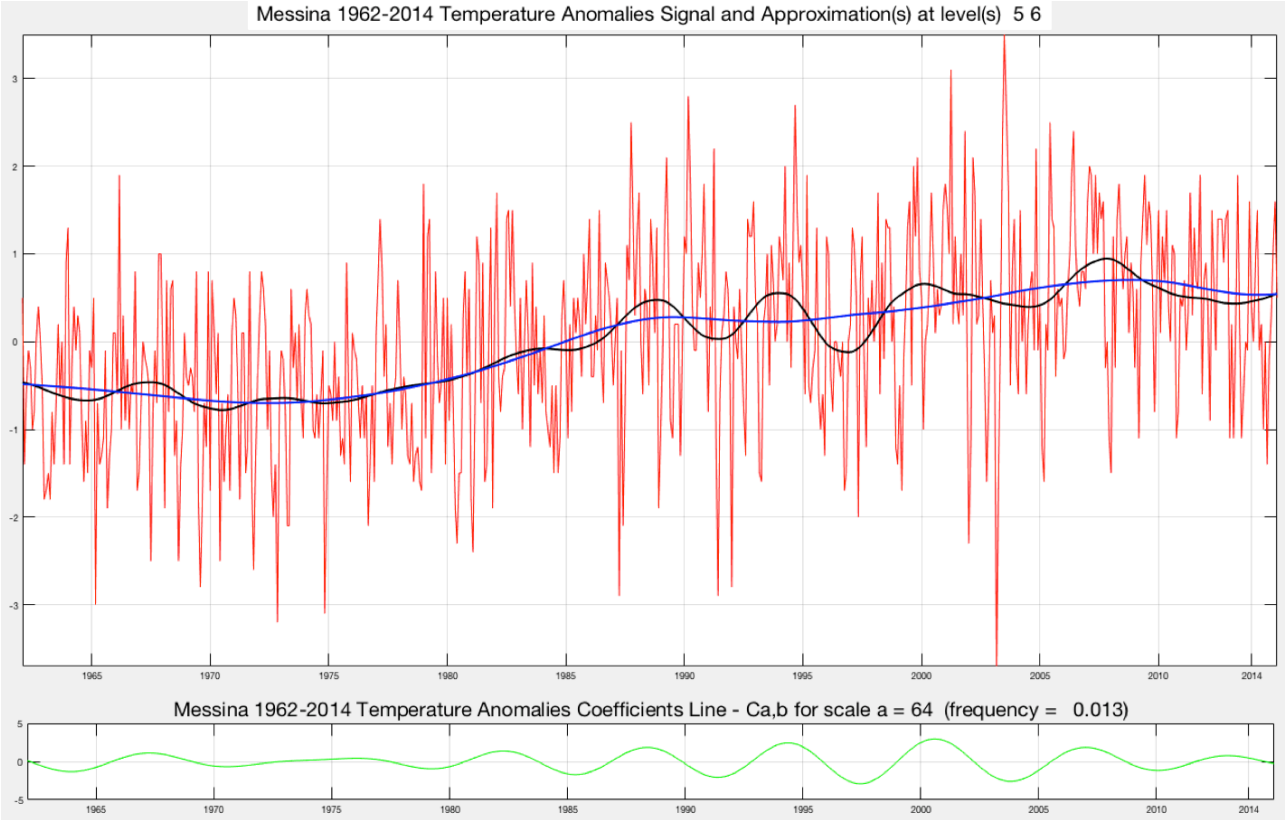

Fig. 51 Messina 1962-2014 Temperature Anomalies analyzed signal (red) with superimposed DWT approximation level 5 (black) and 6 (blue) and coefficient line for scale 64 months (green).

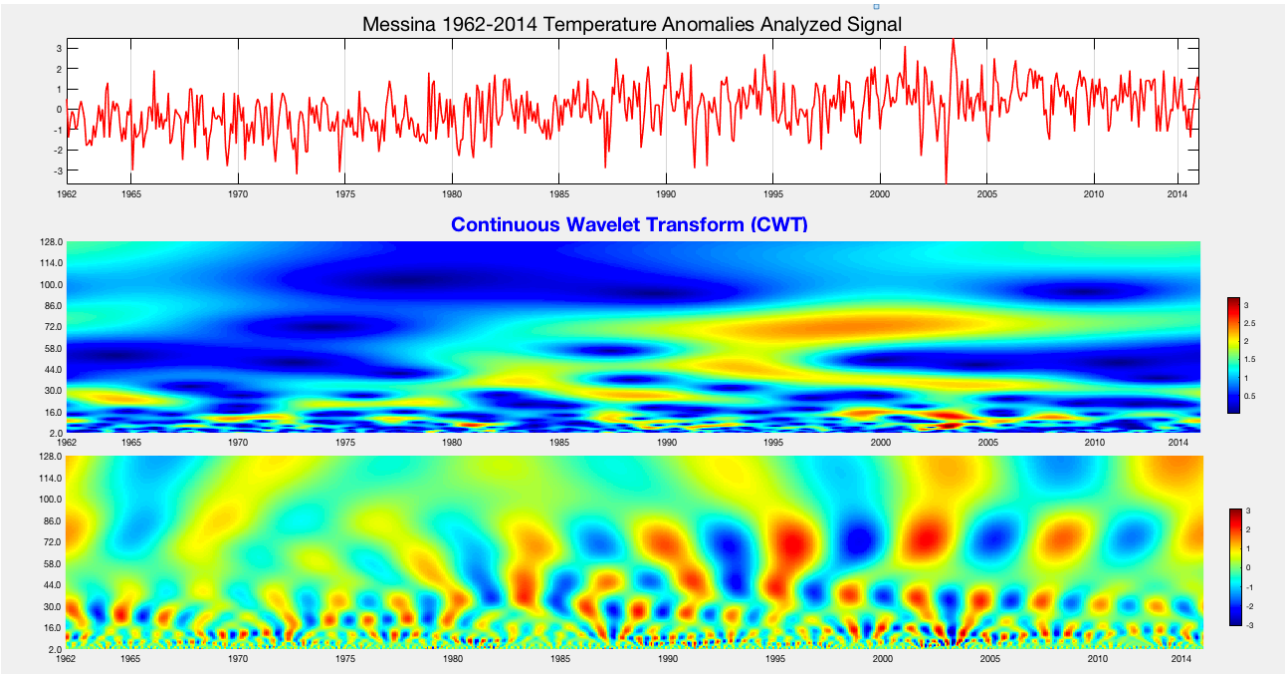

Fig. 52 Messina 1962-2014 Temperature Anomalies analyzed signal (upper), CWT Modulus (middle) and Real part (bottom).

The series of Trapani is the one that in some aspects differs most from the previous ones. Firstly, because between 1962 and 1980, while all the other series shows stationarity or negative trend, it shows a positive trend undulation that culminates in 1972 and then declines rapidly until 1978. Between 1978 and 1985, the temperatures return to grow. Then follows a period of negative trend until 1993, which again follows a thermal increase. The 64-month periodicity is very weak and covers the period between 1983 and 2009. The most marked single episodes are evident in the CWT and concerns 1977, 1987 and a series of minor episodes between 2000 and 2003.

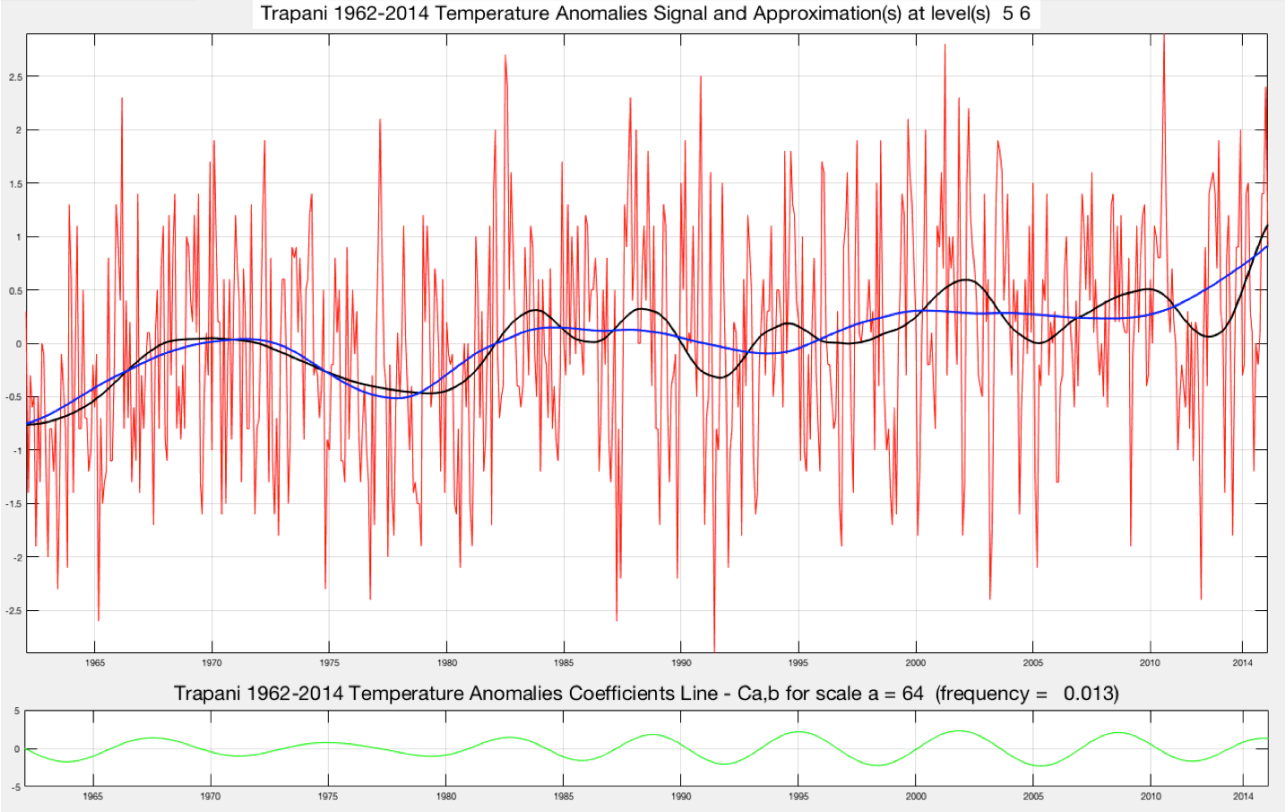

Fig. 53 Trapani 1962-2014 Temperature Anomalies analysed signal (red) with superimposed DWT approximation level 5 (black) and 6 (blue) and coefficient line for scale 64 months (green).

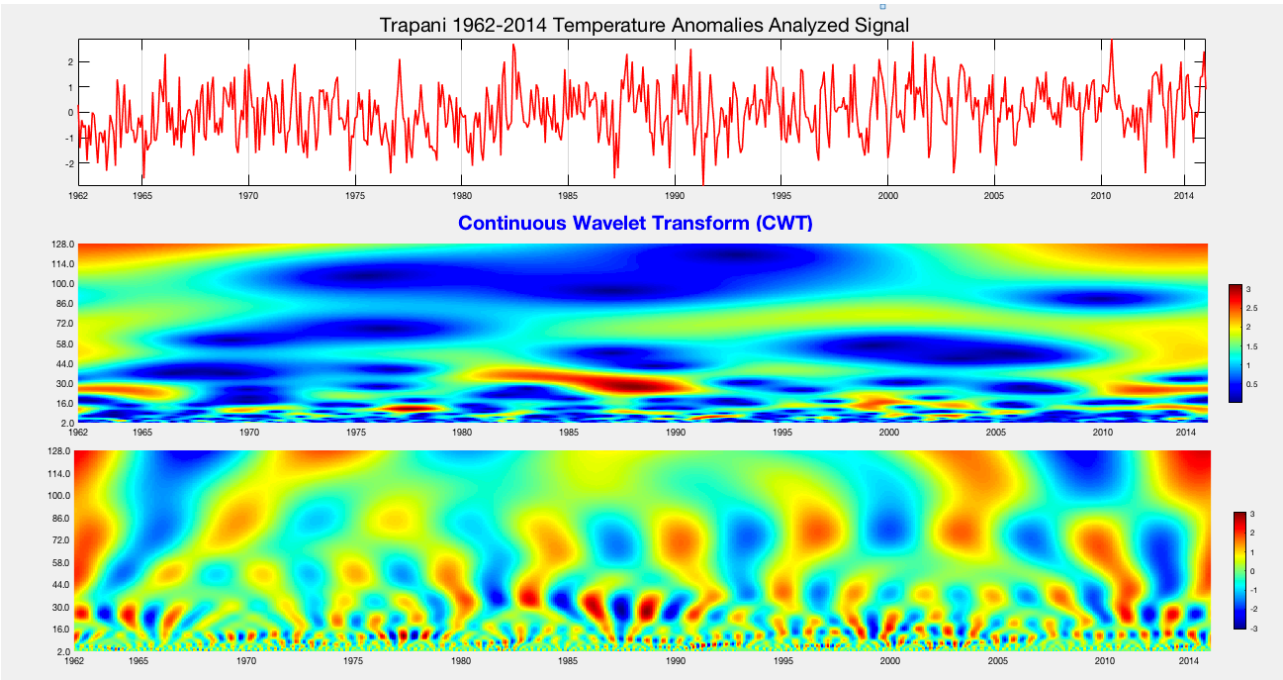

Fig. 54 Trapani 1962-2014 Temperature Anomalies analysed signal (upper), CWT Modulus (middle) and Real part (bottom).

Finally, the analysis of the temperature data series reconstructed by the CRU for grid point 3775-1375 between 1900 and 2016 shows a general trend in line with both the global warming observed at planetary scale and with that observed in the last century in the Mediterranean area. In a positive overall trend, it is possible to observe and distinguish various characteristics:

- The early years of the twentieth century open with a rather cold period and characterized by a negative trend;
- From 1905 to 1928 there is a long period characterized by constantly increasing temperatures;
- Between 1928 and 1940 the temperatures returned to show a weak tendency to decrease;
- Between 1941 and 1947 there was a rapid increase of short duration followed by a long period with stationary or decreasing temperatures that lasted for more than 30 years between 1948 and 1978;

- The beginning of the eighties registers a real change of trend line direction, which shows a steep upward trend until 2016, interrupted only by a couple of weak decreases that occurred around 1990 and 2005 (Figure 55).

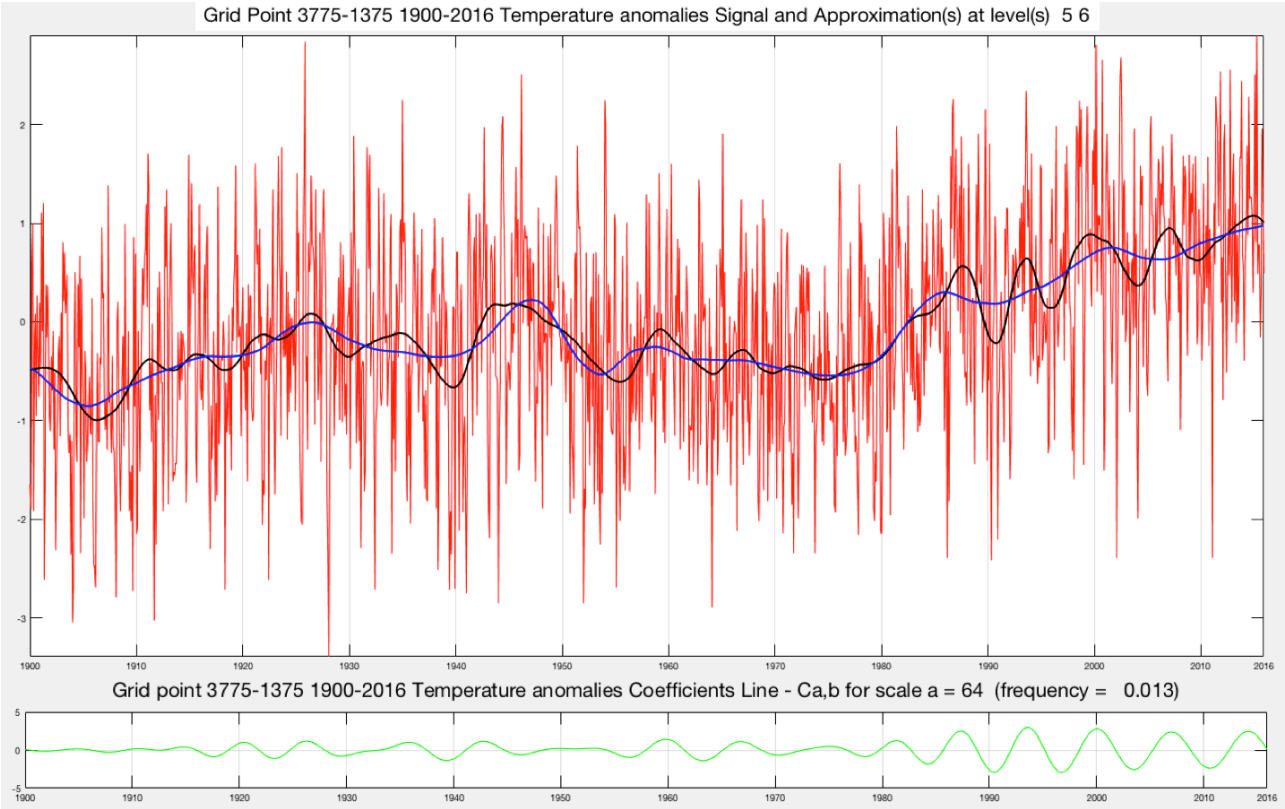

Fig. 55 Grid point 3775-1375 1900-2016 Temperature Anomalies analysed signal (red) with superimposed DWT approximation level 5 (black) and 6 (blue) and coefficient line for scale 64 months (green).

The CWT analysis highlights further characteristics about the ways and times with which climate change manifests. If we consider the two phases, in which the warming was greater, that is the periods 1905-1928 and 1978-2016, it is possible to observe how in the same years there are signals of a period longer than 48 months. Specifically, a component of the 50 months period appears between 1905 and 1928 and a period of 64 months, much more marked than the previous one appears between 1978 and 2016. It is also possible to highlight a component with a period of around 24 months between 1905 and 1914, a series of very

close single episodes of quasi-annual period between 1925 and 1945, and finally other single episodes in 1951, 1978, 1987, 1998, 2003 and 2011 (Fig.56).

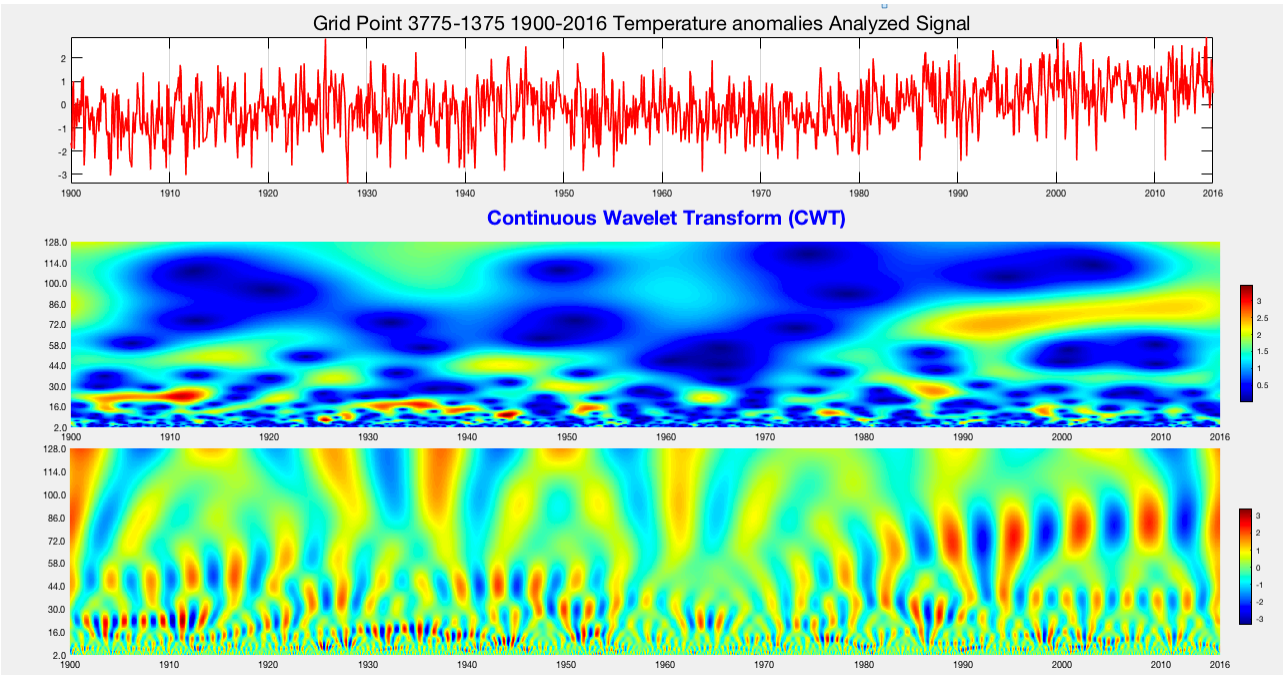

Fig. 56 Grid point 3775-1375 1900-2016 Temperature Anomalies analyzed signal (upper), CWT Modulus (middle) and Real part (bottom).

Conclusion

The challenge of the climate change is not just a scientific issue, but concerns the whole of humanity. The complexity of the Earth's climate system does not allow us to fully understand the mechanism that caused the global warming observed at the planetary level. The aim of this thesis was primarily to try to understand the ways and the times in which the global warming has affected the Sicily and more generally the entire area of Mediterranean Sea during last century. In order to proceed systematically and provide an overall view of the problem, we described the historical framework of the science of climate change, starting from the philosophical concepts of Thales of Miletus and Aristotle and from the first attempts to deal systematically and completely the study of the climate, up to the modern and more complex theories developed during the twentieth century. We have then described the causes, internal and external to the planet, both of natural and anthropic origin, able to determine climate changes at different time scales and then we've described the main climatic changes observed both globally and at the regional level, circumscribing the area of interest to the Mediterranean region. Finally, some of the main signal analysis methods, which are able to extract additional information on climatic dynamics starting from simple historical series, have been reviewed. Among the described methods, in particular we have chosen to use the Wavelets analysis.

The research activity concerned the analysis of the time series of two meteorological parameters that better than others are able to describe climate change: rainfall and air temperature. In order to have results that can cover the entire territory of Sicily, four locations distant from each other and located along the coast, have been chosen. For these four locations the time series regards the monthly averages of the data observed between 1962 and 2014. In addition, in order to extend the time window of analysis and to cover the territory in a more homogeneous way, data of the period 1900-2016 coming from the data base of the Climatic Research Unit (CRU) of the University of East Anglia, were also collected. The analysis performed on precipitation, using the discrete wavelet transform (DWT), shows a substantial stability over time without significant trends. Also the Continuous Wavelet spectra (CWT) highlight the natural annual frequency, showing no other significant characteristics. Very different have been the results obtained by the Wavelet analysis of temperatures: they show in fact the same trend recorded globally, whit a rapid increase occurred specially after the eighties of the last century. Moreover, the Wavelet analysis performed, allows us to obtain information on the climatic dynamics, not otherwise derivable through the use of other spectral techniques. Among the most interesting, there is undoubtedly the sign left in 1987. Between the months of March and October the anomalies of temperatures undergo a real thermal jump that reaches and exceeds in many places the values of 6 ° C. This characteristic is very evident in all CWT spectra as well as by simple comparative analysis of the signals (Fig. 57)

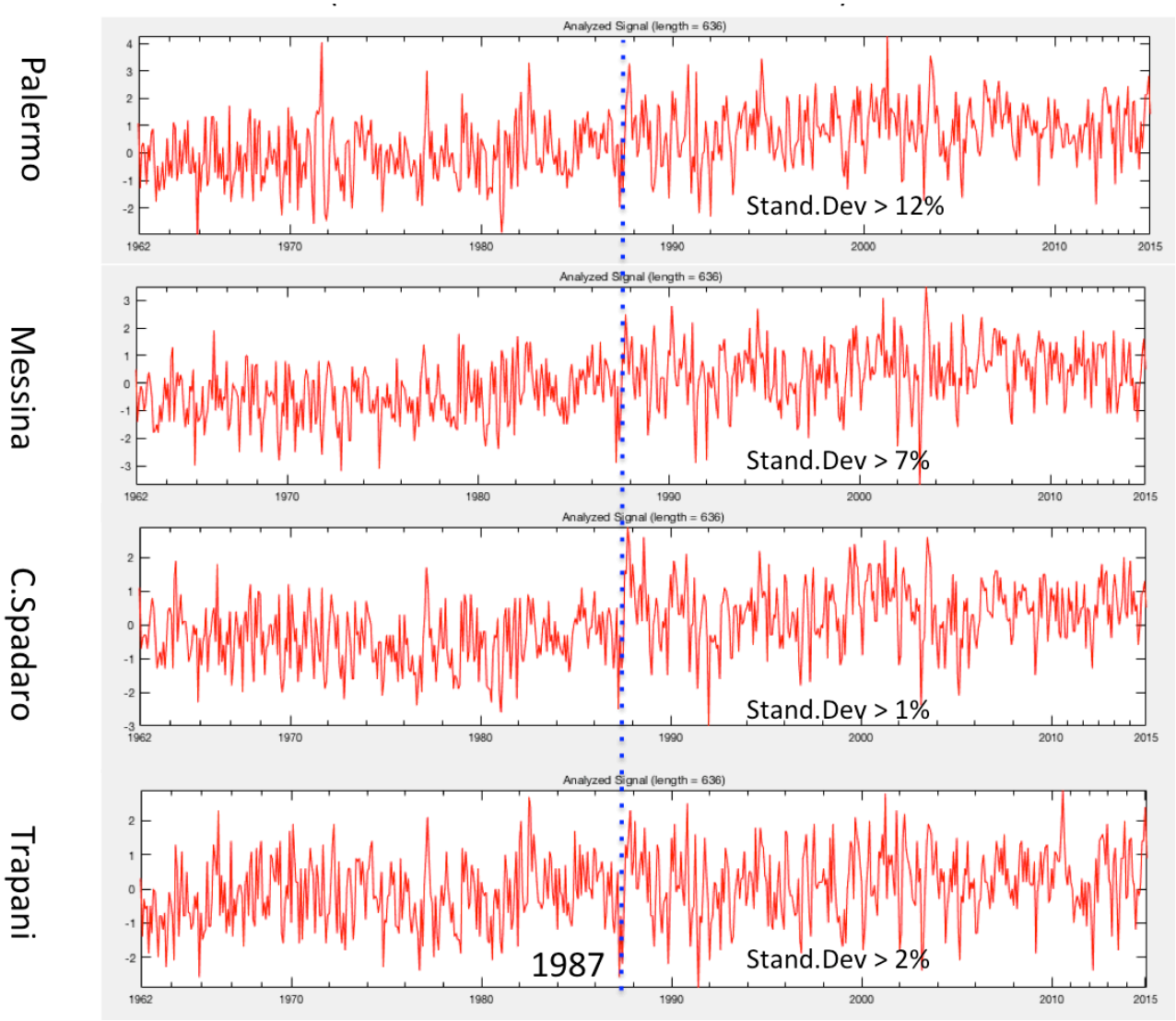

Fig.57 Comparative analysis of anomalies in which is visible the "jump" of temperature occurred on 1987

That 1987 marks a turning point in climate is confirmed by the statistical analysis performed on the first part of the series, that is between 1962-1987 and then on the second part between 1988-2014. The results obtained and summarized in Table 6 show how the Standard Deviation, calculated as a reference parameter using the formula: $s = \sqrt{\frac{1}{n-1}\sum(x_i - \overline{x})^2}$ is always higher after 1987 in all the locations.

	Palermo		Messina		Cozzo Spadaro		Trapani	
	1962-1987	1988-2014	1962-1987	1988-2014	1962-1987	1988-2014	1962-1987	1988-2014
Mean	-0,057	0,744	-0,451	0,440	-0,401	0,409	-0,184	0,188
Stand.Dev	0,910	1,032	0,987	1,056	0,908	0,911	0,993	1,011
Diff. %		+12%		+7%		+1%		+2%

Table 6 percent difference in Standard Deviation of temperature obtained comparing data from 1962 to 1987 and from 1988 to 2004

The differences of Standard Deviation range from just over 1% for Cozzo Spadaro up to 12% in Palermo. Other confirmations on the "climate change" that took place in the Mediterranean area in 1987 have also been found in scientific literature. An interesting and intriguing hypothesis is described in different works and regards the interaction Sea-Atmosphere. Conversi et al. 2010 [84] states “1987 appears to be a year of change for the entire Mediterranean basin surface circulation”. Furthermore Demirov and Pinardi’s [85] simulations of the interannual surface Mediterranean circulation from 1979 to 1993 identify two periods, 1981–87 and 1988–93, which differ in precipitation and winter wind regimes. Pinardi et al. [86] and Korres et al. [87], using data-validated simulations describe the dramatic reversal of the Ionian gyre in the summer of 1987 from its ‘‘usual’’ cyclonic state to an anticyclonic pattern. In particular, they show a reversal in the surface current directions in the Ionian Sea, with the Atlantic/Ionian stream (and associated nutrients and hydrographical properties), branching further northward, at 35.5° N, and link it to the surface circulation changes to the previous winter anomalies in the winds and heat fluxes. The alteration lasted approximately 10 years, until 1997, when the gyre re-reversed.

The second climatic element that emerged from the Wavelet analysis of Sicilian data, concerns the presence of a signal with a periodicity of 64 months in correspondence with the warming that took place in the eighties. The presence of this pattern could be clarified by means of

climate cycles. Cyclical variations in the Earth's climate occur at multiple time scales, from years to decades, centuries, and millennia. Cycles at each scale are caused by a variety of physical mechanisms. Climate over any given period is an expression of all of these nested mechanisms and cycles operating together. In previous chapter we have already seen how, for example, the Milankovithc cycles affect the climate of the Earth on multi-millennial time scales. Ocean-atmosphere interactions regularly cause climate cycles on the order of years to decades. The most studied and well-known climate cycles are

- The Quasi-biennial oscillation (QBO)– about 30 months
- The El Niño Southern Oscillation (ENSO) – 2 to 7 years
- The North Atlantic Oscillation (NAO)- no particular periodicity
- The sunspot cycle – about 11 years

and other oscillations with longer period. The periodicity of 64 months, that is present in the four localities and visible in their CWT, is compatible only with ENSO. El Niño-Southern Oscillation (ENSO) is an interaction between ocean temperatures and atmospheric patterns (commonly known as El Niño or its opposite effect, La Niña). ENSO events occur every 3 to 7 years, and bring different weather conditions to different parts of the world. There is some evidence that global warming may be intensifying ENSO events [84]. The studies of historical data show the recent El Niño variation is most likely linked to global warming. El Niño events cause short-term (approximately 1 year in length) spikes in global average surface temperature (Fig. 58). A further confirmation of the relationship between the ENSO cycle and the temperatures observed on Sicily could be provided by the cross-wavelet analysis.

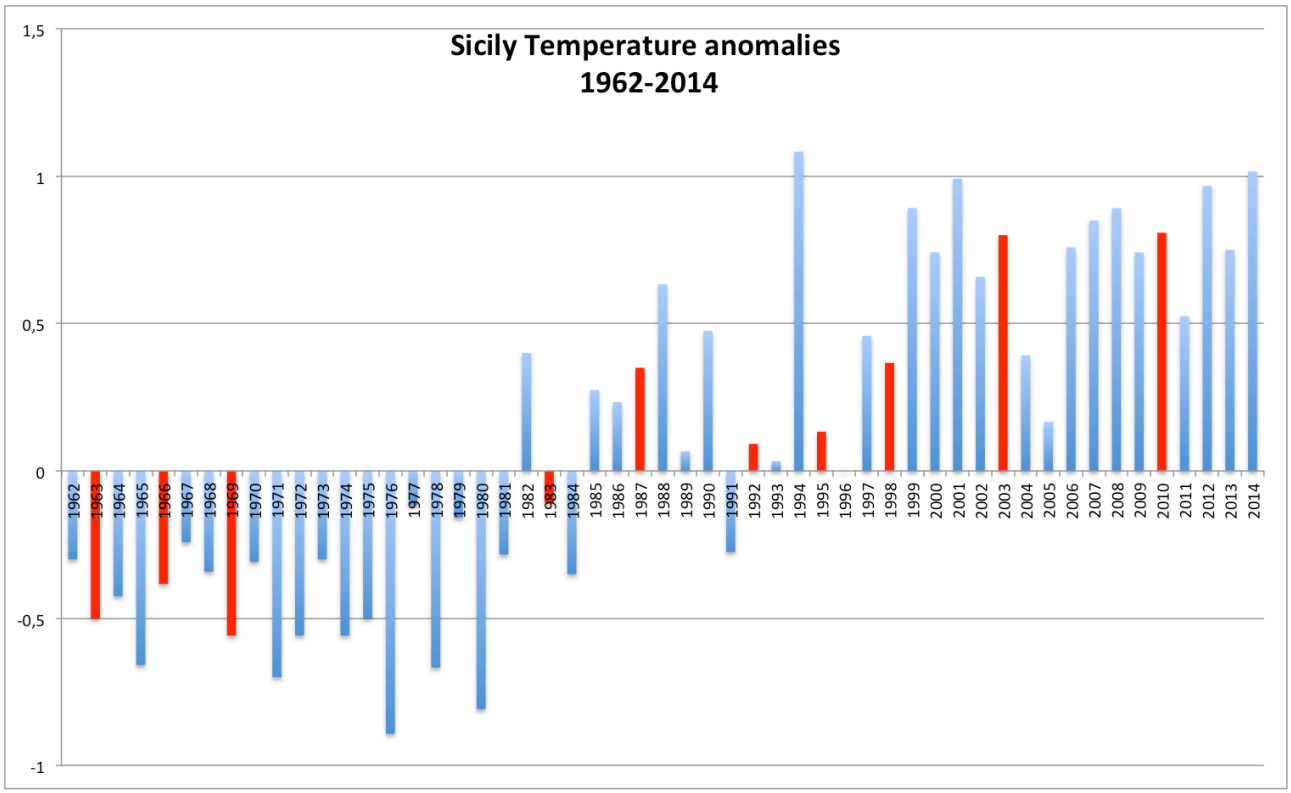

Fig. 58 Sicily temperature anomalies 1962-2014 for grid point 3775-1375. The red lines indicate the occurrence of El Niño.

The concepts of cross-wavelet analysis provide appropriate tools for (i) comparing the frequency contents of two time series, (ii) drawing conclusions about the series' synchronicity at certain periods and across certain ranges of time. The results of cross-wavelet analysis performed crossing the Sicilian temperature anomalies and the Oceanic Niño Index (ONI) are shown in fig. 59. It is inevitable that the understanding of the complex climatic dynamics, which occur on time scales ranging from a few months to thousands of years and involving multiple agents, can not be exhausted in a simple doctoral research. This was not my goal, nor is this thesis supposed to be. It is evident that further analyses, as well as more in-depth studies are necessary to try to better understand the problem of climate change and try to give answers to better face the adaptation of society to the new climate scenarios that will occur in the near future.

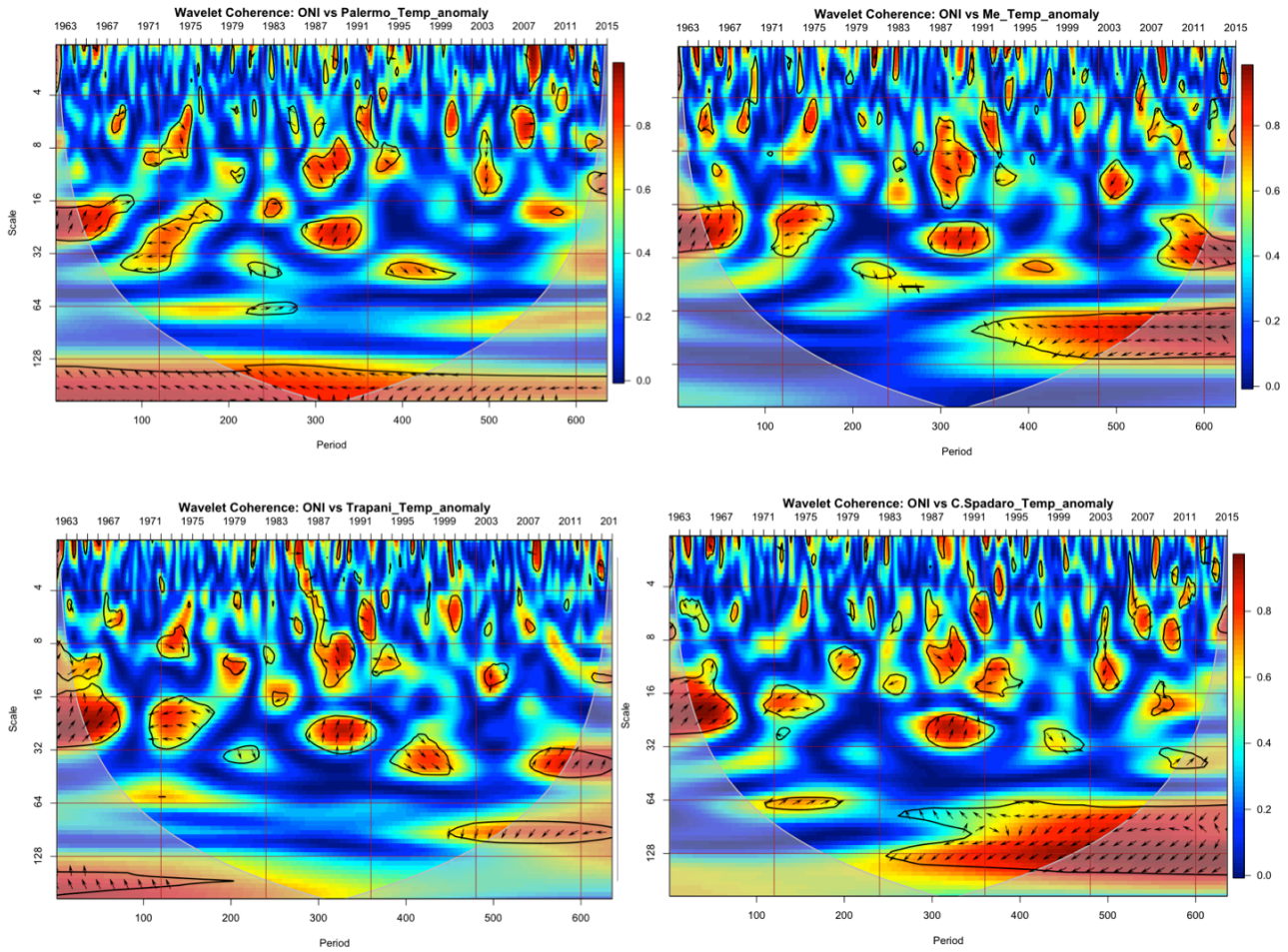

Fig. 59 Wavelet coherence obtained crossing temperature anomalies of Sicilian data of Palermo (upper left), Messina (upper right), Trapani (bottom left) and Cozzo Spadaro (bottom right) with Oceanic Niño Index (ONI).

Acknowledgements

This PhD thesis is the result of a fruitful and close collaboration between the University of Messina and the Italian Air Force, which I am honored to be part of and to which my heartfelt thanks go. I hope that in the future this collaboration may increasingly expand and consolidate.

A big thank you goes to the Doctorate Tutor, Prof. Salvo Magazù, for his advice, patience and availability shown every day.

A heartfelt thanks to Pippo Pellegrino for his valuable contribution and help in English translations.

Finally, an immense "thank you" goes to my whole family: first of all to my wife for the patience she had in the endless hours of study spent in front of the computer; to my sons Giuseppe, Giovanni and Cristina to whom I hope to have transmitted a bit of my love for study and knowledge.

References

[1] Wisniak J. , Svante Arrhenius and the Greenhouse Effect, Indian Journal of Chemical Technology Vol.9 March 2002, pp165-173

[2] Crawford E., Arrhenius' 1896 Model of the Greenhouse Effect in Context, Ambio, Vol. 26, No. 1, Arrhenius and the Greenhouse Gases (Feb., 1997), pp. 6-11

[3] Hays,J.D.,J.Imbrie, and N.J. Shackleton, Variations in the Earth'sorbit: Pacemaker of the ice ages, Science 1,94, 1121-1132, 1976.

[4] Imbrie, J., J. D. Hays, D. G. Martinson,A. Mcintyre, A. C. Mix, J. J. Morley, N. G. Pisias,W. L. Prell, andN.J. Shackleton, The orbital theory of Pleistoceneclimate: Support from a revised chronology of the marine record, in Milankovitch and Climate, Part1, edited by A. L. Bergeret al., pp. 269-305, D. Reidel,Norwell, Mass., 1984.

[5] Eddy J.A. 1976 "The Maunder Minimum". *Science*. **192** (4245): 1189–1202.

[6] Dorian J. Burnette and David W. Stahle, Historical perspective on the dust bowl drought in the central United States, *Climatic Change*, **116**, 3-4, (479), (2013).

[7] J. O. Murphy, Australian Tree Ring Chronologies as Proxy Data for Solar Variability, *Publications of the Astronomical Society of Australia*, **8**, 03, (292), (1990).

[8] Lockwood, M.; et al. (February 2010). "Are cold winters in Europe associated with low solar activity?". *Env. Res. Lett*. **5** (2): 024001.

[9] Cubasch U, Wuebbles D, Chen D, Facchini MC, Frame D, Mahowald N, Winther JG. Introduction. In: Stocker TF, Qin D, Plattner GK, Tignor M, Allen SK, Boschung J, Nauels A, Xia Y, Bex V, Midgley PM (Eds). *Climate Change 2013: The Physical Science Basis. Contribution of Working Group I to the Fifth Assessment Report of the In- tergovernmental Panel on Climate Change*. Cambridge, United Kingdom and New York, NY, USA: Cam- bridge University Press; 2013. p. 119-58; DOI:10.1017/ CBO9781107415324.007

[10] Alexander, L. V. et al., 2006: Global observed changes in daily climate extremes of temperature and precipitation. *Journal of Geophysical Research*, **111**, 22, doi:10.1029/2005JD006290.

[11] Gillett, N. P., V. K. Arora, G. M. Flato, J. F. Scinocca, and K. von Salzen, 2012: Improved constraints on 21st-century warming derived using 160 years of temperature observations. *Geophysical Research Letters*, **39**, 5, doi:10.1029/2011GL050226

[12] Santer, B. D. et al., 2013: Identifying human influences on atmospheric temperature. *Proceedings of the National Academy of Sciences*, **110**, 26-33, doi:10.1073/pnas.1210514109

[13] Stott, P. A., N. P. Gillett, G. C. Hegerl, D. J. Karoly, D. A. Stone, X. Zhang, and F. Zwiers, 2010: Detection and attribution of climate change: A regional perspective. *Wiley Interdisciplinary Reviews: Climate Change*, **1**, 192-211, doi:10.1002/wcc.34.

[14] Kington, J., 1988: The Weather of the 1780s over Europe. Cambridge University Press, Cambridge, UK, 164 pp.

[15] Quetelet, A., 1854: Rapport de la Conférence, tenue à Bruxelles, sur l'invitation du gouvernement des Etats-Unis d'Amérique, à l'effet des'entendre sur un système uniform d'observations météorologiques à la mer. Annuaire de l'Observatoire Royal de Belgique, 21, 155–167.

[16] WMO Statement on the State of the Global Climate 2017. ISBN 978-92-63-11212-5

[17] Peterson TC, Vose R, Schmoyer R, Razuvaëv V (1998) Global historical climatology network (GHCN) quality. Int J Climatol 18:1169–1179

[18] Chen, M., Xie, P., Janowiak, J. E. & Arkin, P. A. Global land precipitation: A 50-yr monthly analysis based on gauge observations. *J. Hydrometeorol.* **3**, 249–266 (2002).

[19] Adler, R. F. *et al*. The version-2 global precipitation climatology project (GPCP) monthly precipitation analysis (1979-present). *Journal of hydrometeorology* **4**, 1147–1167 (2003).

[20] Rudolf, B., H. Hauschild, W. Rüth, and U. Schneider, 1994: Terrestrial precipitation analysis: Operational method and required density of point measurements. *Global Precipitation and Climate Change,* M. Desbois and F. Desalmand, Eds., NATO ASI Series I, Vol. 26, Springer–Verlag, 173–186.

[21] Mitchell, T.D. and Jones, P.D. 2005: An improved method of constructing a database of monthly climate observations and associated high-resolution grids. Int. J. Climatol. 25: 693 – 712.

[22]Lionello, P (Ed), 2012. The climate of the Mediterranean region: From the past to the future. Elsevier Edit. 584 pages.

[22a] Köppen, W., 1900. Versuch einer klassifikation der klimate, vorzugsweise nach ihren beziehungen zur pflanzenwelt. Geogr. Z. 6, 593–611. 657–679.

[23] New, M.G., Hulme, M., Jones, P.D., 2000. Representing twentieth century space time climate fields. Part II: development of a 1901–1996 mean monthly terrestrial climatology. J. Clim. 13, 2217–2238.

[24] Xoplaki, E., Gonzalez-Rouco, F. J., Luterbacher, J., Wanner, H., 2003. Mediterranean summer air temperature variability and its connection to the large-scale atmospheric circulation and SSTs. Clim. Dyn. 20, 723–739. doi: 10.1007/s00382-003–0304-x.

[25] Dünkeloh, A., Jacobeit, J., 2003. Circulation dynamics of Mediterranean precipitation variability 1948–98. Int. J. Climatol. 23, 1843–1866.

[26] Lionello, P., Galati, M.B., 2008. Links of the significant wave height distribution in the Mediterranean Sea with the north hemisphere teleconnection patterns. Adv. Geosci. 17, 13–18.

[27] Mariotti, A., Zeng, N., Lau, K.M., 2002. Euro-Mediterranean rainfall and ENSO—a seasonally varying relationship. Geophys. Res. Lett. 29, 1621.

[28] Alpert, P., Baldi, M., Ilani, R., Krichak, S., Price, C., Rodó, X., et al., 2006a. Chapter 2. Relations between climate variability in the Mediterranean region and the tropics: ENSO, south Asian and African monsoons, hurricanes and Saharan dust. Dev. Earth Environ. Sci. 4 (C), 149–177.

[29] Carrion, J.S., Fernandez, S., Jimenez-Moreno, G., Fauquette, S., Gil-Romera, G., Gonzalez-Samperiz, P., et al., 2010. The historical origins of aridity and vegetation degradation in southeastern Spain. J. Arid Environ. 74, 731–736.

[30] Reale, O., Shukla, J., 2000. Modeling the effects of vegetation on Mediterranean climate during the Roman classical period: Part II: model simulation. Global Planet 25, 185–214.

[31] Zampieri, M., Lionello, P., 2011. Anthropic landuse cools down summer season in Europe. Clim. Res. 46, 255–268.

[32] Carrion, J.S., Fernandez, S., Jimenez-Moreno, G., Fauquette, S., Gil-Romera, G., Gonzalez-Samperiz, P., et al., 2010. The historical origins of aridity and vegetation degradation in southeastern Spain. J. Arid Environ. 74, 731–736.

[33] Colombaroli, D., Marchetto, A., Tinner, W., 2007. Long-term interactions between Mediterranean climate, vegetation and fire regime at Lago di Massaciuccoli (Tuscany, Italy). J. Ecol. 95, 755–770.

[34] Luterbacher, J., García-Herrera, R., Akcer-On, S., Allan, R., Alvarez-Castro, M.C., Benito, G., et al., 2012. A review of 2000 years of paleoclimatic evidence in the Mediterranean. The

Climate of the Mediterranean Region, 87–183.

[35] Mann, M.E., Zhang, Z., Rutherford, S., Bradley, R.S., Hughes, M.K., Shindell, D., et al., 2009. Global signatures and dynamical origins of the little ice age and medieval climate anomaly. Science 326, 1256–1260.

[36] New, M., Hulme, M., Jones, P.D., 1999. Representing twentieth century space-time climate variability. Part 1: development of a 1961–90 mean monthly terrestrial climatology. J. Clim. 12, 829–856.

[37] Plan Bleu and European Investment Bank, 2008. Climate Change and Energy in the Mediterranean.

http://www.planbleu.org/publications/changement_clim_energie_med_EN.pdf

[38] Giorgi, F., Lionello, P., 2008. Climate change projections for the mediterranean region. Global Planet. Change 63, 90–104.

[39] Blackman, R.B., Tukey, J.W. 1958. The Measurement of Power Spectra. Dover, New York.

[40] Shaphiro H.S. and Silverman R.A., 1960, "*Alias free sampling of random noise"* J. Soc. Ind.Appl.Math.

[41] Jonhes R. H. , 1972, " *Alising with unequally spaced observations",* J. Appl. Meteorol.

[42] Thomson D.J., 1982, "*Spectrum estimate and harmonic analysis*", IEEE Proc. 70(9) pag. 1055-1096.

[43] Chatfield C, 1984, "*The analysis of time series: An introduction"*, 3rd ed., Chapman and Hall, New York.

[44] Jenkins G.M. and Watts D.G., 1968, "*Spectral Analysis and its Applications*", Holden-Day, San Francisco.

[45] Burg J.P., 1967, "*Maximum entropy spectral analysis"*, in 37th Ann.Intern.Meeting. Soc. Explor. Geophis., Oklaoma City, OK.

[46] Childers D.G.(ed), 1978*, "Modern Spectrum Analysis"* IEEE Press, New York.

[47] Haykin S.(ed), 1983, "*Nonlinear Methods of Spectral Analysis. Topics in Applied Phisics"*, 2nd ed.,Springer-Verlag, Berlin.

[48] Pestiaux P., 1984, "*Approche spectrale en modellisation paleoclimatique*", PhD Thesis, Universitè Chatolique de Louvain, Belgium.

[49] Press W.H., Flannery B.P., Teulosky S.A. and Vettering W.T., 1988, "*Numerical recipes: The art of science computing*", Cambridge University Press, Cambridge.

[50] Martin N., 1984, "*Developpements de Mèthodes d'Analyse Spectrale Autoregressive: Application à des Signaux Rèels Non Stationnaires a n Dimension"* , Thèse de docteur ingenieur, Institut Polytechnique de Grenoble, France.

[51] Benoist J.P., 1986, "*Analyse Spectrale de Signaux Glaciologique: Etude des Glaces Sèdimentaires Deposèes à Dome C, Morphologie du Lit d'un Glacier"*, Thèse d'Etat, USMT Grenoble, France.

[52] Lindberg C.R., 1986, "*Multiple Taper Spectral Analysis of Terrestrial Free Oscillations"*, PhD Thesis, Scripps Institution of Oceanography, University of California, San Diego.

[53] Park J., Lindberg C.R. and Vernon F.L.I., 1987, "*Multitaper spectral analysis of high frequency seismograms"*, J.Geophys. Res. 92, pag. 12675-12684.

[54] Lanzerotti L.J., Thomson D.J., Meloni A., Medford L.V. and Maclennan C.G., 1986, "*Electromagnetic Study of the Atlantic continental margin using a section of a transatlantic cable"*, J. Geophys. Res. 91, pag. 7417-7427.

[55] Ghil M. and Vautard R., 1991, "*Interdecadal Oscillations and the warming trend in global temperature time series"*, Nature 350 (6316), pag. 324 – 327.

[56] Mann M.E., Park J. And Bradley R.S., 1995 , "*Global Interdecadal and Century-scale climate oscillations durin the past five centuries"*, Nature 378 , pag. 266-270.

[57] Thomson D.J., 1990, "*Quadratic-inverse spectrum estimate :applications to paleoclimatology*", Phil. Trans. R. Soc. London A 332, pag 539-597.

[58] Berger A.L., Mèlice J.L. and Hinnov L., 1991 "*A strategy for frequency spectra of quaternary climate records"*, Clim. Dyn. 5, pag. 227-240.

[59] Park J. and Maasch K.A., 1993, "*Plio-pleistocene time evolution of the 100-Kyr cycle in Marine paleoclimate records"*, J.Geophys. Res. 98, pag. 447-461.

[60] Yiou P., Ghil M., Jouzel J., Paillard D. and Vaultard R., 1994, "*Nonlinear variability of the climatic system, from singular and power spectra of late Quaternary records*", Clim. Dun. 9, pag 371-389.

[61] Yiou P., Genthon C., Jouzel J., Ghil M., Le Treut H, Barnola J.M., Lorius C. and Korotkevitch Y.N., 1991, "*High-frequency paleovariability in climate and in CO_2 levels from Vostok ice-core records*", J. Geophys. Res. 96(B12), pag. 20365-20378.

[62] Slepian S., 1978, "*Prolate spheroidal wave functions, Fourier analysis and uncertainty – V: the discrete case*", Bell. Sys. Tech.. J. 57, pag. 1371-1430.

[63] Rögnvaldsson O.E., 1993, "*Spectral estimation using the multi taper method*" Technical Report RH-13-13 Science Institute, University of Iceland, Reykjavik, Iceland.

[64] Mann M.E., Lees J.M., 1996, "*Robust estimation of background noise and signal detection in climatic time series"*, Clim. Change 33, pag. 409-445.

[65] Berger A.L., Mèlice J.L. and Van der Mersch I., 1990 "*Evolutive spectral analysis of sun spot data over the past 300 Years"*, Phil. Trans. R. Soc. London A 330, pag. 529-541.

[66] Birchfield G.E. and Ghil M., 1993, "*Climate evolution in the Pliocene-Pleistocene as seen in deep sea δ^{18} records and in simulations: internal variability versus orbital forcing"*, J.Geophys. Res. 98 (Do), pag. 10385-10399.

[67] Grossmann A., Kronland-Martinet R. and Morlet J., 1989, "*Reading and understanding continuous wavelet transforms"*, in J.M. Combes, A. Grossman and P. Tchamitchian (eds.), Wavelets: Time-Frequency Methods and Phase Space, pp. 2-20, Springer-Verlag, Berlin

[68] Meyer Y., 1989, "*Ondelettes et Operateurs I: Ondelettes"*, Hermann, Paris.

[69] Mallat S.G., 1989, "*A theory for multiresolution signal decomposition: the wavelet representation"*, IEEE Trans. Pattern Anal. Mach. Intell. 11(7), pag. 674-693.

[70] D. B. Percival and A. T. Walden (2000). Wavelet Methods for Time Series Analysis. Cambridge UK: Cambridge University Press.

[71] Baliunas, S., P. Frick, D. Sokoloff, and W. Soon (1997), Time scales and trends in the central England temperature data (1659 – 1990): A wavelet analysis, *Geophys. Res. Lett.*, *24*(11), 1351–1354, doi:10.1029/97GL01184.

[72] Torrence, C., and G. P. Compo (1998), A practical guide to wavelet analysis, *Bull. Am. Meteorol. Soc.*, *79*(1), 61–78.

[73] Sonechkin, D.M., N.M. Astafyeva, N.M. Datsenko, N.N. Ivachtchenko, and B. Jakubiak, Multiscale oscillations of the global climate system as revealed by wavelet transform of observational data time series, Theor. Appl. Climatol., 131-142, 1999.

[74] Park, J., and M.E. Mann, Interannual temperature events and shifts in global temperature: A multiple wavelet correlation approach, Earth Interact. 4, Pap. 1, 2000.

[75] Datsenko,N .M., D. Novotna, and D.M. Sonechkin Analysis of climate change for 200 years from air temperature observations in Prague-Klementinum, Russ. Meteorol. Hydrol., 23-30, 1998

[75a] Combes, J. M.,A. Grossman, and P. Tchamitchian, 1989: Wavelets: Time Frequency Methods and Phase Space. Springer, 315pp.

[75b] Birchfield, G. E. and M. Ghil, Climate evolution in the Pliocene and Pleistocene from marine-sediment records and simulation: internal variability versus orbital forcing, J. Geophys. Res., 98, 10385-10399, 1993

[76] Farge, M. (1992). Wavelet Transforms and their Application to Turbolence, Ann. Rev. Fluid Mech., 24, 395-457.

[77] Harris, I., Jones, P.D., Osborn, T.J. and Lister, D.H. (2014), Updated high-resolution grids of monthly climatic observations - the CRU TS3.10 Dataset. *International Journal of Climatology* **34**, 623-642

[78] Drago, A.F., Boxall, S.R., 2002. Use of the wavelet transform on hydro-meteorological data. Phys. Chem. Earth 27 (32–34), 1387–1399.

[79] Chou, C.-M., 2007. Applying multi-resolution analysis to differential hydrological grey models with dual series. J. Hydrol. 332 (1–2), 174–186.

[80] Fugal, D.L., 2009. Conceptual Wavelets in Digital Signal Processing: An In-depth, Practical Approach for the Non-mathematician, first ed. Space & Signals Technologies LLC.

[81] Chou, C.-M., 2007. Applying multi-resolution analysis to differential hydrological grey models with dual series. J. Hydrol. 332 (1–2), 174–186.

[82] Bruce, L.M., Koger, C.H., Jiang, L., 2002. Dimensionality reduction of hyperspectral data using discrete wavelet transform feature extraction. IEEE Trans. Geosci. Remote Sens. 40 (10), 2331–2338.

[83] de Artigas, M.Z., Elias, A.G., de Campra, P.F., 2006. Discrete wavelet analysis to assess long-term trends in geomagnetic activity. Phys. Chem. Earth 31 (1–3), 77–80.

[84] Li, J. *et al.* El Niño modulations over the past seven centuries. *Nature Clim. Change* **3**, 822–826 (2013).